Title
Design Optimization of Cementitious Reinforced Orthotropic Sandwich Composite System

Author
Mirnateghi, Ehsan

Publication Date
2017

Peer reviewed|Thesis/dissertation

UNIVERSITY OF CALIFORNIA,
IRVINE

DESIGN OPTIMIZATION OF CEMENTITIOUS REINFORCED ORTHOTROPIC SANDWICH COMPOSITE SYSTEM

DISSERTATION

submitted in partial satisfaction of the requirements
for the degree of

DOCTOR OF PHILOSOPHY

in Civil Engineering

by

Ehsan Mirnateghi

Dissertation Committee:

Professor Ayman Mosallam, Chair

Assistant Professor Mohammad Javad Abdolhosseini Qomi

Assistant Professor Mo Li

2017

DEDICATION

To my Wife Mahsa

TABLE OF CONTENTS

LIST OF FIGURES

LIST OF TABLES

ACKNOWLEDGMENTS

First, I thank God the most merciful, the most gracious and the cherisher and sustainer for giving me the strength to complete this research.

I wish to express my deep gratitude to my supervisor, Professor Ayman Mosallam for his continuous support during all stages of this research. I am grateful for his vast knowledge and keen insight into the most challenging problems. It has been his continuous help and guidance that helped improve the quality of this work.

I would like also to thank my committee members, Professor Mohammad Javad Abdolhosseini Qomi and Professor Mo Li for their time and patience and serving as members of my Ph.D. Committee. Their valuable advice, comments and suggestions have enhanced the quality of my research. I would like also to thank all my colleagues, Mr. Islam Rabie, Mr. Ibrahim M. El Demerdash, Mr. Brian Botello for their sincere assistance in the experimental program. I would also like to thank MSC Software Engineering company, for the providing internship opportunity at the company and software's technical support. Special thanks go to both Ms. Krysia Baker and Mr. Joe Satkunananthanoe for their continuous technical input and support in numerical modeling. Thanks also goes to Enbuil Co. for providing project photos that were used in Chapter 2.

Finally, I would like to thank my family and my wife for their unconditional love, support and understanding.

CURRICULUM VITAE

Ehsan Mirnateghi

Education:

2004-08 Bachelor of Science in Civil Engineering (*magna cum laude*),
American University of Dubai, UAE

2010-12 Master of Science in Civil Engineering, emphasis: Structural Engineering
University of California Irvine, USA

2012-17 Ph.D. in Civil Engineering, emphasis: Structural Engineering
University of California Irvine, USA
Dissertation Title: "*Design Optimization of Cementitious Reinforced Orthotropic Sandwich Composite System"*

Work Experience:

2008-09 Field Engineer at the Dubai Mall Mega Project (World's tallest tower)
Consolidate Construction Company, Dubai, UAE

2012-15 Technical Support Engineer for MSC Marc and Mentat
MSC Software, Newport Beach, CA, USA

2014-15 Teaching Assistance, University of California Irvine

2015-16 Research Assistance, University of California Irvine

Honors and Awards

2006-08 Deans Honors List of Academically Distinguished Student

2007-17 Golden Key International Honor Society

ABSTRACT OF THE DISSERTATION

Design Optimization of Cementitious Reinforced Orthotropic

Sandwich Composite System

By

Ehsan Mirnateghi

Doctor of Philosophy in Civil Engineering

University of California, Irvine, 2017

Professor Ayman S. Mosallam, Chair

This study focuses on structural optimization of the orthotropic sandwich cementitious composite systems. In order to develop a sandwich panel with high structural performance, design optimization techniques must be utilized to achieve full composite action as well as light weight, and high thermal insulation. This study involves both linear and nonlinear finite element analyses and parametric optimization. The verification and calibration of the numerical models will be based on the experimental results of numerous full-scale tests that were performed on two types of commercially produced sandwich panels under different loading scenarios at University of California Irvine.

In order to minimize the number of design variables required for producing an optimum sandwich panel, the Taguchi statistical method for quality control is utilized. In this method, statistically planned experiments (or numerical simulation runs) are used to identify the settings of the sandwich panel design parameters that result in optimum design.

Additionally, the Genetic Algorithm (GA) is used as an alternative approach for optimization, in order to evaluate the optimum design and build further confidence in our optimum design. GA combines Darwin's principle of survival of the fittest and a structured information exchange using randomized crossover operators to evolve an optimum design for the cementitious sandwich panel.

Among the different initial parameters to be evaluated in the study are: (i) shear connectors' geometry, volume fraction, and distribution; (ii) The thickness of exterior cementitious face sheets; (iii) The size and geometry of the exterior face sheets steel reinforcement details.

Ultimately, the proposed optimization method reduced the cost of material of CSP by the by almost 48% using genetic algorithm. In the same time, alternative design for CSP have been proposed where the optimization process increased the thermal resistance of the CSP by 40% compare to the conventional models currently available in the market while meeting the design Criteria's based on the ACI Code. Pareto-optimal front and Pareto-optimal solutions have been identified. Correlation between the design variables of CSP is verified and design recommendation have been proposed for CSP manufacturers and structural designers.

CHAPTER 1

INTRODUCTION

1.1. General

In response to the increasing global awareness of the energy consumption and environmental impact, engineers and the construction industry are facing great challenges in developing energy-efficient and environmentally compatible civil infrastructures systems. [1]. Cementatious Sandwich Panel (CSP) construction system is an example of alternative building systems that satisfies these major challenges. Compared to traditional reinforced concrete, CSP can meet all of the above demands with its modular design, efficient use of cementitious material, and insulator core.

The standard cross-section of a typical CPS can be seen in Figure (1.1). It consists of a several components each made of a specific material for desired purpose. Two steel wire mesh faces are provided on either side of the panel and connected by diagonal transversal truss wires. In between the wire mesh faces and held by the truss diagonals is the insulator foam core. Both faces then have cementitious mortar applied to develop the final complete CSP system.

The idea of sandwich panel comes from optimizing the allocation of material where there is demand. As seen in Figure (1.2) and Figure **(1.3**), the facing skins of a sandwich panel can be compared to the flanges of an I-beam, as they carry the bending stresses load which the beam is subjected, with one facing skin in compression, the other is in tension.

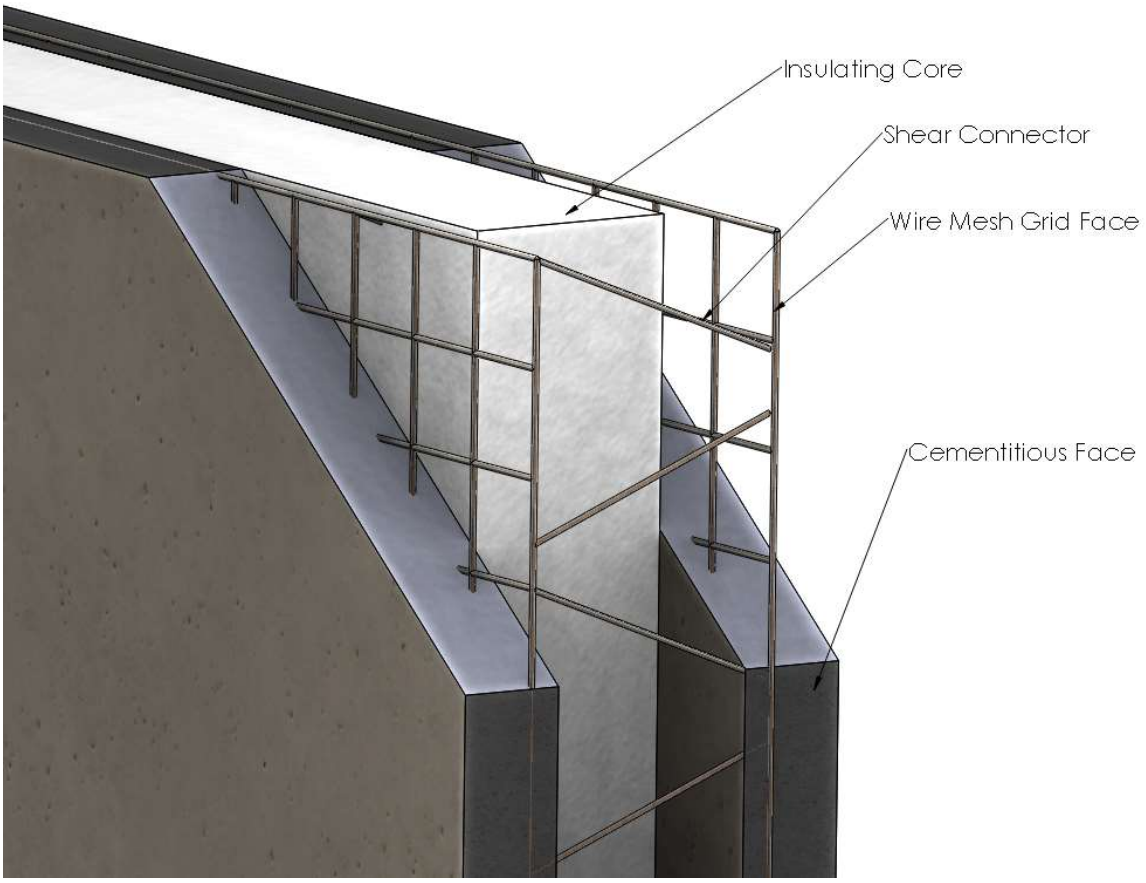

Figure (1.1): Example of Cementitious Sandwich Panel (CSP)

Similarly, the shear connectors in the core of sandwich panel corresponds to the web of the I-beam. The core resists the shear loads, increases the stiffness of the structure by holding the facing skins apart, it gives continuous support to the flanges or facing skins to produce a uniformly stiffened panel.

Cementatious sandwich panel is much lighter compare to conventional reinforce concrete structural systems. Although concrete has considerable compressive strength in compression but it has a very low tensile strength (about 10% of its compression strength) which is why it requires tensile reinforcing. As a result, the concrete used on the tensile side from the Neutral Axis is only used for shear. However, it is huge penalty for shear.

Concrete has low shear strength (square root of its compression strength) compare to its weight which is why it is more efficient to rely on reinforcing for shear to reduce the weight of the structural elements.

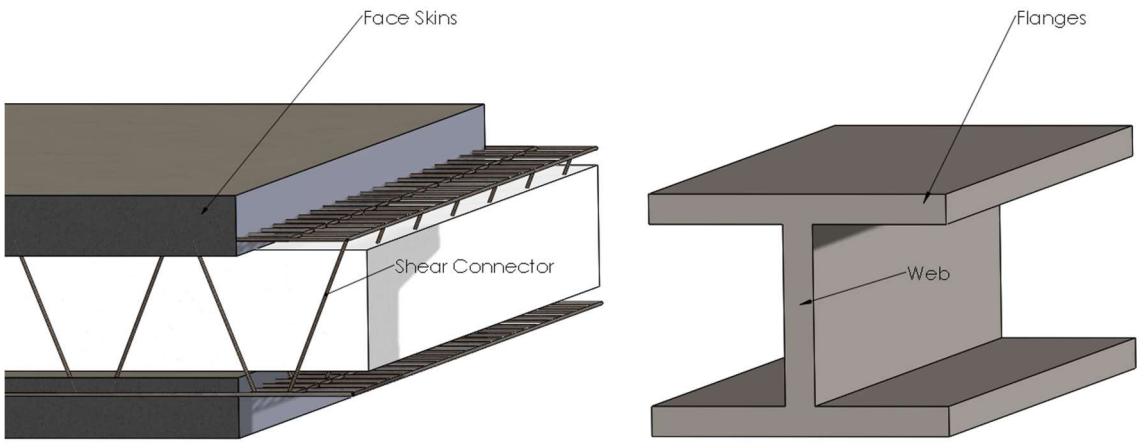

Figure (1.2): Construction of Sandwich Panel Compared to an I Beam.

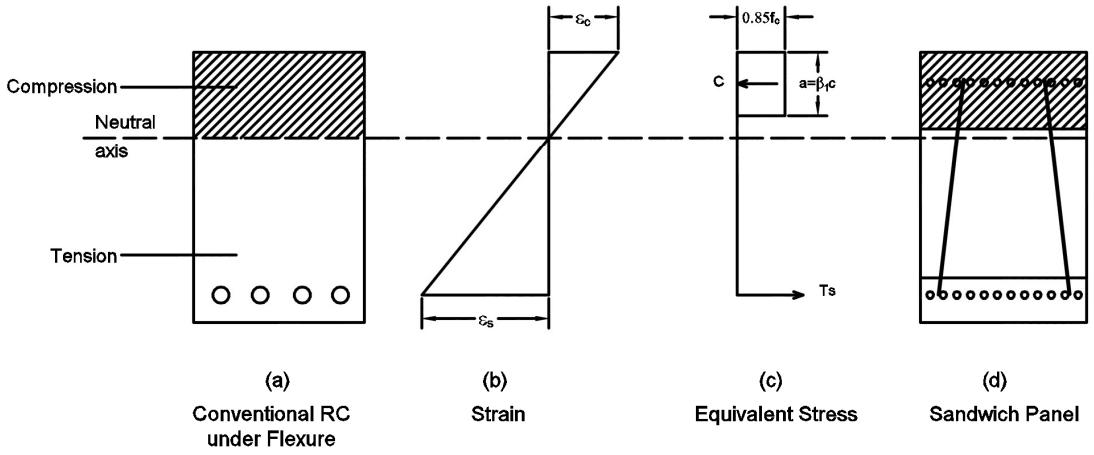

Figure (1.3): Sandwich Panel Optimization Philosophy Based on the Stress Distribution

In CSP the shear connectors are designed to take the shear instead of heavy concrete. However, some of the currently produced CSP systems, the designed shear connectors are not providing adequate, sufficient or compete transfer of shear. For Example, Schnell or Emdue sandwich panel systems have only parallel component for vertical shear as seen in Figure (1.4). However, the shear transfer that happens horizontally, that is called conjugate shear, which happens at the same time as vertical shear, is not available in this design. Unless after a minimum curvature then we would have the horizontal component of the shear connector transferring the load. However, by the time the sandwich panel reaches the required curvature, then the deflection might violate the deflection limit provided by the code.

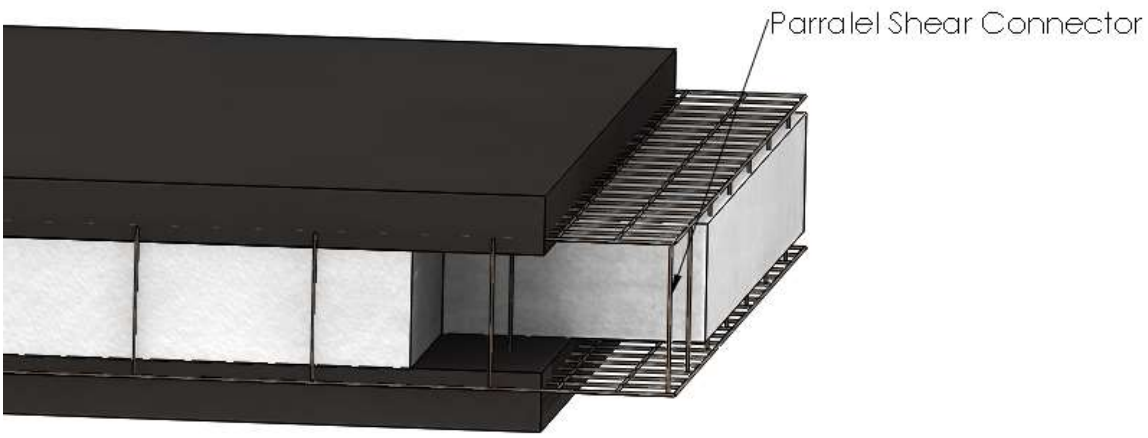

Figure (1.4): Design of Sandwich Panel with Parallel shear Connectors

Another issue in the current design of commercially produced sandwich panels are the number of webs and stiches of the shear connectors. For example, a company like Entwicklungs- und Verwertungs-Gesellschaft (EVG) is producing sandwich panels with

100-125 stiches per 1 m^2 (10.7 ft^2) [2]. On the other hand, a company like Schnell is producing the sandwich panels with 31 stiches per 1 m^2 (10.7 ft^2) using shear connectors with 3mm (0.11in) [3]. This is a wide range for the design of shear connectors and there are no bases from the structural engineering codes on these designs. As a result, manufacturers are dictating the design to the structural engineers, and structural engineers are refusing to use the commercially available designs.

Following the goals of sandwich panels to reduce the weight and cost of the panels, other designs specs of the panels become important. For example, in case of the bidirectional steels wire reinforcing meshes, the manufacturers are producing the Meshes with 5cm x 5cm (2″ x 2″) [2] and 8cm x 13cm (3.14″ x 5.11″) [3] without considering the principal of structural engineering. For example, On Tension side, the steel reinforcement, the reinforcing can be adjusted to the flexural demand and compression side, the excessive steel reinforcement can be reduced, to reduce both deadweight and cost.

This research focuses on implementing an optimization procedure to identify the optimum design for orthotropic sandwich panels. This procedure is defined based on accurate numerical models that will be optimized using the Taguchi statistical method for quality control. This optimization approach is one of the most unbiased and efficient methods to help in finding the optimum lightweight design that meets desired design limits. In addition, for the first time, the Genetic Algorithm (GA) procedure will be customized for optimization of the CSP to evaluate the optimum design and compare the results from the Taguchi statistical method.

Panels used as structural members such as slabs, beams, and walls, can be optimized for efficient structural performance and enhance the special qualities of sandwich panels. In general, sandwich construction members consist of two high-strength reinforced face sheets, core insulator and some form of shear transfer elements. Some of the advantages of such sandwich construction are: (i) its lightweight, (ii) thermal and acoustical insulations properties, and (iii) modular design that lead to an economic, environmental-friendly and energy-efficient building system. These benefits have favored their application in residential, commercial, and industrial buildings in North America. [4].

1.2. Research Motivation and Objective

According to the United Nation Environment Program website, Buildings and Construction sectors account for 40% of global energy use, 30% of energy-related greenhouse gas emissions, approximately 12% of water use, nearly 40% of waste, and employs 10% of the workforce, including many SMEs. Two billion additional urban inhabitants are expected by 2030, the majority of whom will be in the rapidly growing cities of Africa, Asia, and Latin America. [5] With this rapid growth comes an urgent need for affordable, sustainable, and energy efficient building systems. CSP construction system is an example of alternative building systems that satisfies these major challenges.

Available commercially produce sandwich panel systems have been developed by machine manufacturers rather than structural engineers. As a result, there is an urgent need to evaluate both the structural value as well as studying the sustainability benefits of the CSP system. Currently, engineers are designing the CSP system as a doubly-reinforced section without the consideration of the three-dimensional truss action of the orthotropic panel

system. This leads to uneconomical design of the system and underestimating both the strength and stiffness of such system that underutilizes the major benefits of the 3D panel structural system. The composite action of CSP is based on the shear connectors (diagonals wire) connecting the two exterior reinforced mortar faces. (See Figure (1.5))

As mentioned earlier, the major deficiency of the current design practice followed by the structural engineers today is neglecting the major effect of shear connectors (*truss wire diagonals)* when calculating the ultimate capacity of the panels under various loading conditions (normal loads, in-plane loads, out-of-plane, etc.). The two exterior reinforced mortar faces of the panel (refer to Figure (1.5)) are treated separately during design without taking into consideration the shear stress distribution performed by the shear connectors. That leads to overdesigning the cross-section. Overdesign has caused the panels to require more materials and larger cross-sections thus being less economical as an alternative building method.

This study aims at structural optimization of the orthotropic CSP composite systems. It looks into both structural optimizations of CSP as well as optimizing CSP insulation capability. This study involves both linear and nonlinear finite element analyses and optimization. The verification and calibration of the numerical models is based on the experimental results of numerous full-scale tests that were performed on two types of commercially produced sandwich panels under different loading scenarios at UCI Structural Engineering lab.

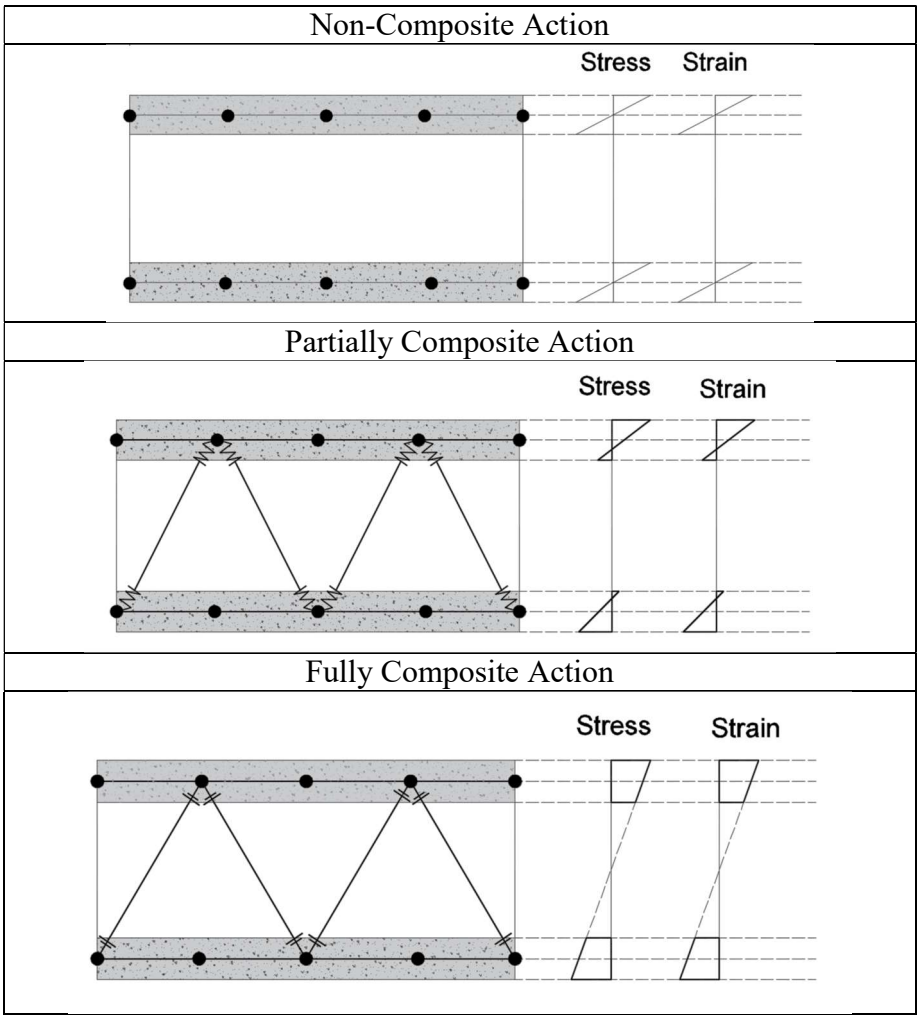

Figure (1.5): Different Types of Possible Composite Action in CSP.

1.3. Research Methodology

In order to be able to do an optimization on CSP a reliable numerical modeling is required that accurately mimics the experimental behavior and is able to predict the failure criteria comparable to the experimental results in finding strength and cracking locations. Later, an optimization procedure can be used to optimize the CSP. The following research methodology was followed:

- An extensive literature review was completed, covering all the topics pertaining to the manufacturing, usage, benefits and structural behavior of CSP. The literature reviews also included studying different optimization procedure used for optimizing similar structural systems.
- A series of large-scale testing that were conducting at UCI Structural engineering which involved various structural elements using CSP were observed and studied. The specimens tested were of various properties, dimensions and reinforcements.
- Experimental analysis was performed on each individual specimen tested as well in depth comparisons between different specimens constructed for the same structural element in study.
- A procedure to develop a Finite Element Model (FEM) to model CSP were developed using state-of-the-art nonlinear finite element analysis software MSC MENTAT and MARC general purpose finite element analysis program. This numerical model was used to predict the failure modes, load capacity, stress and strain distribution and the general behavior of the elements during the various stages of loading.
- The result of FE analysis and experiments were compared in order to verify the accuracy of developed FE analysis predictions.

  Following the maturity of the reliable numerical model, for the first time an optimization methodology is defined that incorporates a combination of mathematical and numerical optimization methodologies to identify the optimum CSP design. The Taguchi statistical method for quality control is customized to be used as sensitivity analysis for different design parameters of CSP.

- Additionally, for the first time, the Genetic Algorithm will be used in optimization of CSP and results were compared to the available commercial designs that were tested at UCI.
- Conclusion on the most effective design for CSP were determined as well as proposed recommendations.

1.4. Organization of The Dissertation

This dissertation is comprised of five chapters. Chapter one present the objectives and motivations of the research along with the research methodology undertaken in order to achieve the aforementioned research goals as well as the content of the dissertation. Chapter two demonstrate the literature review conducted on the history of sandwich panels with focus on development of cementations sandwich panel for civil and structural engineering. It also includes the previous studies conducted on sandwich panels as well as any study on optimization of similar structural elements. Chapter three, introduces two methods for optimization of CSP. First it introduces Tagushi method for sensitivity analysis of CSP Design parameters. Next, it introduces Genetic Algorithm for overall optimization of CSP design. In this chapter, an example of CSP under out of plane loading is evaluated and optimized using the modified GA introduced in this method. Chapter four described the development of finite element model for evaluation of CSP and evaluates the performance of the optimized design of CSP and compares it with results from large-scale test of commercially produced sandwich panels performed at UCI. Chapter five provides the conclusion as well as the recommendation proposed for the future work.

CHAPTER 2

BACKGROUND AND LITERATURE REVIEW

2.1. Background

The present-day designs of buildings have been known to consume large amounts of physical resources such as materials, energy and money in their construction and continued maintenance that have resulted in the loss of amenity and biodiversity [6]. The construction industry has been one of the main culprits of such atrocities to the environment and thus has accepted the mass usage of different construction techniques and materials in order to diminish the harmful effects to the environment. Three essential requirements for a habitable tenement are; strength, stability (*sturdiness in extreme weather, etc.),* and thermal insulation [7]. The utilization of sandwich panels has been deemed as sensible replacement to traditional methods regarding the environment. Other huge and various aspects and benefits arise with the use of sandwich panels such as no need for skilled labor, high heat and sound insulation and lower costs of construction amongst others that will further be demonstrated and tackled in the literature and research. Figure (2.1) shown the picture of former president J. Carter Through his charity foundation promoted the use of 3D panels for low-income housing in 1970s. [Courtesy of Enbuil]

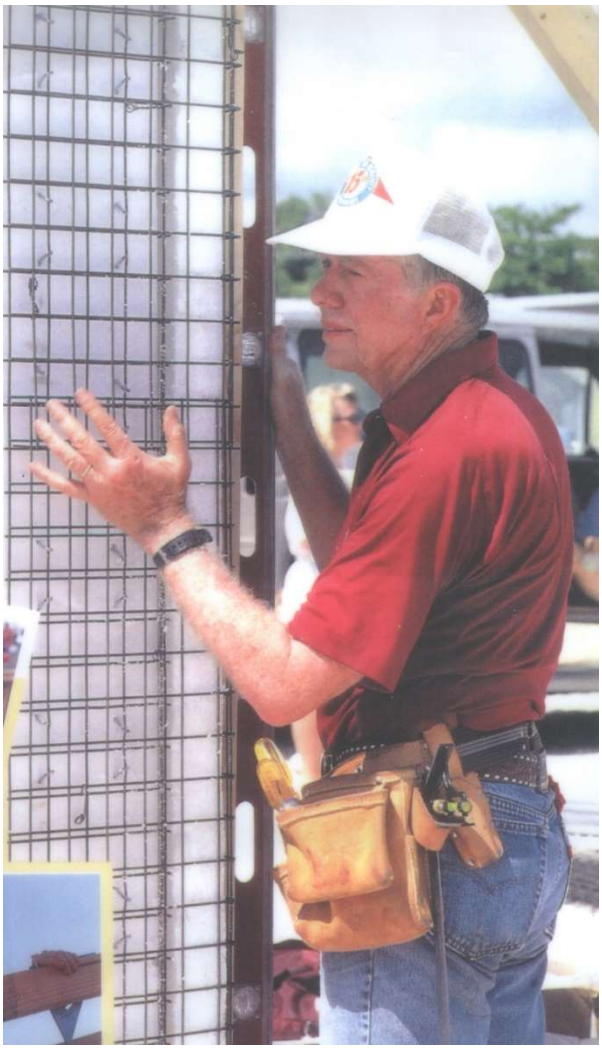

Figure (2.1): Former President J. Carter Through His Charity Foundation Promoted The Use of 3D Panels For Low-Income Housing. [Courtesy of Enbuil]

According to the United Nation Environment Program website, Buildings and Construction sectors account for 40% of global energy use, 30% of energy-related greenhouse gas emissions, approximately 12% of water use, nearly 40% of waste, and employs 10% of the workforce, including many SMEs. Two billion additional urban inhabitants are expected by 2030, the majority of whom will be in the rapidly growing cities of Africa, Asia, and Latin America [5]. The usage of sandwich panels as main

building elements has emerged as one of the leading solutions to provide faster speed of construction and delivery to the residential housing market. The faster method of construction has been proved by various companies in the industry that utilize such methods as opposed to building with the traditional timber, steel or reinforced concrete structures with timber being one of the first materials used for the building of the first dwellings. Figure (2.2) shows three stages of construction of Eco Village and Eco Resort using CSP for dome home designed by Hubble in California, USA.

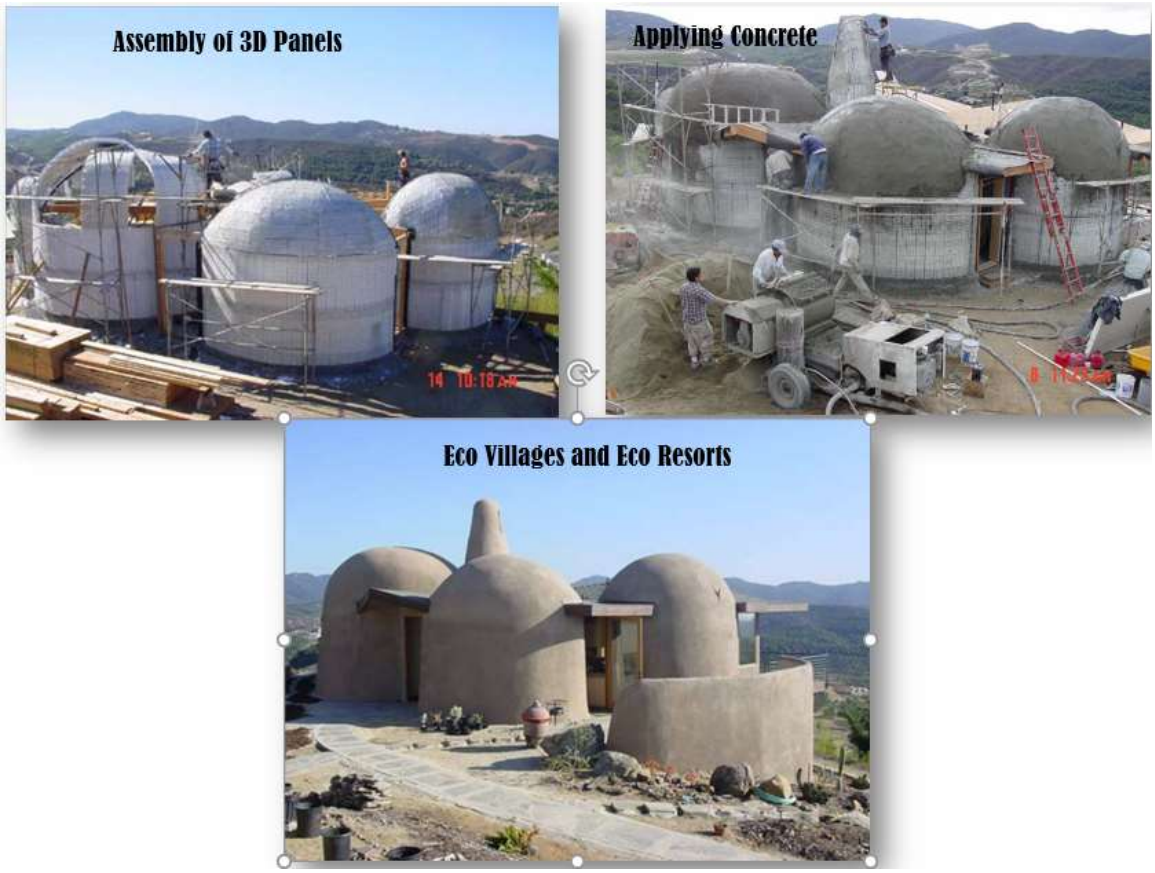

Figure (2.2): Eco Villages and Eco Resorts, Hubbell Dome Home, California, USA [Courtesy of Enbuil]

Sandwich panels are also considered a new groundbreaking method of construction in reference to the invention of concrete as a patented material in 1824 and the usage of reinforced concrete in construction in the mid-1900s whereas steel was largely used starting around 1850. The usage of sandwich panel system enables the mass production of the panels in factories thus standardizing the units produced and furthermore cutting down on time and cost of construction. By altering the technique of construction as opposed to the conventional methods; it allows the interaction between the design phase and the phase of production in order to improve and expedite construction. Designing buildings with a regular configuration in plan and elevation help achieve this objective [8].

The earliest use of sandwich panel dates back to the First World War, when a fiberboard core accompanied by 2 asbestos faces on each side was used. However, it's the acceptance of the uses of various types of adhesives in the United States and England in the early 1930s that paved the way for the utilization of bonded sandwich panels. During the Second World War its mass production was used in light aircraft by the aerospace industry [9].

On the other hand, in building construction, earliest use of sandwich panel technology dates back to 1930 in the Usonian houses designed by Frank Lloyd Wright and was referred to as Structural Insulated Panels (SIPs). It consists of three plywood layers glued by two tar layers in between and didn't provide any sufficient insulation. Afterwards Alden B. Dow, a student of Wright's incorporated an insulating core to the structural element. Styrofoam cores were used between the plywood faces for load bearing walls. Figure (2.) shows the sandwich panels used as walls and slabs.

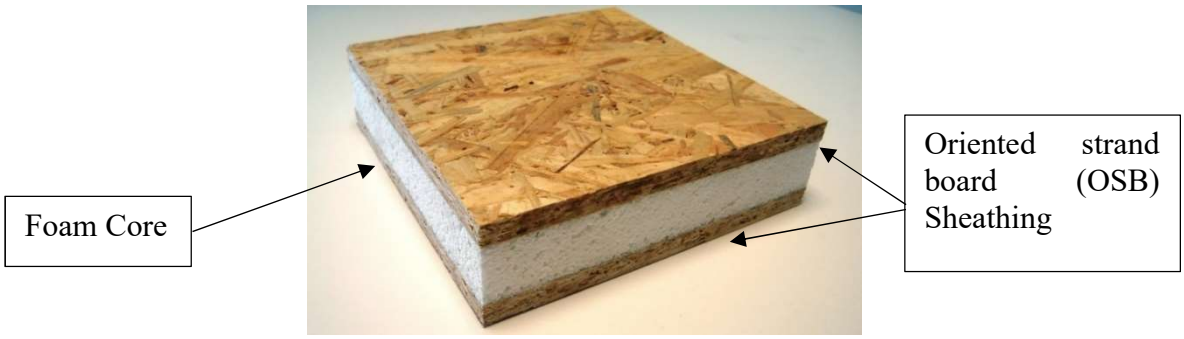

Figure (2.3): Structural Insulated Panel (SIP) (Source: Insulation Corporation 2016)

According to Mashal 2011 [10] the Oriented Strand Board (OSB) was first developed in the 1980's; it is a wood panel that has been engineered for housing and construction, OSB uses harvested trees from forests or tree farms. The trees are processed into precise strands averaging 4 inches (100mm) long and 1 inch (25mm) wide. The strands are oriented length-wise on the exterior and crossaligned on the interior. The alternating layers are then bonded with resins under high heat and pressure. The resulting product shares many of the same properties as plywood.

2.2. Cementitious Sandwich Panel System

The Cementitious Sandwich Panel (CSP) construction system is a rather new, cost efficient construction system that bases on insulated core, Cementitious faces reinforced with steel mesh and steel wire truss system connecting the two faces. One of the very first type of CSP was developed by a company called Impact in California, USA in early 1970. A sample is shown in Figure (2.4). In this design no machinery was required to develop the panels, whereas for the newer design of CSP in market (i.e. Entwicklungs- und Verwertungs-Gesellschaft (EVG) panels, a machinery is required to insert the shear connector through the core. Figure (2.6). In CSP designed by Impact, the two steel mesh faces on each side is connected using continues diagonal shear connectors. Later small

pieces of insular foam in rectangular cuboid shapes are inserted between the parallel shear connectors as shown in Figure (2.4). The foam design had grooves to create interlocking between the foam core and concrete. The problem with this design was that in order to prevent the foam from moving in center when the concrete is sprayed, a stopper is required to keep the foam in the center. The 2D cross section of Impact panels is shown in the Figure (2.5).

Figure (2.4): One of the First Designs of CSP With Continues Truss Shear Connectors

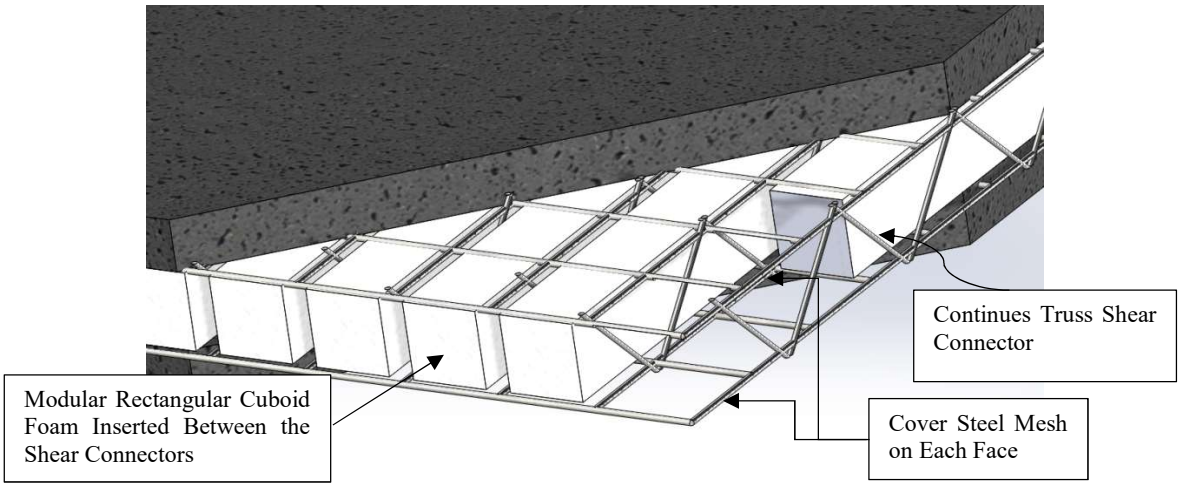

Figure (2.5): Typical CSP Cross Section with Continues Shear Truss Connectors

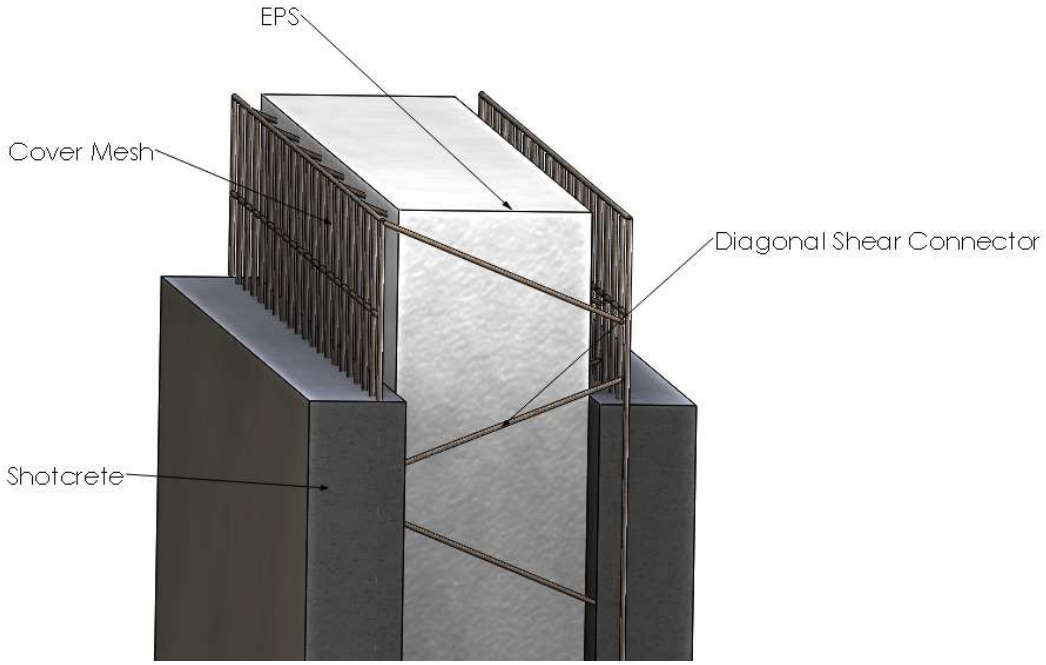

Figure (2.6): Typical CSP Cross Section designed with Diagonal Shear Connectors

In the design of CSP by EVG the expanded polystyrene core with a thickness ranging from 40 to 100mm sandwiched between two plane-parallel welded wire mesh sheets (cover meshes) and inclined diagonal wires in between that go through the EPS core and that are welded to the cover mesh's line wires. Both 3D panel faces then have cementitious mortar

applied to develop the final complete EPS 3D panel system as shown in Figure (2.6). In order to be able to evaluate the structural effectiveness of 3D panels by EVG, a comprehensive series of compression, bending and shear tests was carried out by El Demerdash et al. in 2015 at UCI Structural lab. [11] The tests were based on the material properties and behavior as well the usage of sandwich panels as different structural members. When the 3D panels are used as structural members, both steel meshes are poured or sprayed with concrete or mortar to provide an effective structural system which is capable of withstanding the respective loads applied. The use of concrete in particular is due to its availability as well as the presence of in depth knowledge on how concrete behaves when subjected to different types of loads and forces. It is also due to vast studies made on the way concrete behaves with steel and the bonding capabilities of these two materials together. The sandwich panels were tested as different structural and non-structural elements that comprise the structure. The top view of CSP during fabrication for slab specimen is shown in Figure (2.7).

Figure (2.7): EVG 3D Panel Slab Speciment prior to Mortar application at UCI [11]

2.3. Material Characteristics

2.3.1. Insulator Core

The principle of sandwich structures is the separation of the skins, which carry the load by a low density core. [12] The process of separating the load carrying faces from the center increases the moment of inertia of the element with little increase in weight. Expanded polystyrene is used as the core of the sandwich panel and thus it is vital to describe its manufacturing process and properties. It is the foam core within the EPS panels that provides an insulated outer shell to buildings thus reducing the heating and cooling costs for the structure [13] .

The core selection is based on its mechanical properties, low cost, low density, resistance to fluctuations in temperature, resistance to moisture and chemicals, good formability and easy machinery [12]. EPS panels possess low Moisture Absorption: Moisture absorption rates decrease as density increases, but are still a minimal. Material thickness can increase moisture absorption performance. EPS foam demonstrates no chemical breakdown over time. It also possesses no nutrient value to living organisms and will not contaminate the surrounding environment. The foam core is often the weakest part of the sandwich panel and therefore in many ways governs the capacity and lifetime of the whole sandwich structure [14]. The modified Expanded PolyStyrene (EPS) core has a density of 0.9 lb/ft3 (*complying with ASTM Specifications C578-07a*)

The raw material used to manufacture EPS is virgin plastic beads with approximately 6% pentane. The pentane is used as a blowing agent for expansion. Virgin plastic can be

replaced by a recycled product. The first step is pre-expansion where the beads are placed in a hopper with steam injected at about 104 degrees ºC (220 ºF). The steam releases the pentane causing the beads to expand. The density of the foam is controlled by the steam exposure time which is directly proportional to bead expansion. This aging period varies from one to five days after which the beads are gravity-fed into a rectangular mold. Vacuum below the mold helps extract the steam while steam is continuously injected until a uniformly distributed pressure is achieved. The pressure-temperature combination releases the residual pentane from the beads causing them to fuse. The molding process is complete once the mold wall pressures are balanced. The foam blocks are then aged for three to five days to allow for expansion and contraction. Then finally hot wires are used to cut the blocks to the required dimensions and then the foam blocks are ready for transportation [15].

The small cell size and low volume fraction of solids in closed-celled foams makes them excellent insulators for building panels [14]. The purpose of thermal insulation is to help energy conservation and create comfortable living conditions. The heat resistive quality of Insulated Panels such as those with an EPS foam core have an R-Value that is 40% greater than the conventional framing and batt insulation of a like-sized wall. That increase in R-Value describes a relatively higher insulation for EPS sandwich panels than traditional walls. EPS can easily withstand temperature cycling in cold environments. The maximum use temperature is 167 F for continuous exposure, and 180 F for intermittent exposure. [16].

The thermal brake within each 3D panel is mainly modified EPS. In its standard core of EPS, a 60mm core with 40mm of concrete yields an R-11 rating whereas a 100mm core with 50mm concrete gives a highly efficient R-18 rating [2].

The presence of concrete surfaces on the interior and exterior of the structure separated by an EPS insulating core allows a thermal flywheel behavior to take place. When interior of the house is heated or cooled the wall system absorbs that heat or cool. When the temperature in the house changes the walls will begin emitting the retained heat or absorbing it as the case may be. The exterior skin behaves in the same manner by preventing the heat or cool to radiate inward. Their energy efficiency is maximized in warmer climates, especially those with large temperature differences between day and night [16]. The EPS core thickness used in the panels varies from 1.5 inches to 5 inches in thickness depending on the demands of the designer and the structural element for which it is used [17]. This allows for flexibility of dimensions when constructing walls, slabs, roofs or beams. As previously described, the increase in EPS thickness increases the thermal insulation of the panel as well as increasing the moment of inertia and the second moment of area of the load carrying element. That in turn increases the element's stiffness and the ability of the element to resist deflection due to flexure and rotation whilst still using the same amount of concrete or mortar along each face of the EPS core [12].

2.3.2. Steel Wire Mesh Grid Faces

When manufacturing the EPS foam panels, the wire mesh grid is most commonly formed by having a 2″ X 2″ (50mm X 50mm) grid from the centerline of each wire to the next in the same direction. The wire diameters used vary from gauge 14 steel up to gauge 9 and

they can be altered during the manufacturing process providing flexibility that meets the need of the design and structural element being produced. A typical steel wire mesh used in EPS panels that was tested at UCI by El Demerdash et al. can be seen in Figure (2.9). The steel reinforcement of the sandwich panel is in the form of three dimensional (3D) cold-rolled welded wire space trusses. Each mesh size at each face of the panel is 2″ in both longitudinal and transversal directions. However, only longitudinal steel wires take the bending load, therefore, one idea that is looked at in this study, is to have other steel mesh ratio between lateral and longitude mesh. For example, as seen in Figure (2.8) is to have 2:1 ratio between longitudinal and lateral steel wire grid. In the conventional panel tested by El Demerdash, the panels had 11 gauge with 0.09″ (2.31mm) diameter wire mesh fabric along on each side and the diagonal cross wire were made with 9-gauge wire with 0.11″ (2.91mm) diameter. The wire mesh fabric along with the 9-gauge diagonal cross [17]. By applying a cold rolling technique and annealing process to the 6mm original wire, the final product is 3.5 mm of steel wire. The stress-strain curve of the final product is demonstrated in Figure (2.11) [11].

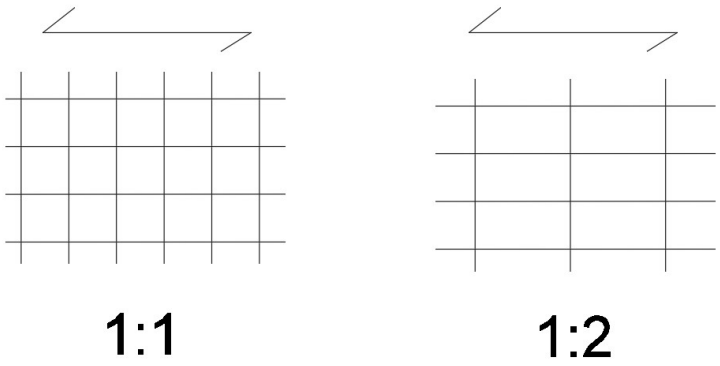

Figure (2.8): Different Grid ratio between Lateral and Longitudinal Steel wire Mesh

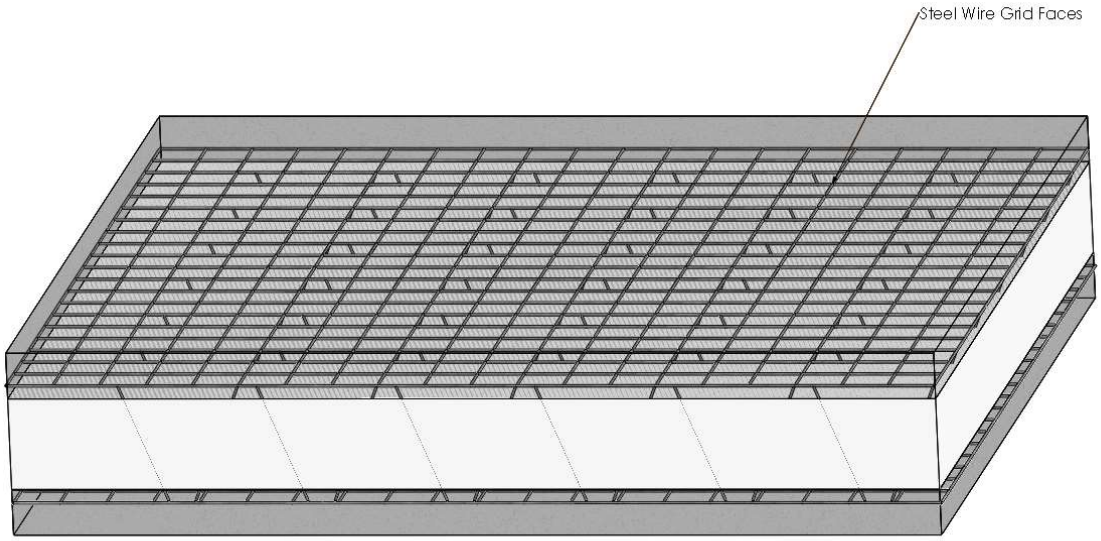

Figure (2.9): Conventional 1:1 Steel Wire Mesh Grid Face

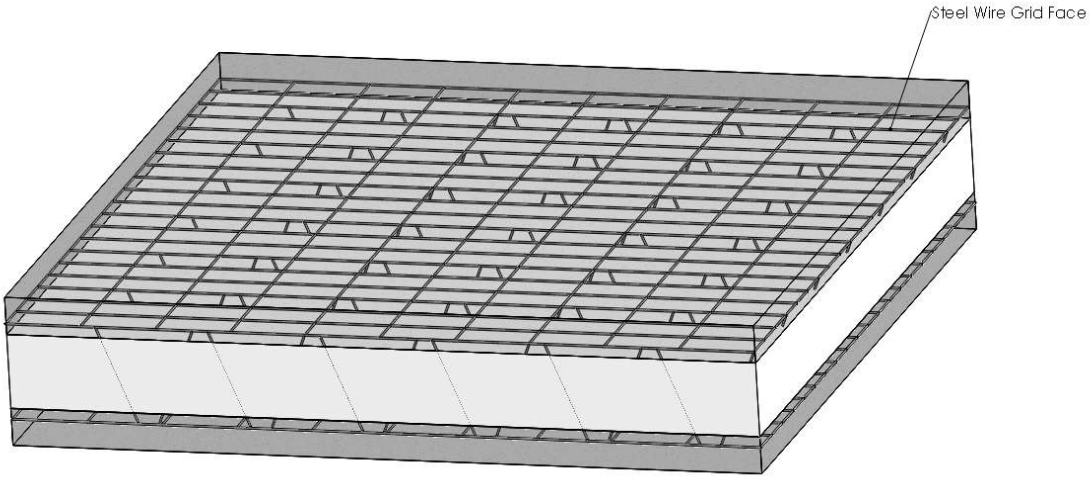

Figure (2.10): 2:1 Long. to Lat. Steel Wire Mesh Grid Face

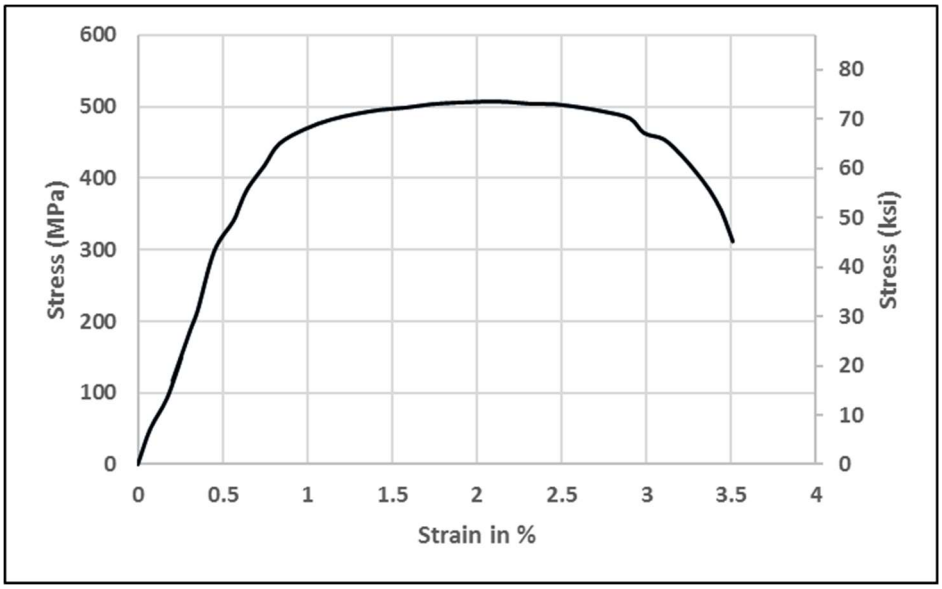

Figure (2.11): Stress and Strain Curve for Cold Wire Steel [11]

2.3.3. Shear Connectors

The transversal steel truss wires are also known as diagonal truss wires or shear connectors. They can come in various sizes or variable thickness during the manufacturing process depending on the required strength the element is required to withstand. The number of diagonal wires per square meter can also be altered and are determined on the basis of the shear strength required. In general, the diagonal wire diameters range from 2.3 – 3.67 mm (0.09″ – 0.14″). The number of diagonal wires may range from 50 – 200 per m^2 [2]. The wall panel receives its strength and rigidity from the diagonal cross wires welded to the welded-wire fabric on each side. This combination creates a truss behavior, which provides rigidity and shear terms for the full composite behavior [18]. The diagonal truss wires undergo shear deformation with the extent of the deformation being the governing factor that determines the degree of composite action.

According to study by Stine, to take full advantage of the strength of the two wythes and to prevent individual wythe buckling, the shear connectors should be designed to provide for full shear transfer between the two concrete wythes. [19] Wythes is another name for the relatively high strength faces on of sandwich panel.

In series of test performed by Kabir in 2005 [18] on performance of 3D panel under flexural loading, the effect of full composite vs. non-composite action was illustrated via Load-Displacement curve and compared to the results of the test as shown in Figure (2.12)

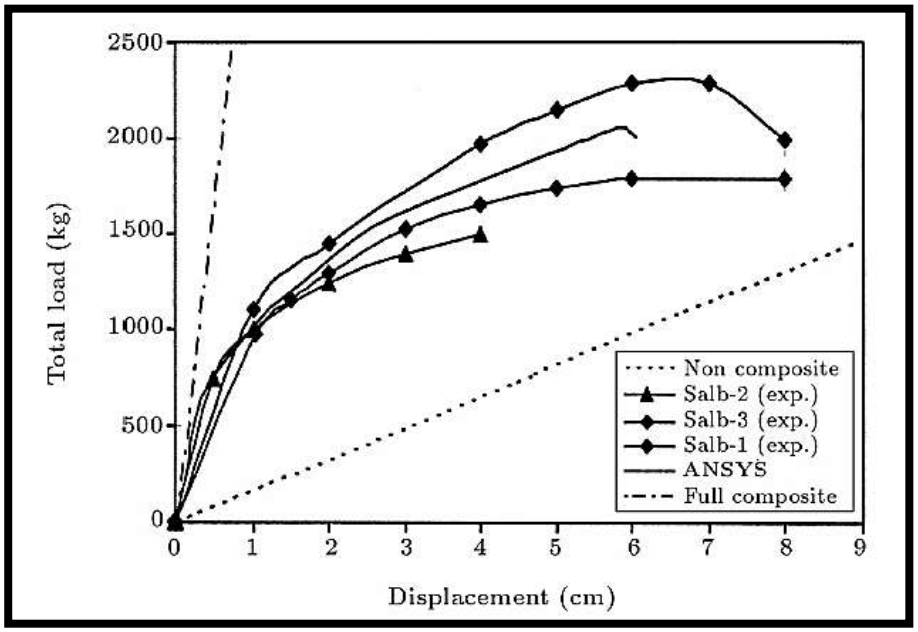

Figure (2.12) Load-Displacement Curves of Cementatious Sandwich Panel compared to their Potential Composite Action [18]

Two of commercially available cementitious sandwich panels' configurations are shown in Figure (2.13). In 2013 El Demerdash [11] did an extensive large scale experimental tests at UCI on CSP panel with Diagonal Shear Connectors as shown in Figure (2.13) (a) and in 2015 Botello [20] did similar tests on CSP with vertical shear connectors as shown in

Figure (2.13) (b). Results of studies reported by El Demerdash and Botello et al. on the flexural performance of CSP with both steel wire shear connectors configuration indicate that the performance of CSP is highly dependent on the number, the spacing, and the mechanical properties of the steel connectors which also contribute to the global strength of the panels. It was also shown that the both flexural strength and stiffness of these sandwich panels decreases as the angle between the connectors decreases [21].

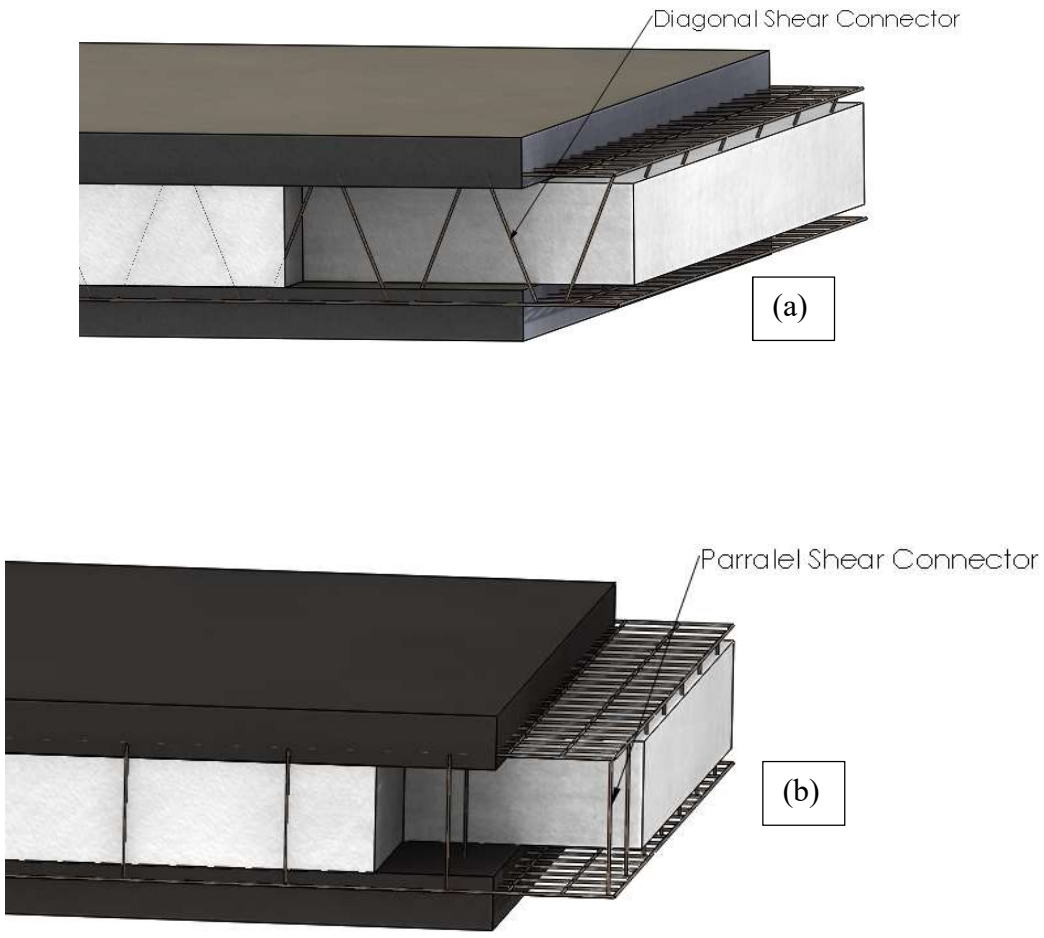

Figure (2.13): Two Common Types of Sandwich Building System: (a) Diagonal shear connectors, (b) Parallel shear connectors [11, 2].

On the other hand, the shear connectors, connecting the two faces of the CSP panels creates a local thermal bridge through the insulator core of CSP. The effect of local thermal bridges due to the truss wires of the CSP is dependent on the number and the cross section of them. As a result, there is a tradeoff between the stiffness and strength of CSP due to the shear connectors and thermal insulation capacity of the CSP. Considering that, thermal Insulation is one of main advantages of CSP vs. other structural elements, designing the optimum strength-to-weight and stiffness-to-weight ratios, which satisfies the highest composite action but in same time maximizing the thermal insulation capacity of the CSP is a vital to the benefits of CSP.

2.3.4. Wythe of CSP

As mentioned previously, the structure of sandwich panel consists of two layers of high strength panel herein called wythe and are separated by a lower strength core. The wythe are relatively thin while the core relatively thick and light in weight. The common materials used for wythe are steel, aluminum, wood, fiber reinforced plastic or mortar. In CSP mortar is applied on each face. hence the name CSP. The advantages of mortar for wythe of the sandwich panel vs other materials mentioned above, include: lower cost, availability, workability, relatively good thermal conductivity (k = 0.4 W/mk) and good average compression strength 20MPa (3ksi).

In study done by El Demedash 2015, two methods of mortar application were investigated. The mortar was hand applied on some specimens while others had the mortar applied pneumatically. The concrete or mortar mix is created using the traditional methods of concrete mixing by determining the desired compressive strength that the concrete should

achieve in the design then creating a mix that produces that strength in 28 days. Another factor that controls the mix at the beginning is the workability requirement for the workers mixing and applying the mortar or concrete to the faces of the CSP. The concrete has to be workable during the time of application and in both methods of application, however, when using the hand applied method the workability of the mortar is lower than that applied pneumatically. It is essential that when the mortar is applied pneumatically that it is very workable so it can flow freely through the pipes and opening of the nozzle [11]. That in turn should not affect the expected concrete strength of the different applied mortars as the comparison performed after testing is only between the method of application and not the mortar strength.

Pneumatically applied mortar is applied using what is commercially known as a Hopper Spray as shown in Figure (2.14). It is different from shotcrete as the velocity by which the mortar is pumped out of the Hopper Spray is much lower and with less volume than that of shotcrete. Shotcrete is a form of application of almost any type of aggregate and binder like sand, cement and water. It is performed using shotcrete equipment which consists of a compressor, mixer, cement gun, nozzles, miscellaneous hoses and on occasion a pressure pump. The cement gun is the equipment which releases the materials from the nozzle onto the surface required at high velocity. The pneumatically applied method is also known as low velocity shotcrete. Figure (2.14) shows application of mortar on wall using hopper spray.

Figure (2.14): Pneumatically Application of Mortar on CSP using Hopper Spray

2.4. Cost Optimization of Concrete Structures

A great majority of structural optimization papers deal with minimization of the weight of a structure (Vanderplaats 1984; Arora 1989; Adeli and Kamal 1993; Adeli 1994; to mention a few). Though weight of a structure constitutes a significant part of the cost, minimization of the cost is the final objective for optimum use of available resources. In cost minimization, however, additional difficulties are encountered. These difficulties include definition of the cost function and uncertainties and fuzziness involved in determining the cost parameters. As a result, only a small fraction of the structural optimization papers published deal with minimization of the cost.

Most of the papers published on cost optimization of concrete structures are about beams or girders. The general cost function for reinforced, fiber, or prestressed concrete beams can be expressed in the following form:

$$C_m = C_{cb} + C_{sb} + C_{pb} + C_{fb} + C_{sbv} + C_{fib} \quad \text{Eq. 1}$$

where C_m = total material cost; C_{cb} = cost of concrete in the beam; C_{sb} = cost of reinforcing steel; C_{pb} = cost of prestressing steel; C_{fb} = cost of the formwork; C_{sbv} =: cost of shear steel; and C_{lib} =: cost of fiber in the concrete. This is a general equation can be reduced for special cases. For example, in case of sandwich panel, cost of prestressing steel, cost of fiber in concrete can be set to zero.

Goble and Lapay [22] minimize the cost of posttensioned prestressed concrete T-section beams based on the ACI code by using the gradient projection method (Arora [23]). The cost function includes the first four terms in Eq (1) They state that the optimum design seems to be unaffected by changes in the cost coefficients. But this conclusion is rebutted by subsequent researchers. Kirsch [24] presents minimum cost design of continuous two-span prestressed concrete beams subjected to constraints on the stresses, prestressing force, and the vertical coordinates of the tendon by linearizing the nonlinear optimization problem approximately and solving the reduced linear problem by the linear programming (LP) method. His cost function includes only the first and third terms in Eq (1). Friel [25] finds closed-form solutions for optimum ratio of steel to concrete for minimum-cost, simply-supported rectangular RC beams using the ultimate moment constraints of the ACI code. The cost function is similar to Eq (1) but neglects the costs of prestressing steel (C_{pb}) and fiber (C_{lib}) and adds an additional term for increasing the cost due to an increase in the

building height. The author concludes that the costs of the formwork and the increase in the height do not influence the optimum cost significantly.

Brown [26] presents an iterative method for minimum cost selection of the thickness of simply supported uniformly-loaded one-way slabs using only the flexural constraints of the ACI code. The cost function includes only the first two terms in Eq (1). The author reports cost savings of up to 17%.

Naaman [27] compares minimum cost designs with minimum weight designs for simply-supported prestressed rectangular beams and one-way slabs based on the ACI code. The cost function includes the first, third, and fourth terms in Eq (1) and is optimized by a direct search technique. The writer concludes that the minimum weight and minimum cost solutions give approximately similar results only when the ratio of cost of concrete per cubic yard to the cost of steel per pound is more than 60. Otherwise, the minimum cost approach yields a more economical solution, and, for ratios much smaller than 60, the cost optimization approach yields substantially more economical solutions. The writer also points out that, for most projects in the United States, the aforementioned ratio is less than 60. Considering that it is the first time that an optimization process is used for optimization CSP, a new methodology based on previous works on similar structures needs to be used. In previous studies by Lemonge et al. [28] an optimization process is applied to the structural configuration considering weight minimization of a space truss structure (consisting of standard modules that includes a steel truss roof), presenting both continuous design variables, such as the coordinates of the nodes, as well discrete variables, such as the cross-sectional areas of the bars, which are to be chosen from commercially available sizes.

CHAPTER 3

DESIGN OPTIMIZATION OF CEMENTATIOUS SANDWICH PANEL (CSP) USING NUMERICAL MODELING

3.1. General

Design optimization refers to the process of attempting to arrive at certain ideal design parameters, which, when used within the model, satisfy prescribed conditions regarding the performance of the design and at the same time minimize (or maximize) a measurable aspect of the design. The main structural materials in CSP are the mortar and steel, which their mass densities and unit costs are taken into account in the computation of the objective function.

The performance requirements of the optimum design might not necessarily have to be limited to the response of the structure under the load, but also to different concepts such as packaging, design envelope, or even maintenance. However, the current scope of this research is based on the optimization of the design variables while the response of structure is controlled within ACI recommended constraints.

The goal of the optimization is to obtain the highest strength to weight ratio while maximizing thermal resistance of the CSP. The optimization model is based on a simply supported sandwich panel subjected to out of plane loading with fixed thickness where the deflection (response) will directly reflect the strength of the sandwich panel. However, the same methodology can be used for all loading conditions, such as seismic, blast etc.

Considering that it is the first time that an optimization process is used for optimizating Cementatious Sandwich Panel (CSP), a new methodology based on previous works on similar structures is used. In previous studies by Lemonge et al. [28] an optimization process is applied to the structural configuration considering weight minimization of a space truss structure (consisting of standard modules that includes a steel truss roof), presenting both continuous design variables, such as the coordinates of the nodes, as well discrete variables, such as the cross-sectional areas of the bars, which are to be chosen from commercially available sizes. Similarly, in this optimization process, first a base design is chosen from available commercial design of CSP. In 2013, an extensive study was done in UCI SETH lab, by El Demerdash [11] on CSPs designed by EVG. That design of CSP is chosen as base model for CSP optimization in this study. However, the different element used in the design CSP is set as a design variable which are explained in the next section.

3.2. Design Variable

Due to the fact that the number of degrees of freedom in the design of cementitious sandwich panel is large, this study designates a specific design area as boundary condition. A 1m X 1m X 14cm (40″ X 40″ X 5.5″) (*L X W X D)* where D is the distance between top and bottom steel mesh. The thickness of the foam is also set to be constant 10cm (4″). This boundary condition is used similar to design of commercially available CSP studied by El Demerdash in 2013 at UCI SETH lab [11]. XX shows the cross section defined to be used in this optimization analysis. Next, a series of design variables are introduced for CSP topology optimization including: shear connectors cross section and configuration, number

of bays, number of modules, steel mesh cross section and configuration, cementitious face thickness on top and bottom of CSP, etc. Table (3.1) lists these variables for the optimization process indicating the discrete possible options.

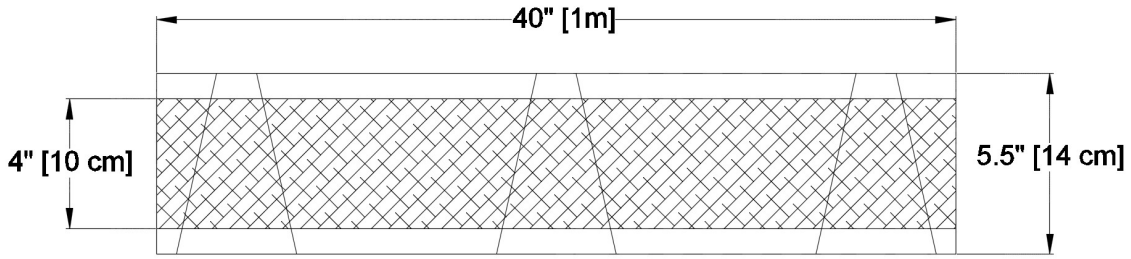

Figure (3.1): Boundary Condition of CSP

Although certain design variables are continuous, in order to reach an optimized design which is both mathematically but also practically feasible, a set of discrete options based on American Wire Gauge (AWG) wire sizes is chosen for steel wire options. (See

Table (**3.2**)). The other parameters in the design of the CSP panel are dependent upon design parameters Table (3.1) and geometry of the specified CSP to be optimized (i.e. foam core thickness, angle of shear connector, etc.).

Figure (3.4) shows the topography of possible designs based on the number of bays and modules listed in Table (3.1). The topography of shear connectors is based on a rectangular distribution except the 3rd row which is based on the star shape distribution that will be studied in the optimization process.

Table (3.1): List of Design variables for optimization of CSP.

Parameter	Unit	Level 1	Level 2	Level 3
Bays / 1.0 m [39.3″] Length	[#]	3	4	5
Modules / 1.0 m [39.3″] Width	[#]	6	8	10
Diam. of Shear Connector	cm [inch]	0.23 [0.09″]	0.27 [0.11″]	0.35 [0.14″]
Diam. of Steel Mesh (Top)	cm [inch]	0.23 [0.09″]	0.27 [0.11″]	0.35 [0.14″]
Diam. of Steel Mesh (Bottom)	cm [inch]	0.23 [0.09″]	0.27 [0.11″]	0.35 [0.14″]
Mortar Thickness (Top)	cm [inch]	2.5 [1.0″]	5.0 [2.0″]	7.5 [3.0″]
Mortar Thickness (Bottom)	cm [inch]	2.5 [1.0″]	5.0 [2.0″]	7.5 [3.0″]
Steel Mesh Ratio	[Ratio]	1:1	1:2	1:4

Table (3.2): AWG wire sizes

AWG Gauge#	Diameter [in]	Diameter [mm]	Area [in^2]	Area [mm^2]
7	0.14	3.67	0.016	10.54
9	0.11	2.91	0.010	6.63
11	0.09	2.31	0.006	4.17

The Figure (3.2) and Figure (3.3) show two possible solutions for the configuration of CSP. Each module is made up of two face sheets, meshes, and shear connectors connecting two faces. In the Figure (3.2) and Figure (3.3) distinct structural solutions are shown for the same area of CSP: Figure (3.2) presents three regular modules whereas the second one, Figure (3.3), five modules. The first solution uses a greater number of modules, probably with ″thinner″ cross-sectional areas, whereas the second solution uses a smaller number of modules, probably with ″thicker″ cross-sectional areas, different number of bays between the CSP panels can be observed in the Figure (3.2) and Figure **(3.3**).

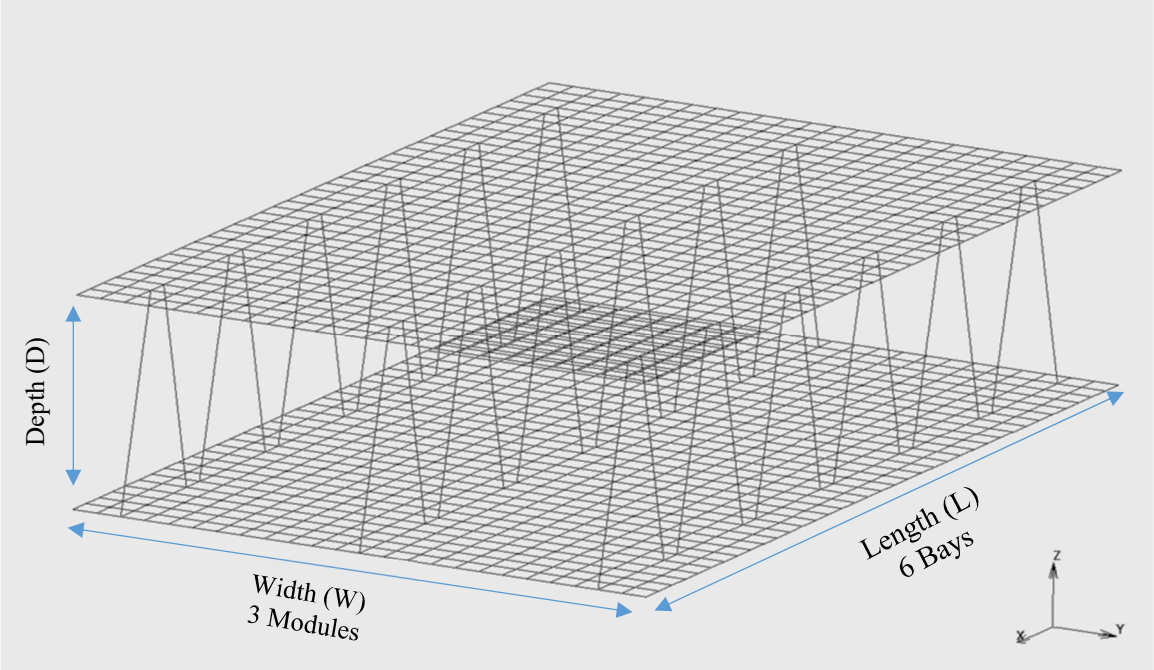

Figure (3.2): Design option for structural configuration of CSP, 3 modules with 6 bays

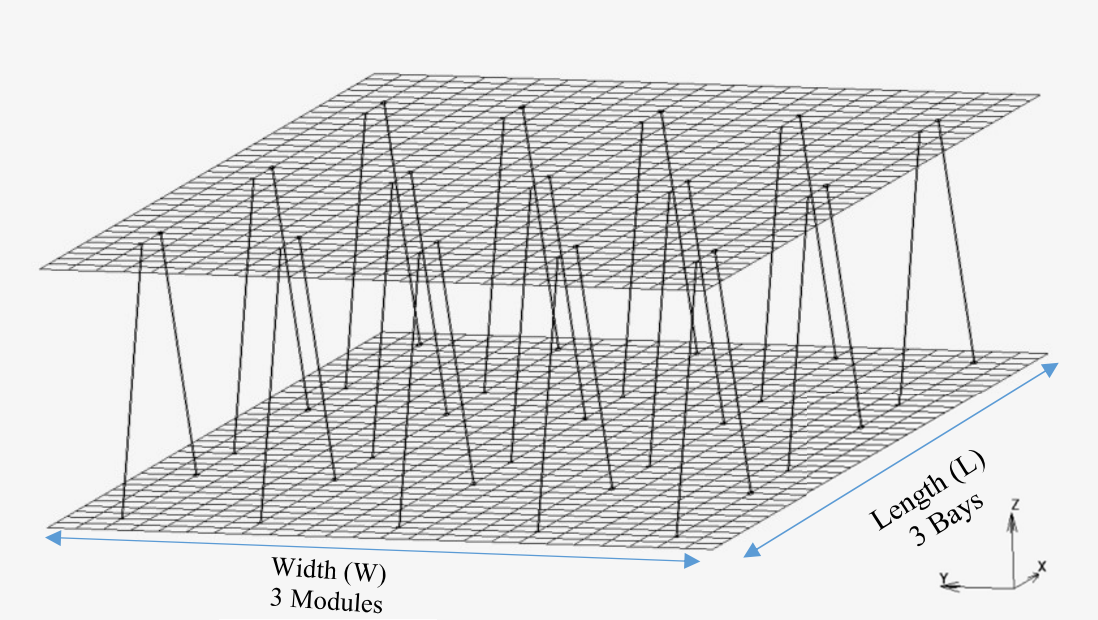

Figure (3.3): Design option for structural configuration of CSP, 5 modules with 3 bays

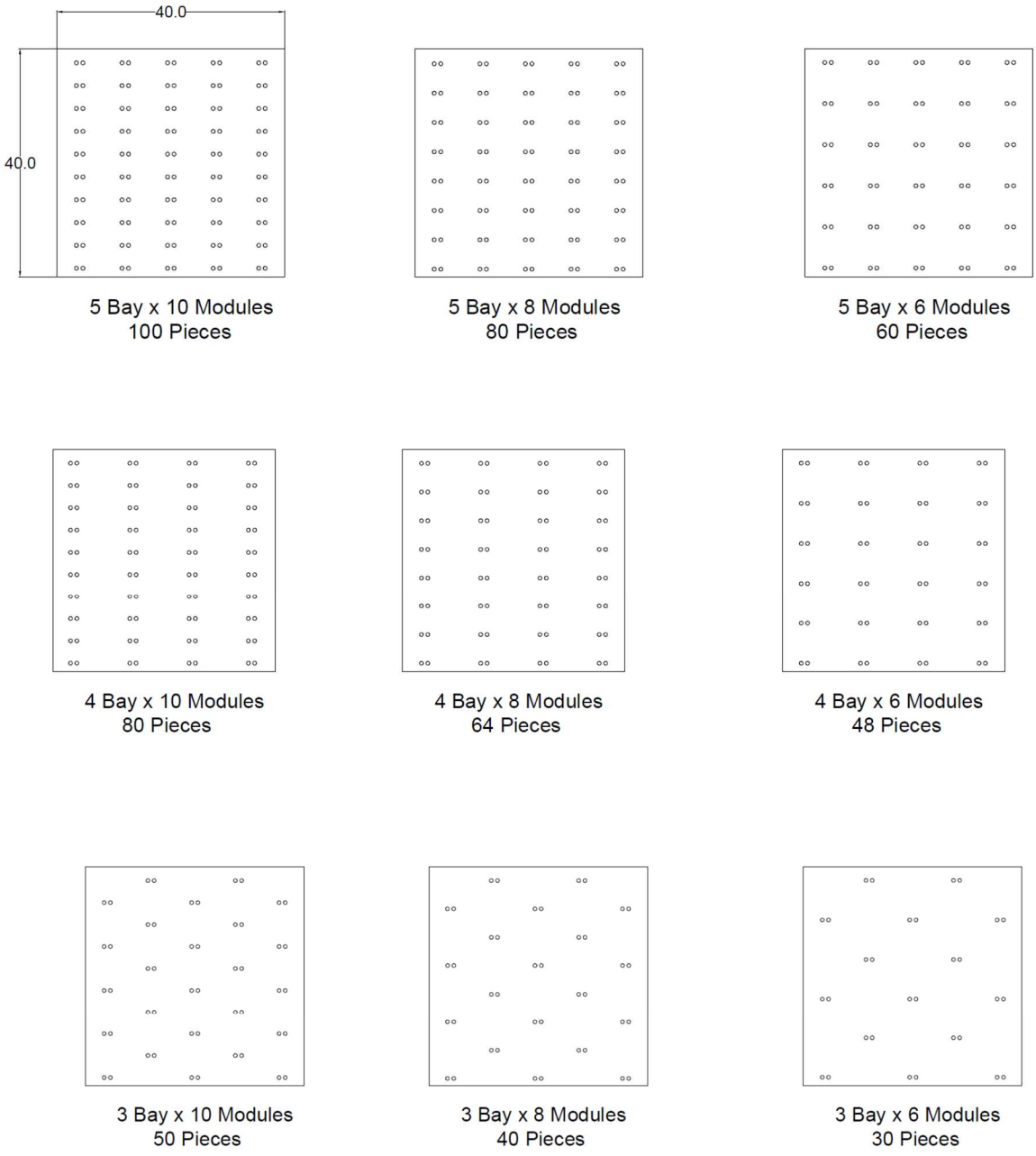

Figure (3.4): Top view of CSP Topography Configuration options for shear connectors.

3.3. Design Constraints

Along with material properties, in order to control the optimization process, design constraints are introduced. For example, when CSP panel is used as slab for residential buildings, based on ACI code 24.2.2, the immediate deflection due to the live load for flat roofs and floors should be less than L/360, where L is the clear span of the floor. Therefore, this an upper limit for the nodal displacement of panel, which is defined by:

$$\frac{u_j}{u_{max}} - 1 \leq 0 \qquad \forall j = 1, 2, \dots, n \qquad \text{Eq. (2)}$$

Where u_{max} is equal to L/360 based on ACI code 24.2.2, for displacement in direction of the load.

In optimization using finite element analysis, the constraints can be imposed on strain, stress and displacement in response quantities. For stresses and strains, the constraints are defined as being on the elements, and for displacements, the constraints are defined as being at nodes. Stress and strain components, as well as various functions of these components (the von Mises equivalent stress and principal stresses, stresses on prescribed planes) and generalized stress quantities can be constrained. Similarly, translation and rotation components of displacement, resultant and directed displacements as well as relative displacements between nodes can be constrained.

3.4. Objective Function

In order to optimize the design of the CSP two different objective function are defined. One objective function is set to minimize the Cost of Material while maintain the Constrains.

As mentioned previously, since this optimization includes more than one material (Mortar and Steel) in the model, the specification of different mass densities and unit costs are taken into account in the computation of the objective function.

The *total cost* is derived from two factors of *cost of material* and *cost of energy*, each of these factors independently as in some situations the industry may have specific goals in mind for which they may decide to define total cost differently. This study therefore provides a guideline of how to achieve optimum result depending on different needs of the industry.

In this study, the objective of this optimization is set to minimize the **total cost** of the panel which can be written as:

$$f(x_1) = \underbrace{C_s\left(\frac{W_s}{W_{sb}}\right)^2 + C_m\left(\frac{W_m}{W_{mb}}\right)^2}_{\text{Cost of Material}} + \underbrace{\alpha\left(\frac{R_{tb}}{R_b}\right)^2}_{\text{Cost of Energy}} + \underbrace{\beta\left[\left(\frac{|u_{FEA}|}{u_{max}} - 1\right)^+\right]}_{\text{Constraint}} \qquad \text{Eq. (3)}$$

Where:

f(x) is the objective function to minimize the *Total Cost* of the panel;

C_s is the weight factor for Steel;

W_s is total weight of steel in proposed design of CSP;

W_{sb} is a constant value based on the total weight of steel in the base model CSP;

C_m is weight factor for Mortar;

W_m is total weight of concrete in proposed design of CSP;

W_{mb} is a constant value based on the total weight of mortar in the base model CSP;

α is a weight factor for Cost of Energy which depends on the specific location weather data and unit price of energy and life span of the building;

R_t is the equivalent Thermal Resistance of proposed CSP;

R_{tb} is the equivalent Thermal Resistance of Base CSP;

β is the constant penalty factor set to 100 for all experiment. This value is subjective to the goals of the optimization.

u_{FEA} is the maximum deflection of proposed CSP in each finite element analysis run.

u_{max} is the maximum deflection allowed per ACI code 24.2.2 and $[x]^+ = x$ if $x > 0$ and $[x]^+ = 0$ otherwise.

3.4.1. Cost of Material

Weight of steel and Mortar can be calculated using the following equations:

$$W_s = \sum_{i=1}^{n} \rho_s A_i L_i \qquad \text{Eq. (4)}$$

Where ρ_s is the density of the steel; L_i and A_i is the length and Area of the *i-th* bar of shear connectors and steel meshes on each face.

$$W_m = \rho_m (t_b + t_t) \times A \qquad \text{Eq. (5)}$$

Where, ρ_m is the density of the Mortar on each face; t_b and t_t are the thickness of cementitious faces on bottom and top of the panel; and A is the CSP Area.

To evaluate the weight factor steel, the approximate unit price of Steel is used. The unit price of steel in wholesale store of M&K Co in USA[1] in the current time (2016) is about \$0.79 for 12ft (3.65m) cold rolled steel diameter 1/8″ (3.175mm) that is equivalent to number 8 steel wire gauge. Density of Cold rolled steel is considered to be: 7850kg/m^3 (0.284 lb/in^3). As a result, the unit price of steel in this study is set to 3.4 Dollar per kg (21.5 Dollar per lb) which is used for evaluation of weight factor for steel in the composite objective function for Multi-objective optimization of this study.

Approximate unit price of ready mix Mortar for this study is taken from Mortar supplier in USA CEMEX[2] for Mortar mix ready for shotcrete as approximately between \$90 to \$100 per cubic yard for Mortar for shotcrete with compression strength of f'_c = 3ksi (20MPa). Density of Mortar is assumed as 0.087lb/in^3 (2400 kg/m^3). As a result, the unit price of Mortar in this study is approximated as 0.055 Dollar per kg (0.025 Dollar per lb) to be used for evaluation of weight factor for Mortar in the composite objective function for the Multi-objective optimization of this study.

However, it should be mentioned that what is important in this study is the ratio of price of steel to price of Mortar not the actual value of steel and Mortar. $C_s/C_c = 60$. In the research by Naaman [27] in optimization of reinforced concrete slab, points out similar ratio for cost of concrete to the cost of steel per pound for most projects in United States is about 60. Also here, the price is just meant to be used as a weight factor for optimization function and the absolute value of objective function does not evaluate the actual cost of the CSP.

---

[1] http://www.mkmetal.net/
[2] http://www.cemexusa.com/

3.4.2. Cost of Energy

One of the key features of sandwich panels is their insulation capabilities. Therefore, it is vital to look at the insulation performance of the CSP when studying the optimization these panels. Most importantly since there is a huge trade off analysis required due to thermal bridging phenomena happening in the CSP panels. The metal shear connectors connecting the two Cementatious layers of the panel creates thermal bridge across the wall and reduces the thermal insulation of the panel. According Oxford Dictionary of Construction, Surveying, ″A thermal bridge, also called a cold bridge or heat bridge, is an area of an object (frequently a building) which has a significantly higher heat transfer than the surrounding materials resulting in an overall reduction in thermal insulation of the object or building″. [29]

Common thermal properties of materials and air spaces are based on steady state tests, which measure the heat that passes from the warm side to the cool side of the test specimen. Thermal resistance is a heat property and a measurement of a temperature difference by which an object or material resists a heat flow. Thermal resistance is the reciprocal of thermal conductance. Daily temperature swings and heat storage effects are accounted for in thermal mass calculations.

The SI units of thermal resistance are kelvins per watt or the equivalent degrees Celsius per watt (the two are the same since the intervals are equal: $\Delta 1\ \mathrm{K} = \Delta 1\ ^{\circ}\mathrm{C}$). In another word, thermal resistance is the temperature difference across a structure when a unit of heat energy flows through it in a unit time.

In order to evaluate the thermal resistance of the sandwich panel, the heat flow can be modelled by analogy to an electrical circuit where heat flow is represented by current, temperatures are represented by voltages, heat sources are represented by constant current sources, absolute thermal resistances are represented by resistors and thermal capacitances by capacitors. If the layers of insulator are on top of each other, they insulator can be modeled in series and their resistance value of the individual insulators will be added together.

However, when the insulators are in parallel to each other, the reciprocal (1/R) value of the individual insulators will be added together. In Cementatious Sandwich Panel however, we have the combinations of series and parallel insulators in the system. Figure (3.5) shows the diagram for an equivalent thermal circuit for a CSP as a combination of cementations skin, insulator core and steel thermal bridges.

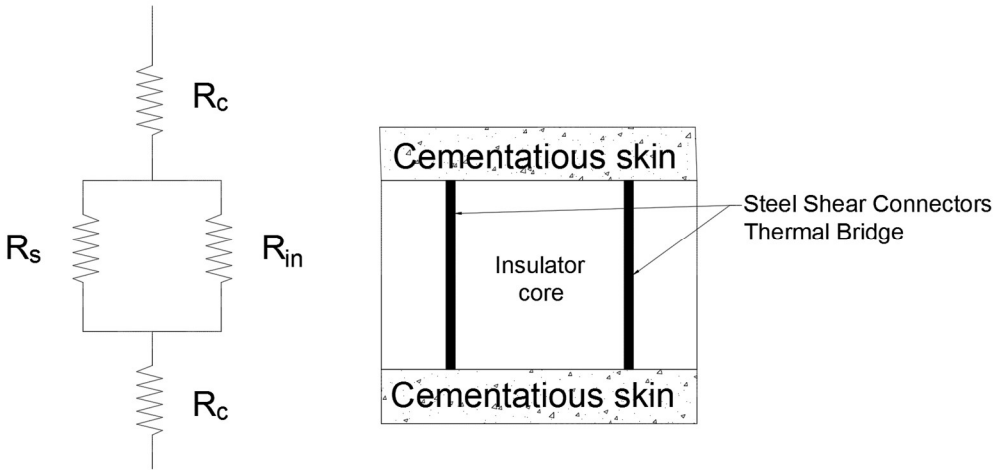

Figure (3.5): The diagram shows an equivalent thermal circuit for a CSP

Equation Eq. (6) shows the parametric formulator to evaluate the Thermal resistance of the CSP based on the diagram illustrated in Figure (3.5).

$$R_t = 2R_C + \frac{(R_{in} \times R_s)}{(R_{in} + R_{in})} \quad \text{Eq. (6)}$$

Where R is the thermal resistance of the material in kelvin per Watt [K/W] and R_c, R_s and R_{in} are the Thermal resistances of Mortar, steel and insulator in order. The thermal resistance of the material. It should be noted that thermal resistance is not a directly a material property, as its depends on the geometry of the material and it is derived from Fourier's Law for heat conduction, the following equation can be derived, and is valid as long as all of the parameters (x and k) are constant throughout the sample.

$$R = {}^{x}/_{(A \times k)} \quad \text{Eq. (7)}$$

where:

R is the absolute thermal resistance (across the length of the material) [K/W]

x is the thickness of the material (measured on a path parallel to the heat flow) [m]

k is the thermal conductivity of the material [W/(K·m)]

A is the cross-sectional area (perpendicular to the path of heat flow) [m^2]

Next following the Equation used by Qomi et al. [30] developed for calculating Energy required to keep certain level of temperature, can be used in this study to calculate the energy loss due to heat loss while maintaining a temperature in the building at base temperature.

$$E = \frac{T_o - T_{out}}{R_{eff}} \times S \times t \quad \text{Eq. (8)}$$

Where: S [m^2] is the surface area of the building E [W.hr] is the heating or cooling energy required to maintain inside temperature of T_o [K] when the outside temperature is T_{out} [K] during the interval exposure, t [hr] and R_{eff} [m^2 K/ W] is the effective thermal resistance of the building material.

In order to evaluate the fluctuation of outside temperature base on the temperature inside the building for any location, Degree-days data can be used. Degree days are a specialist type of weather data, calculated from readings of outside air temperature. Heating degree-days and cooling degree days are used extensively in calculations relating to building energy consumption. There are two types of Degree-day data useful for calculating energy loss in the buildings. Heating Degree Days (HDD) and Cooling Degree Days (CDD). Heating Degree Days are a measure of how much (in degrees), and for how long (in days), the outside air temperature was below a certain level. They are commonly used in calculations relating to the energy consumption required to heat buildings. On the other hand, Cooling Degree Days are a measure of how much (in degrees), and for how long (in days), the outside air temperature was above a certain level. They are commonly used in calculations relating to the energy consumption required to cool buildings. These two data can be added together throughout the year to calculate how much energy is required to maintain the inside temperature (base temperature) of the buildings. At their website[3], there is a database for collecting Degree-day data for different weather stations around the world.

[3] http://www.degreedays.net/

In order to have a reliable data for calculating the Energy loss due through the CSP, a location around the world is selected. Dubai in United Arab Emirates. This is an example of hot city where an air conditioning is required to maintain the inside temperature of the buildings and therefore insulation is important factor in designing the building. Using the Degree day database, a set of Cooling Degree-day data is collected for the past years while setting the base temperature at 20 ^{o}C (68 ^{o}F).

By inserting the Degree-day for one year data as [$\Delta T.t$] in Eq. (8), setting [t = 24hr/day] to convert Degree-Day data to Degree-Hour, [S = 1m^2]; [E] Energy loss through any CSP with its effective Thermal Capacity [R_{eff}] can be calculated for one year. This data would be useful to compare the cost of Material to Cost of Energy at the end of optimization process. As note, we see that Cost of Energy is linearly changes with respect to Degree-Day unit of different locations around the world.

Using the unit price identified for Steel, Mortar and equation for cost of energy and degree-day data for Irvine, CA, the total cost of the base panel is estimated in the Table (3.3). Next a contribution factor for each parameter is identified and normalized to be used as weight factor in this study.

Table (3.3): Estimation of Weight Factors to be used in this Study

Parameter	Steel	Mortar	Heat Loss*	Total
Cost in Base Model	\$11.88	\$12.18	\$2.59	\$26.65
Normalized Contribution Factor	0.42	0.43	0.15	1

***Calculated for Irvine, CA for 10 Years Period**

3.5. Sensitivity Analysis using Tagushi Method

The traditional approach of developing an efficient design of an existing structural element using FEM involves several runs for different models. For each model, the existing and the improved case are compared until a satisfactory design is obtained. This approach may require a large number of iteration cycles including modification to the new model, analysis, and comparison to the previous ones. The number of iterations depends mainly on the knowledge level of the engineer and the complexity of the FE model, especially when the number of design variables is large. In addition, when a satisfactory model is obtained, the possibility of better improvement will still be questionable if slight modifications are introduced. This is due to the lack of independent evaluation of each contributing design parameter.

In the design of CSP panel there are 8 design variables with 3 different options for parametric optimization equals to $3^8 = 6561$ different design to be analysed. Alternatively, using the Taguchi method, a reduced set of models can be used for the optimization process, and simultaneously the individual effect of each parameter can be analyzed using the Taguchi orthogonal matrix. Trends in the performance index are then observed and quantitatively analyzed to construct some meaningful conclusions regarding the design factors. Proposed steps of using the proposed Taguchi method for optimization of CSP is shown in form flow chart in Figure (3.6).

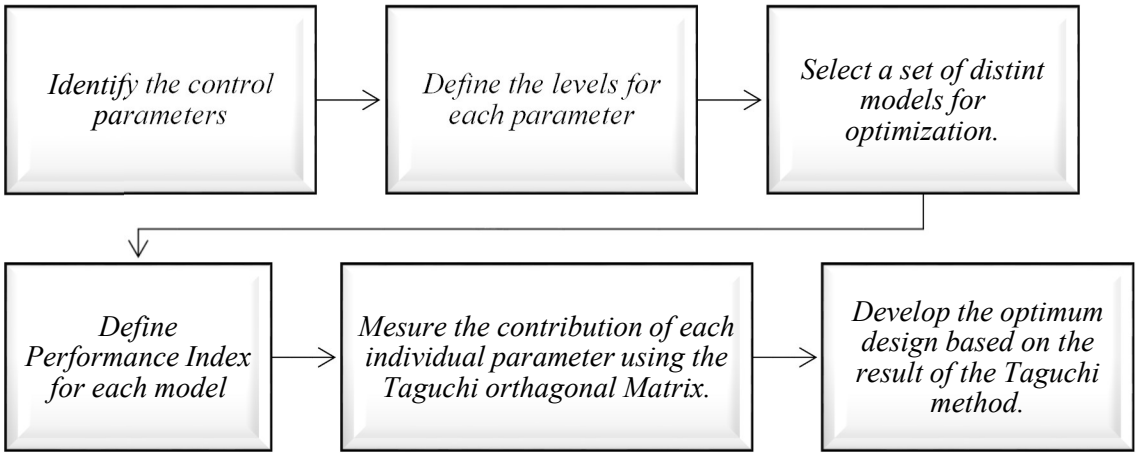

Figure (3.6): Optimization Flowchart Using the Taguchi Method

3.5.1. Identifying Control Parameters

In this optimization problem, the variables affecting the performance of the product is already identified in Table (3.4). Accordingly a table of design factors based on the design variables are identified as Table (3.4) for this optimization process.

Table (3.4): Design Factors for Taguchi Analysis

Factor	Parameter	Unit	Level 1	Level 2	Level 3
A	Bays / 1.0 m [39.3″] Length	[#]	3	4	5
B	Modules / 1.0 m [39.3″] Width	[#]	6	8	10
C	Diam. of Shear Connector	cm [inch]	0.23 [0.09″]	0.27 [0.11″]	0.35 [0.14″]
D	Diam. of Steel Mesh (Top)	cm [inch]	0.23 [0.09″]	0.27 [0.11″]	0.35 [0.14″]
E	Diam. of Steel Mesh (Bottom)	cm [inch]	0.23 [0.09″]	0.27 [0.11″]	0.35 [0.14″]
F	Mortar Thickness (Top)	cm [inch]	2.5 [1.0]″	5.0 [2.0″]	7.5 [3.0″]
G	Mortar Thickness (Bottom)	cm [inch]	2.5 [1.0]″	5.0 [2.0″]	7.5 [3.0″]
H	Steel Mesh Ratio	[Ratio]	1:1	1:2	1:4

3.5.2. Optimization Bracket

Based on the previous studies which used Tagushi method for optimization of structures by Mosallam et al [31] random sample set of a 10 models are selected from the possible solutions using the design factors. Each sample based on its design combination is modeled using FEM in MENTAT and analyzed using MARC based on the model described in Chapter 3. Table (3.5) summarizes these 10 samples with the orthogonal design parameter matrix. The columns of this matrix represent the design parameters, while the rows represent different combinations of test settings. In the last column the objective function is calculated for each combination based on Eq. (3).

Table (3.5): Orthogonal Matrix for Taguchi Optimization

Sample Number	Factor Levels								f(x)
	A	B	C	D	E	F	G	H	
1	1	3	3	2	2	1	3	2	4.4
2	1	3	3	2	2	1	3	1	5.3
3	3	2	3	2	1	2	2	2	6.5
4	1	2	1	1	1	3	3	3	2.0
5	1	1	1	1	1	1	1	3	28.4
6	1	1	1	2	3	2	1	1	4.5
7	1	1	3	3	3	1	1	1	7.0
8	2	3	2	1	1	1	1	1	4.4
9	1	1	1	2	1	3	2	2	2.4
10	3	1	3	3	2	3	1	1	8.8

Figure (3.7) shows the standard boundary condition used for each model following the procedure explained in the previous chapter that is used in the optimization process. It is pin-pin boundary condition on each end. In this model, the load is applied using the Master node which reads the Max displacement of the panel in the same time at the of the analysis.

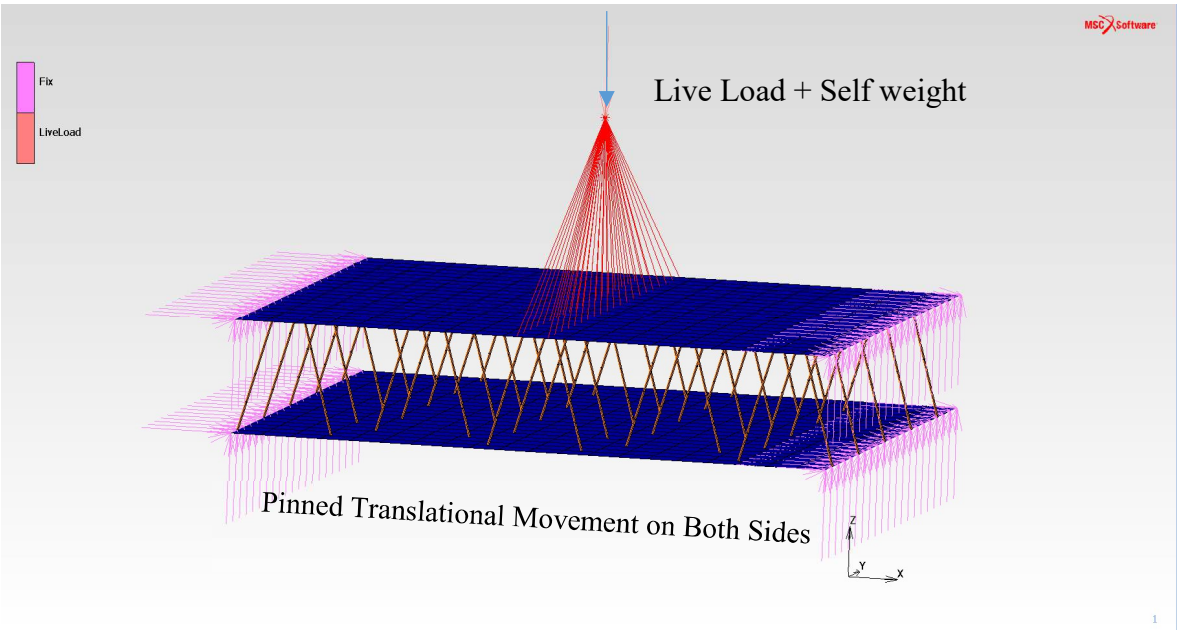

Figure (3.7): Standard Boundary condition used for Optimation models.

Figure (3.8) shows the Load vs displacement of all 10 models used in Tagushi method. The stress applied on each model is normalized by the 100 psf live load plus the self-weight of each model. The result of displacement is normalized by the limit defined by the ACI code for deflection under the live load. This way, it is easy to see, for example model 5 did not pass the deflection control of ACI, therefore it is penalized and the objective function has increases dramatically as seen in the 5th row of Table (3.5).

Numerically combining the contribution of each individual factor for all the CSP configurations listed in Table (3.5), effect of each factor on the objective function is obtained. This is achieved by averaging the Level 1 contributions for each connector separate from Level 2 and Level 3 contributions using Eq. (4).

$$\text{Contribution of each factor} = \sum_{k=0}^{n} \alpha_k / n \qquad \text{Eq. (9)}$$

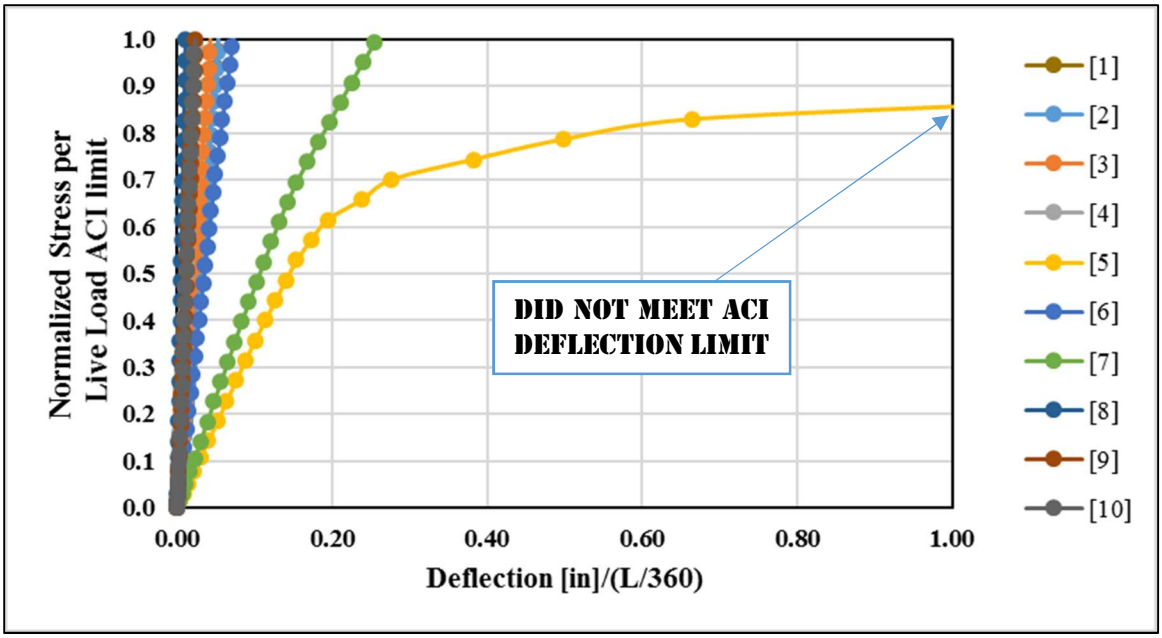

Figure (3.8): Normalized Stress vs. Normalized Deflection by ACI Code Limit

Where α_k is each of the contributing factors and n is the number of levels defined for that factor. The result is listed in Table (3.6). The last row, indicated the optimized design which is obtained by level of factors that minimizes the cost function while meeting the design constraints.

Table (3.6): Contribution Factor to Cost function

	A	B	C	D	E	F	G	H
Level 1	-0.03	0.19	0.75	-0.15	0.50	-0.09	0.22	-0.33
Level 2	0.00	0.00	0.00	0.00	0.00	0.00	0.00	0.00
Level 3	0.42	0.08	0.31	0.42	-0.07	-0.20	-0.10	0.56

This data gives a clear indication of the relative effect each design factor has on the overall cost of the CSP. For a clearer presentation of the contribution factor results, Figure (3.9) is obtained by normalizing the contribution factors based on the minimum factor level

contribution for each factor, as shown in the last row of Table (3.6) and shifting the Level 2 to zero for the 8 design factors.

These charts can be used as sensitivity analysis of the design parameters to the cost of CSP panel. The data is interpreted by noting that a decreasing slope indicates a reduction in cost, and that the higher the magnitude of the slope the more significant the effect on the design. By observing the trends of the curves in Figure (3.9) the designer can see how and in what degree each factor affect the cost function of the optimization process.

3.5.3. Discussion on the Results

By observing the trends of the curves in the charts of Figure (3.9) and contribution factors in Table (3.6) the following conclusions can be made:

1. Increasing Number of Bay [A] and Number of Modulus [B] in connecting the two faces of sandwich panel from Level 1 to Level 2 will decrease objective function, by making the panel stiff enough so it does not violate the ACI requirements. However, increasing them further will result to an overdesigned panel where the objective functions has been increased due to cost of Material and thermal bridging caused by the extra shear connectors.
2. Thickness of shear connectors [C] have similar effect on the objective function of the CSP as factor [A] and [B].
3. Increasing the area of steel mesh on top [D] will increase the objective function, meaning the cost. This is true because still is an expensive and not efficient material to be used for compression side.

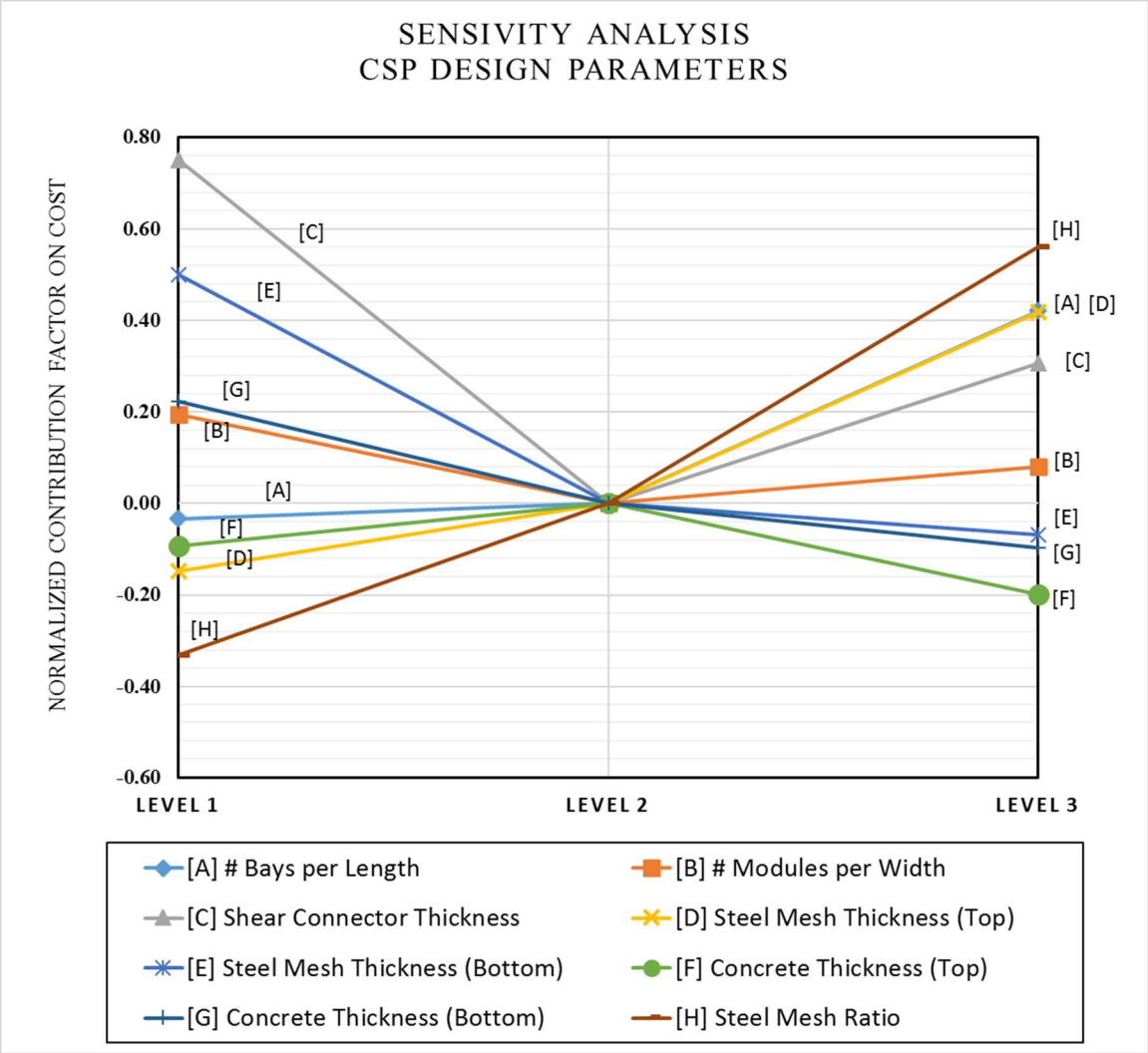

Figure (3.9): Normalized Contribution Factors of Design Parameters of CSP to the Cost of CSP.

4. Thickness of steel mesh in the bottom [E] has to be adjusted carefully, as it has major contribution to bending stiffness of the panel. Minimizing it will result to panel that violate the ACI requirement limits and increase the objective function due to penalty factor defined in the objective function.
5. Increasing the thickness of Mortar on top [F] will minimize the objective function. This can be explained by the fact that Mortar is most efficient material for the

compression zone which is on top of CSP in this case. Also increasing the concrete thickness contributes to increasing the insulation of the panel and reducing Heat loss.

6. Although decreasing the thickness of materials decrees the cost of Material, However, increasing the thickness of concrete in the bottom [G] will contributes to increasing the insulation of the panel and reducing Heat loss.
7. Increasing the Steel Mesh ratio, which is ratio of horizontal spacing to vertical spacing, will minimize the objective function. This is true as these members do not have any structural influence on the response of CSP. Therefore, if the manufacturer can increase this ratio, they can reduce the cost safely. [H]

3.6. Optimization Analysis using Genetic Algorithm

Optimizing sandwich panel systems requires considering design variables as discrete quantities. Genetic Algorithms (GAs) are best suited for unconstrained optimization problems, and it is necessary to transform the constrained problem into an unconstrained one. Therefore, a penalty-based transformation method is proposed. The penalty parameter depends on the degree of constraint violation, which is found to be well suited for a parallel search using the genetic algorithm. A genetic algorithm presented here is a modified Simple Genetic Algorithm (SGA) proposed by Goldberg in 1989, based on natural genetics. It combines Darwin's principle of survival of the fittest and a structured information exchange using randomized operators to evolve an efficient search mechanism.

3.6.1. Optimization Procedure using Genetic Algorithm

Figure (3.10) shows the summary flowchart illustrating the genetic algorithm proposed for a CSP optimization.

Step 1: Define Objective Function and Constraints.

In order to use the genetic algorithm for optimization of CSP, first we need to define the objective function *f(x)* subjected to constants *g(x)*. Objective function and constraints defined by Eq. (3) to reduce the cost of CSP panel due to the cost of material and heat loss used in the previous section for Taguchi method, can be utilized in Genetic Algorithm. This way, a Violation Coefficient *C* is proposed in the following condition: if $g_i(x) > 0$, then $c_i = g_i(x)$; or if $g_i(x) \leq 0$, then $c_i = 0$, where:

$$C = \sum_{j=1}^{m} c_j \qquad \text{Eq. (10)}$$

where: *m* is the number of constraints. In this study, similar constrain for Maximum displacement due to the live load based on ACI code 24.2.2 as defined in the Taguchi method will be used for optimization using genetic algorithm.

Now the modified objective function $\phi(x)$ is written, incorporating the constraint violation as:

$$\phi(x) = f(x)(1+KC) \qquad \text{Eq. (11)}$$

where parameter *K* has to be judiciously selected as penalty parameter depending on the required influence of a violated individual in the next generation. Now the genetic algorithm is used to carry out unconstrained optimization of $\phi(x)$.

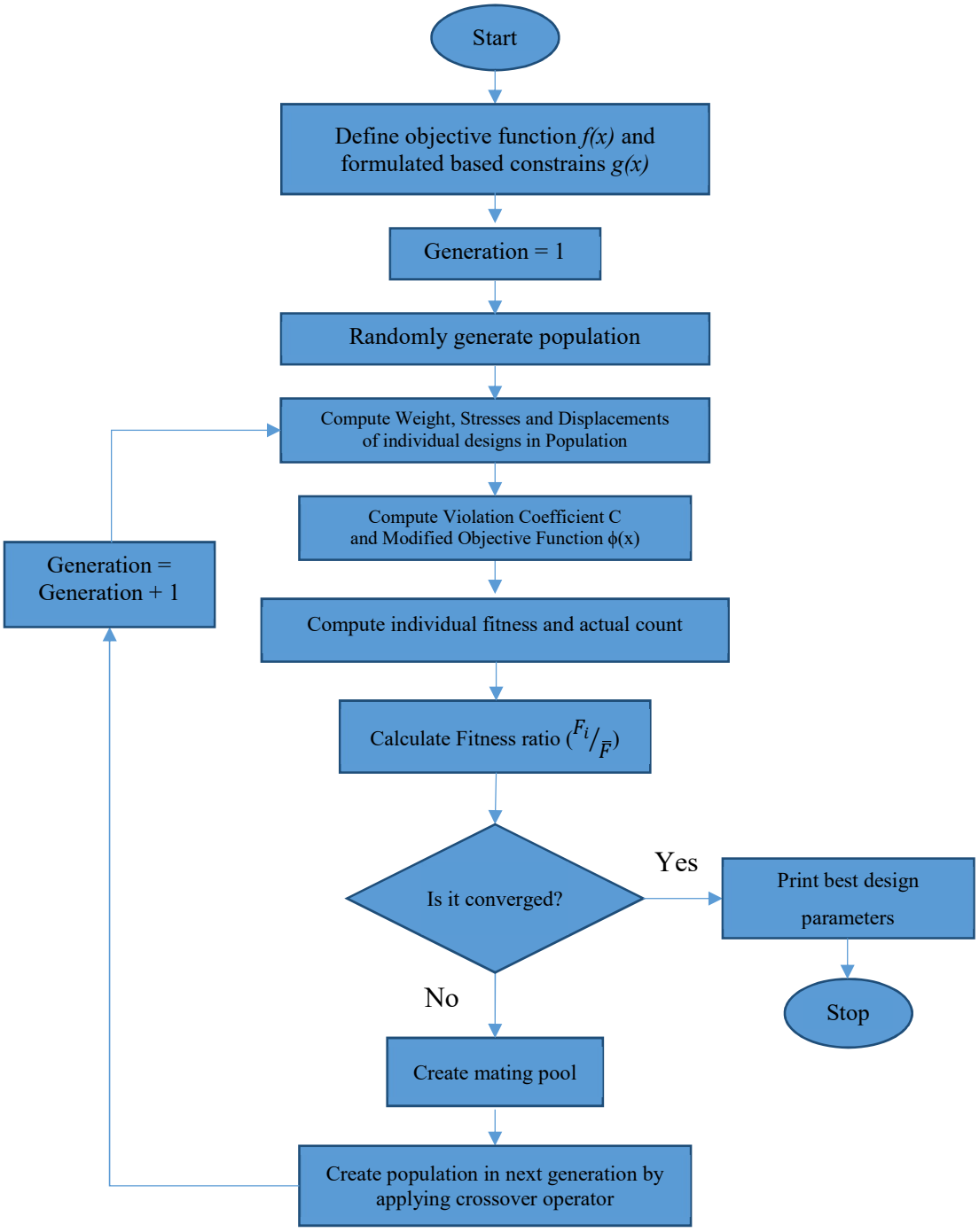

Figure (3.10): Flowchart of Genetic Algorithm for Sandwich Panel Optimization

Step 2: Define the first generation based on the design variables

A discrete list of values that the design variables can take is populated. Since genetic algorithm work on coded design variables, it is necessary to code the design variables into a string. A Trinary code is selected as we have three different values for each design parameter. In Table (3.7) a population group of 5 CSP is generated as per design variables listed in Table (3.4), where 1, 2, and 3, each refer to design parameter values, Level 1, Level 2, and Level 3 accordingly.

Table (3.7): First Generation randomly selected based on design variable pool

Sample Number	**1**	**2**	**3**	**4**	**5**
Gene	13322132	13322131	32321222	12111333	11111113

Step 3: Running the FEA.

Each CSP is modeled using FEM Preprocessor such as MENTAT, and analyzed using FEA solver, MSC MARC in order to obtain the objective function *f(x)* for each model. The violation factor *C* is computed using information in step 1 for each model. Values of the modified objective function f(x) are computed using Eq. (11). The result is listed in Table (3.8)

Table (3.8): Obtain the Objective Function from FEA

Sample Number	**1**	**2**	**3**	**4**	**5**
Gene	13322132	13322131	32321222	12111333	11111113
Objective Function f(x)	20.81	26.54	25.92	10.68	28.42

Step 4: Compute the Fitness function

Now ***f(x)*** has to be converted into corresponding fitness values. This should be done in such a way that the best individual has maximum fitness. Goldberg (1989) suggests that

for minimization problems, ***f(x)*** should be subtracted from a large constant, so that all the fitness values are nonnegative and individuals get fitness values according to their actual merit. In this proposal, the value of this constant is obtained by adding the maximum and minimum values of ***f(x).*** The expression for fitness becomes:

$$F_i = [\boldsymbol{f}(x)_{max} + \boldsymbol{f}(x)_{min}] - \boldsymbol{f}_i(x) \qquad \text{Eq. (12)}$$

where: F_i is the fitness of the i^{th} individual. Here, the subscript i is introduced to indicate the individual in the population (As shown in Table (3.9)).

Table (3.9): First Generation randomly selected based on design variable pool

Sample Number	1	2	3	4	5
Gene	13322132	13322131	32321222	12111333	11111113
Objective Function f(X)	20.81	26.54	25.92	10.68	28.42
Fitness function F_i	**18.29**	**12.56**	**13.18**	**28.42**	**10.68**

Step 5: Cross over and Reproduction

The next step is to generate the population for the next generation, which are the offspring's of the current generation. Two genetic operators, reproduction and crossover, are applied for this purpose. The reproduction operator selects the fit individuals from the current population and places them in a mating pool. Highly fit individuals get more copies in the mating pool, whereas the less fit ones get fewer copies. As the number of individuals in the next generation is also the same, the worst fit individuals die off.

The reproduction operator is implemented in the following manner. The factor $(F_i/\bar{F})$ for all the individuals is calculated, where $\bar{F}$ is the average fitness. This factor is the expected count of individuals in the mating pool. Next, this factor is converted into an actual count

by appropriately rounding off so that individuals get copies in the mating pool proportional to their fitness. This process of reproduction confirms the Darwinian principle of survival of the fittest.

In this step, the crossover operator is applied using crossover parameters that are generated randomly. The first step is to matching individuals in the mating pool which done randomly. Once the pairs are decided, it is necessary to find the crossover sites. The crossover is carried out in the following manner. Consider two strings A and B as follow:

$$\mathbf{A = x_1\ x_2\ |x_3\ x_4\ x_5|\ x_6\ x_7\ x_8} \qquad \mathbf{(A)}$$

$$\mathbf{B = y_1\ y_2\ |y_3\ y_4\ y_5|\ y_6\ y_7\ y_8} \qquad \mathbf{(B)}$$

Let the cross sites generated be 2 and 5. The cross sites are randomly selected and are marked in the strings as vertical lines. After crossover, string A gets transformed into A' and B to B' as shown:

$$\mathbf{A' = x_1\ x_2\ |y_3\ y_4\ y_5|\ x_6\ x_7\ x_8} \qquad \mathbf{(A')}$$

$$\mathbf{B' = y_1\ y_2\ |x_3\ x_4\ x_5|\ y_6\ y_7\ y_8} \qquad \mathbf{(B')}$$

The new optimized population is generated after crossover. The genetic algorithm process is repeated until the Fitness factor ratio ($^{F_i}/_{\bar{F}}$) converges to 1. Table (3.10) continues from the results of objective function listed in Table (3.9) and calculates the fitness factor ratio among the population of the first generation. This fitness factor is used to find a mate for each model for cross over and reproduction of the new generation. Highly fit individuals are assigned 2, less fit individuals are assigned as 1 and worst fit individual dies off. In Table (3.10), Model 1 and Model 4 have higher fitness factor ratios and therefore they are

graded as 2. Model 2 and Model 3 are on the next stage and they are graded as 1. Model 5 is the has the lowest fitness factor ratio and therefore is graded zero and dies off in this generation. This process of reproduction confirms the Darwinian principle of survival of the fittest.

Table (3.10): Genetic Algorithm Analysis of First Generation and Birth of Second Generation

1	Individual Number	1	2	3	4	5
2	1st Generation	13322132	13322131	32321222	12111333	11111113
3	Objective Function f(x)	20.81	26.54	25.92	10.68	28.42
4	Fitness function Fi	**18.29**	**12.56**	**13.18**	**28.42**	**10.68**
5	F_i/F	1.10	0.76	0.79	1.71	0.64
6	Survival of Fittest	2	1	1	2	0
7	Mates	4	3	2	1	0
8	Crossover 1	2	3	3	2	0
9	Crossover 2	4	5	5	4	0
10	2nd Generation	12112132	13321131	32322222	13321333	13111131

The details of all ten generations of genetic algorithm optimization process in this study is listed in in Appendix B.

3.6.2. Optimization Analysis Results

The objective of this optimization process is to reduce the cost of CSP considering both cost of material and cost of energy. The objective function Eq. (3) is developed accordingly to represent both these cost and also penalizing the models which had excessive deflection, more than what is allowed by the ACI code 24.2.2. The result of the optimization process using Genetic Algorithm is shown in Figure (3.11). The result clearly illustrate the objective function is reduced in each generation of Genetic Algorithm thought the process explained in the previous section. However, after tenth generation, the result converges to

certain value of objective function which illustrate the optimized results. This process optimized the CSP from randomly generated models in the first generation, based on the Design variables limits defined in the process, genetic algorithm process reduced the objective function by more than 50% with the average objective function at 50% at tenth generation compare to the first generation.

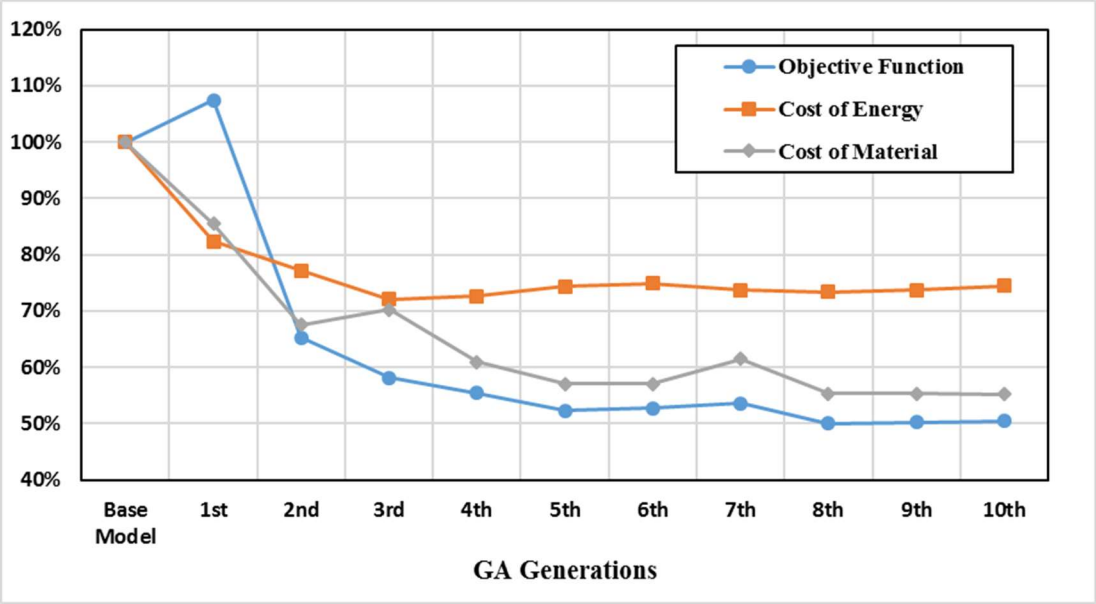

Figure (3.11): History of objective function vs. Genetic Algorithm Generations

This optimization process can be better studied by the parameters of the objective function which are to reduce the total cost of the CSP based on the cost of material and cost of energy loss. As it is also shown in Figure (3.11), in the tenth generation of optimization, the cost of material of CSP has been reduced by 45% and cost of energy by 28% compare to the base model. This is achieved by increasing the thermal resistance of the CSP from 2.06 [m^2.K/W] (R-12) to 2.89 [m^2.K/W] (R-16) achieved by Model 47. At the same time, weight of the panel has been reduced from 225 kg (495 lb) in the base model to 128 kg

(282 lb) in the Model 50. As it is illustrated in Figure (3.12), the average cost of material in optimization process decreased by almost 45% by the tenth generation of genetic algorithm. In the same time, the optimization process increased the thermal transmittance of the CSP by 35% compare to the base model while meeting the design criteria's based on the ACI Code.

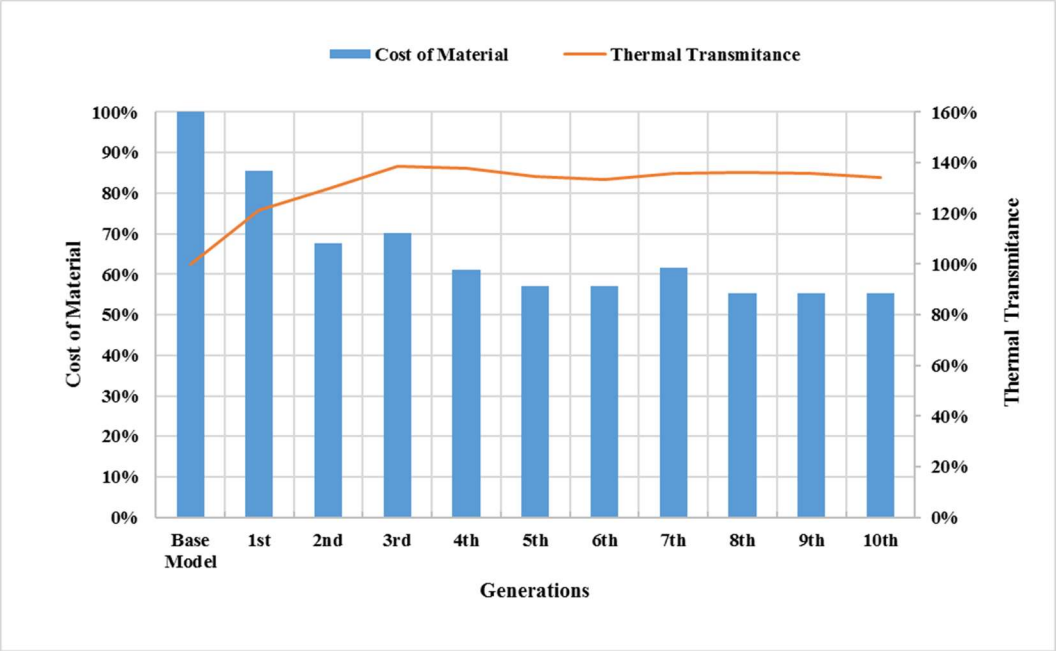

Figure (3.12): History of Cost of CSP and Thermal Resistance (T_r) in GA

3.6.2.1. *Pareto-Optimal Front*

Figure (3.13) shows the search path used of the model to find optimum solutions with respect to both maximizing thermal resistance and minimizing the cost of the panel using genetic algorithm. As it can be seen in Figure (3.13), the result have converged on the bottom right hand side of the objective space. These models on the right hand side, which include the models from the tenth generation of genetic algorithm, have optimized both

cost of material and thermal resistance, however, there exist a trade-of between these models. In the Table (3.11), results of the optimized CSP using genetic algorithm in the tenth generation is compared to In the optimization process, the top and bottom mesh is changed from 1:1 ratio to 1:2 ratios, where the wires perpendicular to direction of the slab has been reduced to the minimum requirement for shrinkage which were not contributing to the stiffness of the slab. The shear connectors configuration has been changed from rectangular array to star shaped array as shown in Figure (3.15) to optimize the thermal resistance of the panel by transfer the shear load more efficiently while meeting the requirement strength constrain defined in the optimization process according the ACI code. On the other hand, in Model 50, higher number of shear connector have been used compare to Model 47 to improve the composite action, and reduced the extra reinforcement on tension side compare to Model 47 to take the bending load. As result, the Model 50 has less amount of steel which reduces the total material cost compare to Model 47, which has higher cost but better thermal resistance. Hence none of these two solutions can be said to be better than the other with respect to both objectives and there is trade-of between the two models. These exist many other solutions in the objective space which are joined together using a curve in the Figure (3.14). This curve is called Pareto-optimal front, and the models lying on this curve are called Pareto-optimal solutions.

Table (3.11): Comparison of the Pareto-Optimal Solutions to Base Model

1	Individual Number	47	49	50
3	Weight of Steel	-38%	-47%	-48%
4	Weight of Mortar	-14%	-14%	-43%
5	Total Weight	-15%	-15%	-43%
6	Thermal Resistance R_t	40%	36%	35.6%
7	Cost of Material	-38%	-47%	-48%

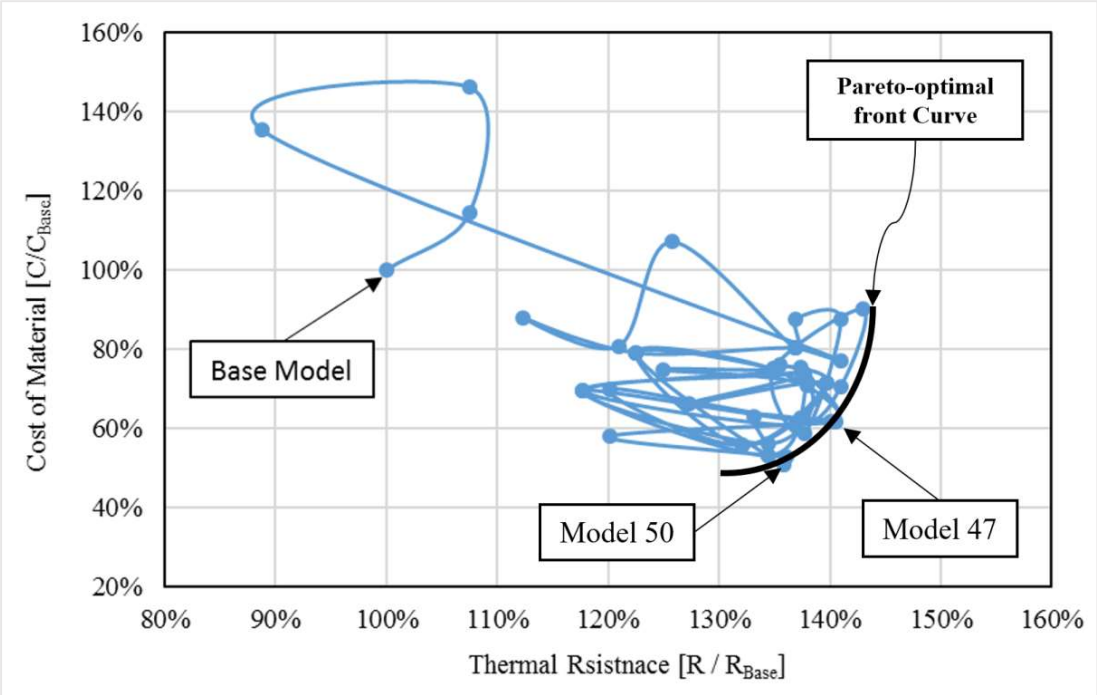

Figure (3.13): Search Path used by GA to optimize Cost and Thermal Resistance Excluding Panelized Members.

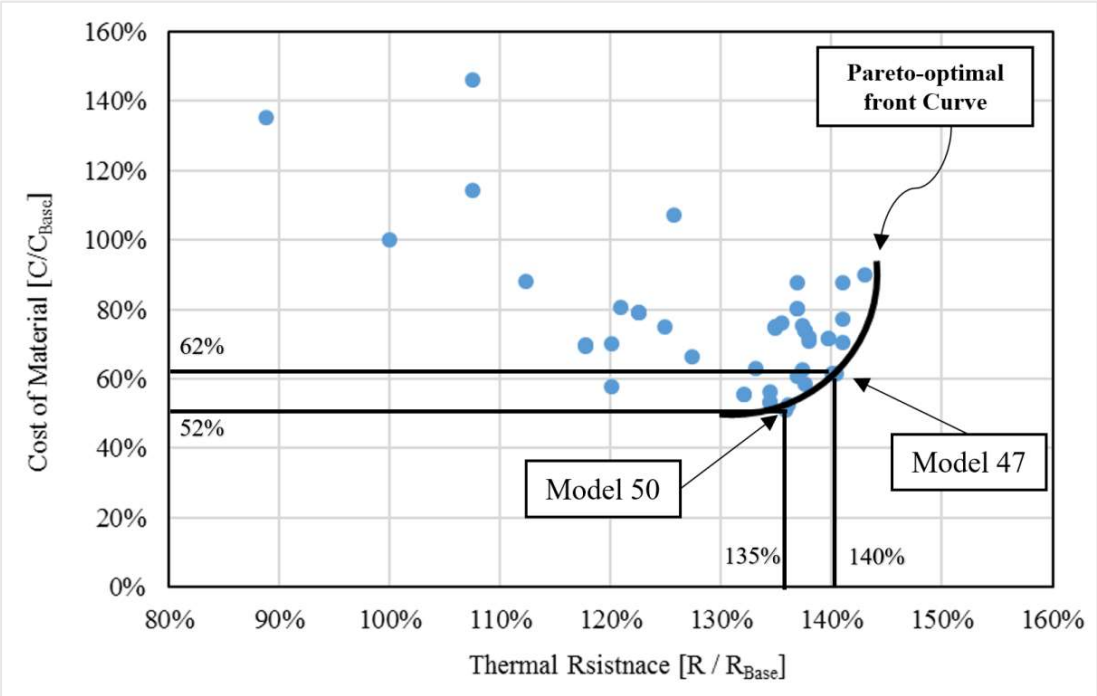

Figure (3.14): Pareto-Optimal Front Plot in the Objective Space

Looking at the optimized models Pareto-Optimal-Frontier, the designer has an option to choose from several optimized design according to design preference. For example, if the cost of material is the priority, while meeting the design requirement, designer can choose model 50 where the cost of material has been reduced by 48% with 35.6% increase in the thermal resistance value; or if the insulation is the priority while meeting the design requirement, designer can choose Model 47 where the thermal resistance value has been increased by 40% while the cost of material has been decreased only by 38%; or any other parameter listed in Table (3.11) such volume of steel, volume of mortar, if any of these two is the priority base on the Market prices, or the following this studies objective function, which is the combination of cost of material and thermal resistance. Comparison of the designs specification of the CSP models in tenth generation vs. the base model is listed in Table (3.12). Figure (3.15) graphically represent the topology optimization of CSP vs. the base model.

Table (3.12): CSP Specification Comparison 10th Generation to Base Model

Parameter	Unit	Base Model	Model 47	Model 49	Model 50
Number of Shear Connector	**Pieces / (per m^2)**	100	40	50	48
Shear Connector Size	**[mm]**	2.9	2.3	2.3	2.3
Top Mesh Wire Sizer	**[mm]**	2.9	2.3	2.3	2.3
Bottom Mesh Wire Size	**[mm]**	2.9	2.9	2.3	2.3
Top Mortar Thickness	**[mm]**	38	50	50	25
Bottom Mortar Thickness	**[mm]**	50	25	25	25
Steel Mesh Spacing (LXW)	**[mm]**	50x50	50x100	50x100	50x100
Weight of Mortar	**[kg]**	220	126	126	126
Weight of Steel	**[kg]**	3.6	2.22	1.9	1.88
Thermal Resistance	**[m^{2}K/W]**	2.06	2.89	2.81	2.79

(1 mm = 0.039 in), (1 m^2 = 10.5 ft^2), (1 kg = 2.2 lbs)
(1 m^2 K/W [RSI] = 5.67 h.ft^2.^{o}F /BTU [R-Value])

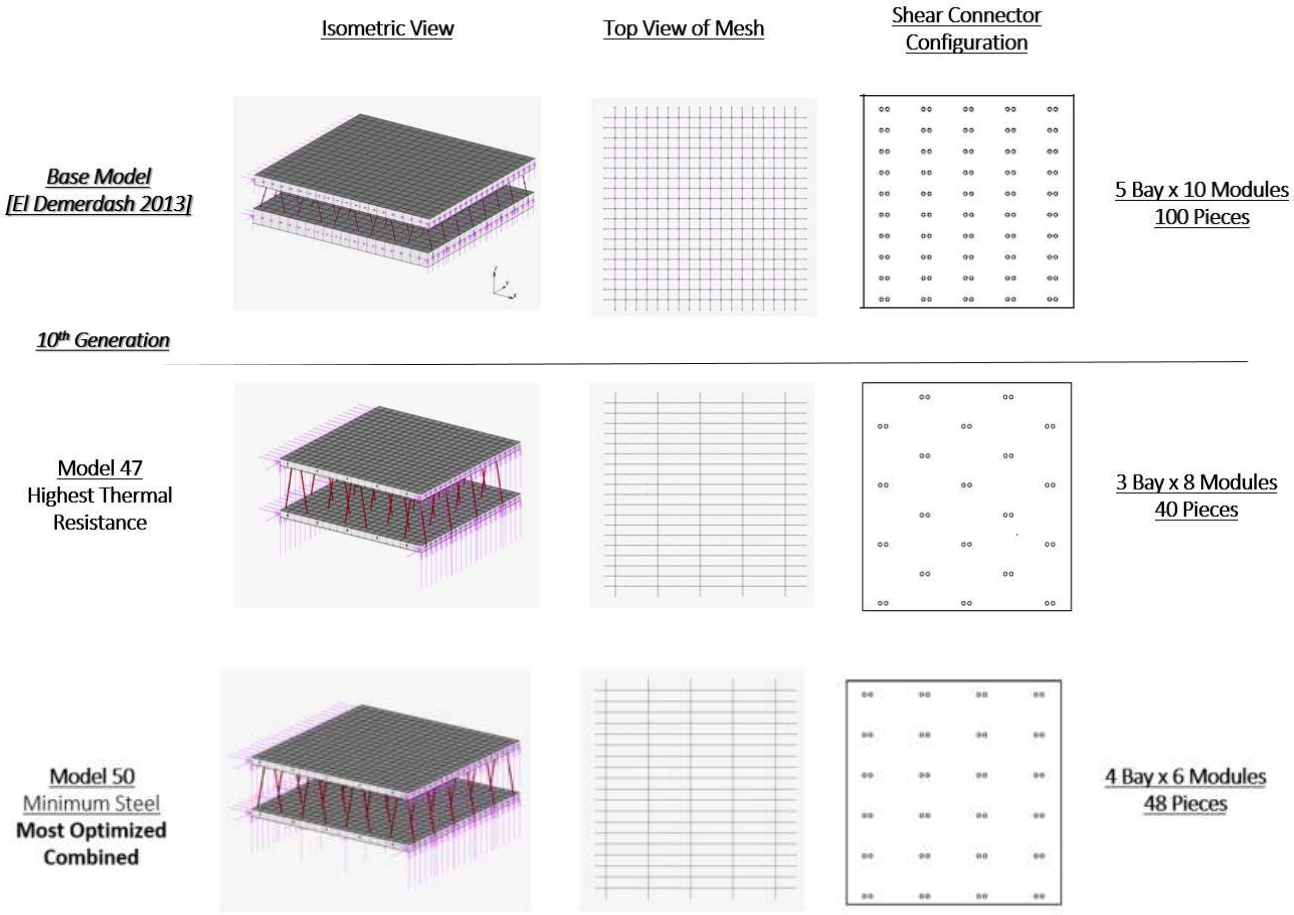

Figure (3.15): Graphical representation of CSP Topology Optimization using GA.

3.7. Correlation of Design Variables

One important topic to look into is the correlation between the variables in any type of parametric optimization. CSP main advantage compare to the conventional structural elements, is in utilizing materials more efficiently and also thermal insulation capability to save energy. Therefore, in the optimization of CSP, the objective is set to reduce Cost of Material and also increasing the Thermal Resistance of the CSP to reduce the Cost of Energy due to Heat loss.

The steel wires connecting the two faces of CSP are the main members contributing the full composite action of the CSP and hence improving the CSP efficient use of material. However, in the same time, these wires create thermal bridge between two faces of the CSP and reduce the thermal resistance of the CSP. Figure (3.16) illustrate the correlation between the steel wires connecting the two faces and the equivalent thermal resistance of CSP. The thermal resistance is normalized with respect to the thermal resistance of the CSP with minimum steel wire ratio in between design variables limit which is 30 wire 11-Gauge per m^2 (10.5 ft^2). As illustrated in this chart, the thermal resistance of the core of the panel decreases up to half, as the steel ratio increases from 30 11-Gauge Wires to 80 7-Gauge Wire, which is equivalent to 0.01% and 0.08% respectively. Figure (3.17) shows the correlation between Thermal Resistance and Stiffness of CSP in different generations of genetic algorithm optimization process. One can see that there is a tradeoff correlation between Thermal Resistance and Stiffness of CSP. This is due to the correlation between the design variables of Shear Connector and Thermal Resistance that described in the previous paragraph and illustrated in Figure (3.16).

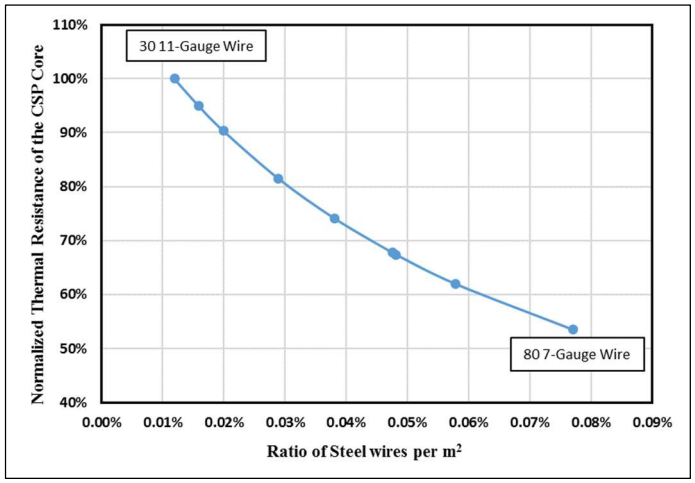

Figure (3.16): Correlation Between Steel Wires And Thermal Resistance Of The CSP

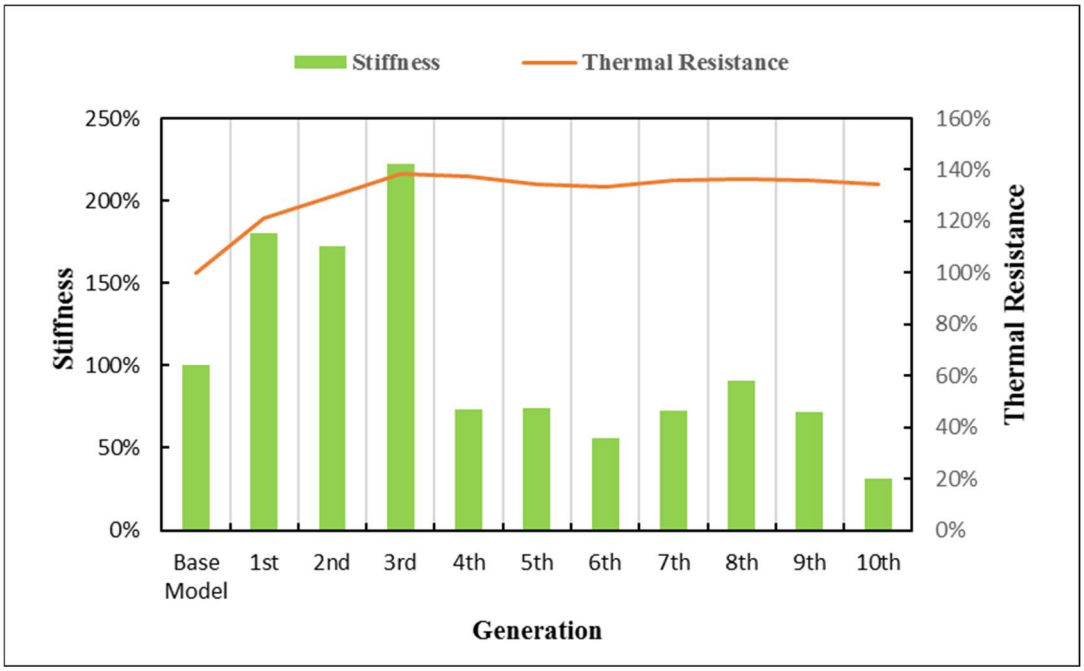

Figure (3.17): Correlation Between Thermal Resistance And Stiffness Of CSP

On a last note, in studying correlation between variables in the thermal insulation of the building material, and the most famous and evident correlation is between the material cost (Insulation Cost) and cost of energy loss that are directly related to the insulation thickness as shown in Figure (3.18). As result, the thickness of foam was kept constant in this study, however, the optimization results can also be implemented in these diagrams to illustrate the benefits of the new design for CSP. In the model outputted from optimization (Model 47), the cost of material has been decreased by 14% and Energy cost which is inversely related to thermal insulation (Eq. 9) has been reduced by 28%. The details of this plot calculation is provided in Appendix E.

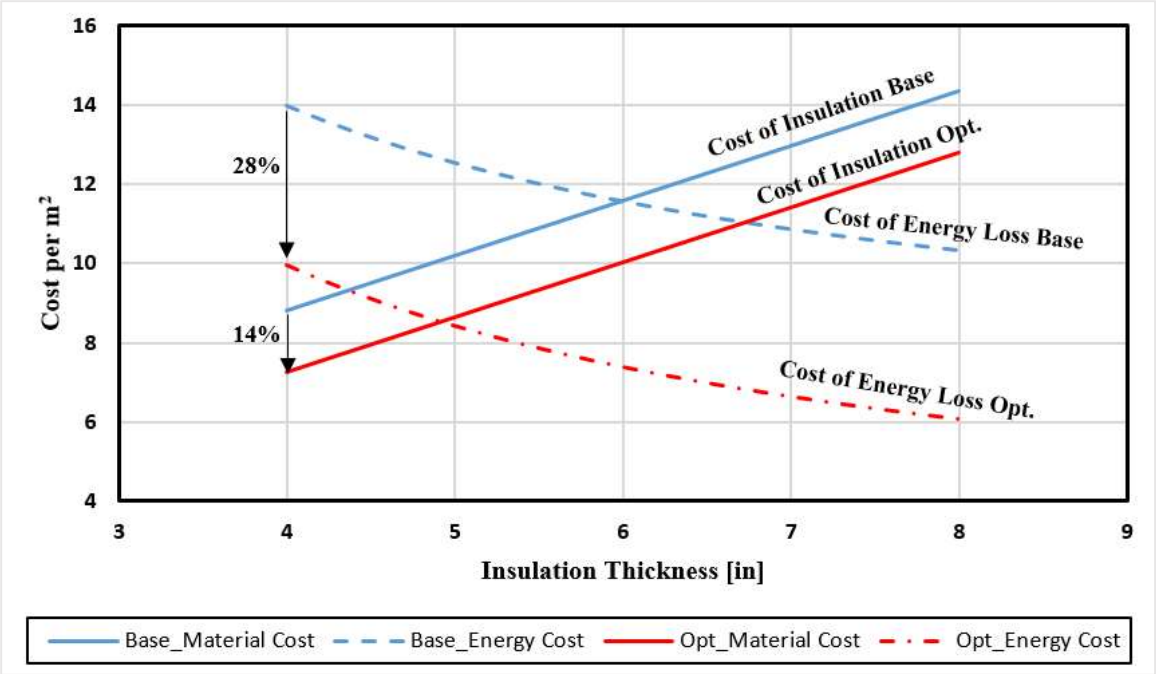

Figure (3.18): Effect of Optimization on Insulation Economy of CSP

CHAPTER 4

PERFORMANCE EVALUATION OF THE OPTIMIZED CSP USING NUMERICAL MODELING

4.1. General

In order to verify the optimum design scheme developed in chapter 3, this chapter aims at comparison between the performance of the optimize design and existing off-the-shelf CSP that were extensively studied using large-scale tests at UCI Structural Engineering Lab. [10]. In this chapter, the following CSP panels have been selected and their performance have been evaluated and compared to each other.

A- Off-the-shelf CSP with diagonal shear connector which was tested at UCI, hereinafter called “Diagonal CSP” [11]

B- Off-the-shelf CSP with parallel shear connectors which was tested at UCI, hereinafter called “Parallel CSP” [20]

C- Numerically modeled of optimized CSP, based on the results of previous chapter, hereinafter called “Optimized CSP”.

The load-displacement curve, and cracking locations, thermal insulation and cost of material of the models are compared in this chapter using numerical modeling’s and results of the full-scale experiments done previously at UCI.

In this study a numerical modeling procedure is developed and verified using the results of the full scale experiments of ″Diagonal CSP″ at UCI Structural lab. The verification of the numerical modeling is important to check the geometric property, material property and

most importantly the boundary conditions defined in the Finite Element Model (FEM) match the conditions of "diagonal CSP" experiments. This verification of FEM is essential to relying on the results of the numerical modeling.

Using the optimized design of CSP obtained in Chapter 3, an "Optimized CSP" is modeled based on the minimum ACI and ASCE code requirements and numerically tested under similar boundary conditions as the experiment of the "Diagonal CSP" done at UCI.

Numerical modeling of reinforced concrete systems using Finite Element Analysis (FEA) structures has been under continuous development in recent decades. The worldwide research effort led to the formulation of sound constitutive models as well as numerical techniques for their implementation in computer software. These advances have made possible the application of non-linear finite element analysis to the practical engineering problems of analysis and design. Several computer programs featuring non-linear material models are now available commercially and claim distinct features.

For numerical simulation, MSC MARC and MENTAT 2016 was used. MARC is a powerful, general-purpose, Non-linear finite element analysis solver which can effectively depict the non-linear behavior of RC structures, has been used in the present study to simulate the behavior of CSP under flexure and shear through the elastic to the ultimate limit states. MENTAT is Pre- and Post-Processor dedicated for MARC.

4.2. Performance Evaluation of Parallel-CSP

In 2014 a series of large scale cementitious sandwich panels with parallel shear connectors were fabricated and tested in UCI Structural Engineering Testing Hall (SETH) lab. [20] The purpose of that structural evaluation test program was to assess the performance of CSP slab panel with parallel shear connectors subjected to out-of-plane flexural loading. The steel mesh in Parallel-CSP tested at UCI lab by Botello et al. were made using 75mm x 80mm (2.95″ X 3.15″) steel mesh using gauge 11, 2.3mm (0.09″) diameter cold-rolled wire on each face. The two faces were connected and welded using 3D dimensional shear connectors using gauge 9, 2.9mm (0.09″) diameter wire with density of 23 connectors per m^2. The thickness of the EPS foam core of this specimen was 16 cm [6.3"]. The thickness of the top cementitious face was 2″ (5.0 cm), while the thickness of the bottom cementitious mortar face was 1.5″ (3.80 cm). Figure (4.) shows the typical dimensions of off-the-shelf Parallel-CSP that were used in this study.

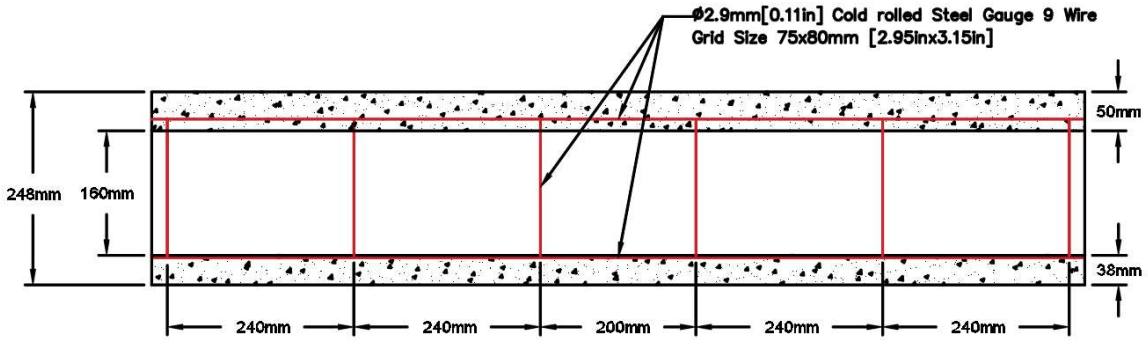

Figure (4.1): ″Parallel-CSP″ Side View and Dimensions tested at UCI

Slab specimens with simply supported boundary conditions and loaded using four-point bending test setup. The slab was rested at both ends of its length onto two steel beams. The distance of contact between the slab specimens and the steel beam supports was 4 inches

on each side and along the whole slab width. Pieces of rubber were placed between each specimen and the steel beam to enable free rotation and prevent immediate damage to the specimen at those locations. The loading was applied using an actuator placed above the specimen. Using a steel beam connected to two steel cylinders the load from the actuator was transferred to the specimen.

The steel cylinders were 15 inches away from the center of the actuator and 30 inches apart. The cylinders rested on rubber pads on the top face of the slab in order to distribute the load and to prevent crushing of the mortar from direct contact due to compression failure. This test setup is also known as a four-point bending test as there are 4 points of load transfer on the slab. 2 points of loading demonstrated by the steel cylinders connected to the actuator and 2 supports producing reaction loads at the points of contact between the slab and steel beams. The set-up of one of the 2.4m (8ft) long slab under out-of-plane flexural loading tests can be seen in Figure (4.2) and Figure **(4.3**).

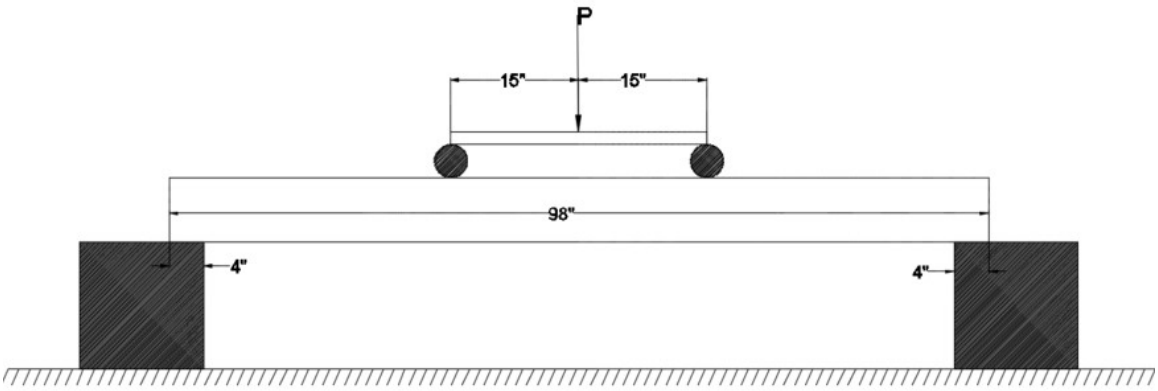

Figure (4.2): Slab Flexural Test Set-up for 2.4m (8ft) Long Specimens

Figure (4.3): Side View of Slab Set-up prior to Testing [11]

Series of Parallel-CSP panels were tested at UCI with different span sizes of single and double spans, using different boundary conditions in study done by Botello et al. [20]. However, in order to be able to compare the performance of Parallel-CSP to other panels in this study, SS-PB-1 test was selected where a 2.4m x 0.6m x 27.3cm [7.9ft x 1.9ft x 10.75in] single span panel was tested under 4 pint loading out-of-plane bending test. A monotonic loading was applied to the top portion of the specimen with the assistance of a 55-kip calibrated servo-hydraulic actuator as demonstrated in Figure (4.3).

According to Botello et al. [20] initially and at a low load level, no cracks were observed. However, as the load was increased, hair cracks were developed at the slab/support interface as shown in Figure (4.4). Flexural cracks appeared at the bottom portion at the mid-span as shown in Figure (4.5).

Figure (4.4): Cracks due to Flexure at Mid-Span for Specimen Parallel-CSP

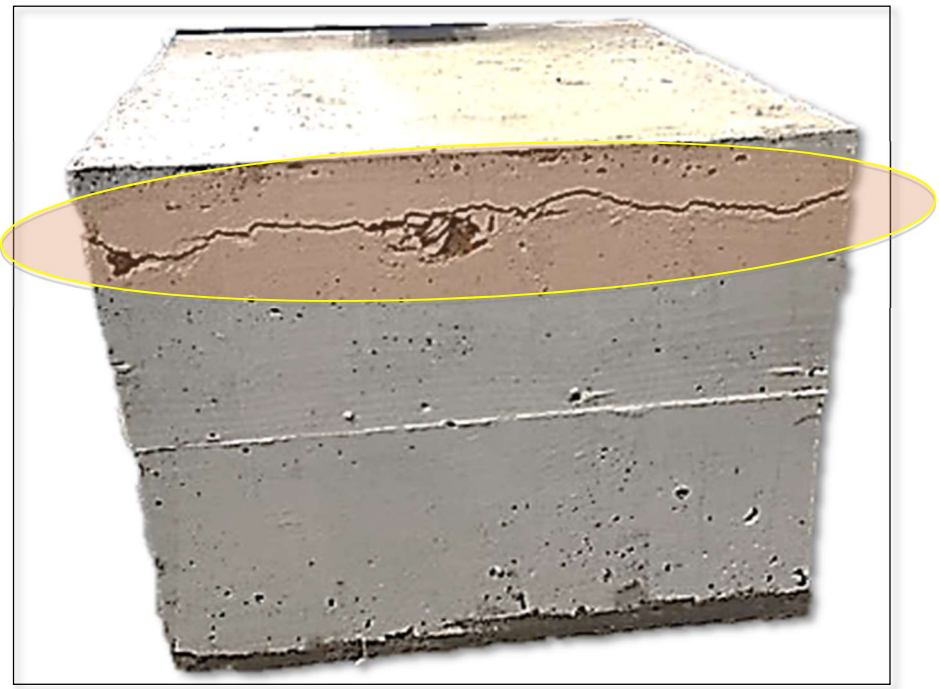

Figure (4.5): Interfacial Cracks at Boundary of Specimen Parallel-CSP

The poor performance of CSP with parallel shear connector is due to not providing adequate, sufficient or compete transfer of shear. In CSP the shear connectors are designed

to take the shear instead of heavy concrete. In design Parallel-CSP have only parallel component for vertical shear. However, the shear transfer that happens horizontally, that is called conjugate shear, which happens at the same time as vertical shear, is not available in this design. Unless after a minimum curvature then we would have the horizontal component of the shear connector transferring the load as illustrated in Figure (4.6). However, by the time the sandwich panel reaches the required curvature, then the deflection might violate the deflection limit provided by the code. Additionally, the cracks on back of the support shown in Figure (4.5) shows the weakness of this design in resisting the horizontal shear.

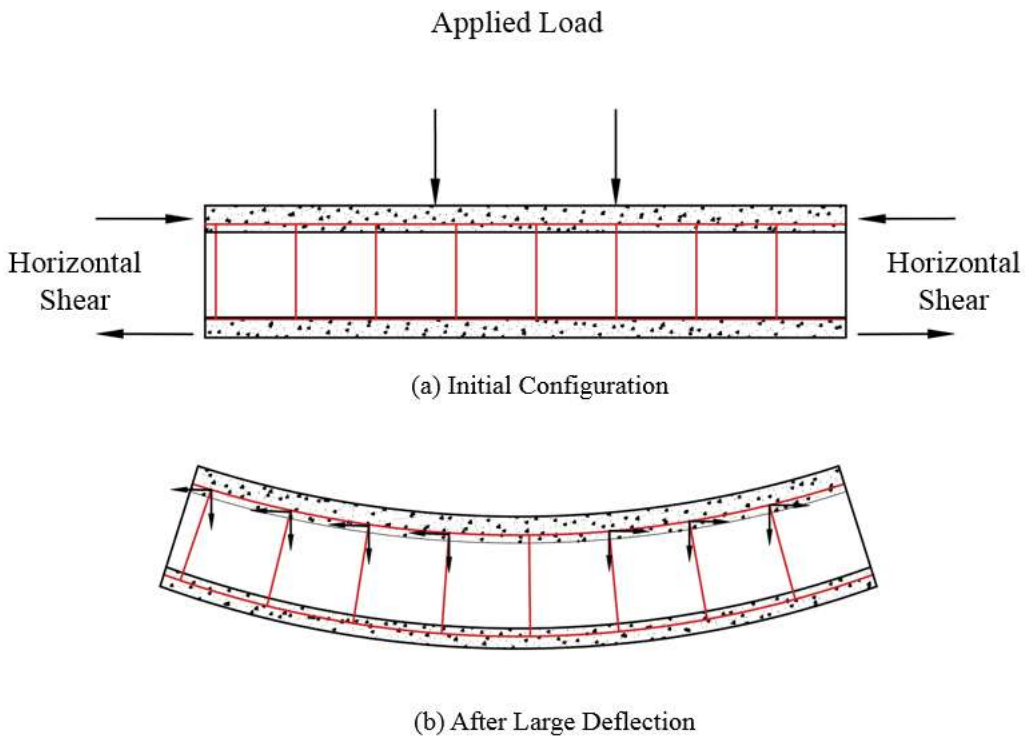

Figure (4.6): Parallel-CSP Resistance to Horizontal Shear After Large Deflection

4.3. Performance Evaluation of Diagonal-CSP

In 2014 a series of large scale cementitious sandwich panels with diagonal shear connectors were fabricated and tested in UCI Structural Engineering Testing Hall (SETH) lab. [11] The purpose of that structural evaluation test program was to assess the performance of CSP slab panel systems subjected to out-of-plane flexural loading. The steel reinforcement in Diagonal CSP tested at UCI lab by El Demerdash were made using 50mm x 50mm (2″ X 2″) steel mesh using gauge 11, 2.3mm (0.09″) diameter cold-rolled wire on each face. The two faces were connected and welded using 3D dimensional shear connectors using gauge 9, 2.9mm (0.11″) diameter wire. The mortar mix is later applied to each face. 50mm (2″) of concrete on compression side, and 38mm (1.5″) concrete on tension side. Figure (4.1) shows the cross view and dimensions of tested Diagonal-CSP.

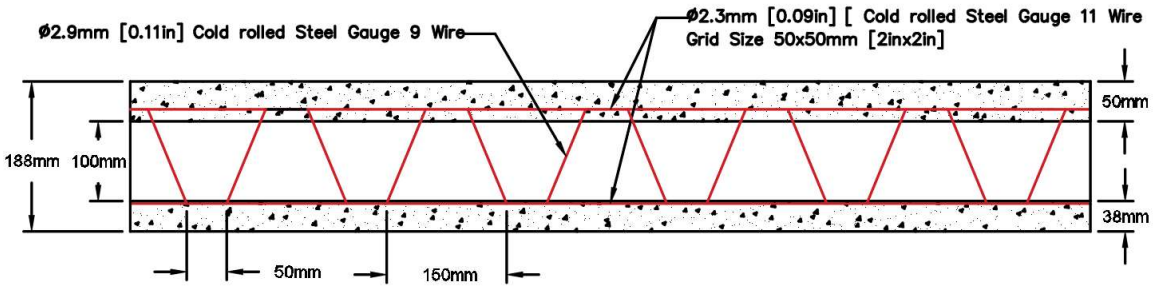

Figure (4.7): ″Diagonal-CSP″ Side View and Dimensions

Slab specimens with simply supported boundary conditions and loaded using four-point bending test setup. The slab was rested at both ends of its length onto two steel beams. The distance of contact between the slab specimens and the steel beam supports was 4 inches on each side and along the whole slab width. Pieces of rubber were placed between each specimen and the steel beam to enable free rotation and prevent immediate damage to the

specimen at those locations. The loading was applied using an actuator placed above the specimen. Using a steel beam connected to two steel cylinders the load from the actuator was transferred to the specimen.

The steel cylinders were 15 inches away from the center of the actuator and 30 inches apart. The cylinders rested on rubber pads on the top face of the slab in order to distribute the load and to prevent crushing of the mortar from direct contact due to compression failure. This test setup is also known as a four-point bending test as there are 4 points of load transfer on the slab. 2 points of loading demonstrated by the steel cylinders connected to the actuator and 2 supports producing reaction loads at the points of contact between the slab and steel beams.

Figure (4.8): Side View of Slab Set-up prior to Testing [11]

The Diagonal-CSP panels were tested with and without additional hot-rolled steel rebars reinforcements were evaluated. The result indicated that CSP without additional hot-rolled

reinforcement had sudden brittle failure on tension side as shown in Figure (4.9) and Figure (4.10) Therefore, it is highly suggested that at least 3#3 hot-rolled reinforcing bars every four feet are placed at the bottom of slabs to improve ductility and mode of failure. The steel wire mesh that comprises the panels is all cold-rolled and thus possesses low ductility, this is why the addition of hot-rolled reinforcing bars changes the behavior of the specimens. (El Dememdash 2014).

Figure (4.9): Brittle Failure Of CSP Specimen Without Additional Hot-Rolled Reinforcements [11].

Figure (4.10): Up-Close Failure of Cold Rolled Wires In The Center Of CSP without additional Hot-rolled reinforcement [11]

Afterwards, another slab specimen 240cm x 120cm x 19cm (8′ x 4′ x 7.5″) (*Length by Width by Thickness*) using Diagonal CSP with addition of 3 #3 hot rolled steel rebars with diameter of 9.5mm (0.375″) was loaded under similar test setup of previous experiment. The specimen demonstrated both flexural and shear stresses depicted by the crack locations that appeared during loading and up to failure. Due to the presence of the additional reinforcement, the slab did not fail due to flexure but due to shear. There were cracks that appeared in the center which is the section that fails due to flexure as can be but the main failure location was next to the location of the loading steel cylinders at a distance close to the depth of the specimen away from the support. The failure was at a 45^{o} angle indicating that the failure due to shear stresses exceeded the capacity of the slab section as seen in Figure (4.11). The maximum load that the slab managed to withstand was also increased indicating that the additional reinforcement had a big effect in the increase of slab capacity. The failure also demonstrates that total collapse and splitting at the center didn't occur, that further underlines the importance of adding additional reinforcement that greatly increases the safety and serviceability of the structural elements' failure for those present within the structure.

Figure (4.11): Shear Failure of Diagonal CSP Specimen at 45^{o} Degree Angle and Flexural Cracks at Centerline of Specimen at Ultimate Load. [11]

Figure (4.12) shows the comparison of the Load displacement curves for the two full scale experiments. In the Diagonal-CSP specimen without additional reinforcement, the load-displacement curve was behaving linearly with high stiffness up to a load of 20 kN (4.3 kips), this is equivalent to a surface load of 635 kgf/m^2 (130 psf), after which the first stiffness drops. Up to this point, the two layer of Diagonal-CSP is working together and full composite action, however, after this load, the slope Load-Displacement curve drops which represent the stiffness of the panel. This can be due to the failure of shear connectors and as a result each layer is taking the load partially (partially composite action). In the Diagonal-CSP without additional reinforcement, the stiffness reduced more significantly than the Diagonal-CSP with additional hot rolled reinforcement. The load increases to a maximum load recorded 56kN (12 kips) which is equivalent to surface load of 2000 kgf/m^2 (400 psf) where deflection of the beam was about 22mm (0.86 in). After this load, the resistance sharply drops, indicating the brittle failure of the specimen. This brittle failure was due to the brittle behavior of all the materials used in the composite Diagonal-CSP specimen, those being the mortar, cold rolled steel wire mesh. The failure can be seen in the Performance Evaluation of Diagonal-CSP), as a major crack the tension side of the panel through both mortar and snapping of the cold wires. The specimen completely split in the middle with all the wires completely broken, again clearly demonstrating its brittle failure.

The Diagonal-CSP with additional hot rolled reinforcement, had a smaller drop in resistance after first change in the slope of load displacement curve at load of at 20 kN (4.3 kips) compare to the Diagonal CSP without additional reinforcement. This is due to

additional reinforcement on tension side of the specimen that resist the load in partially composite action, after loss of the full composite action.

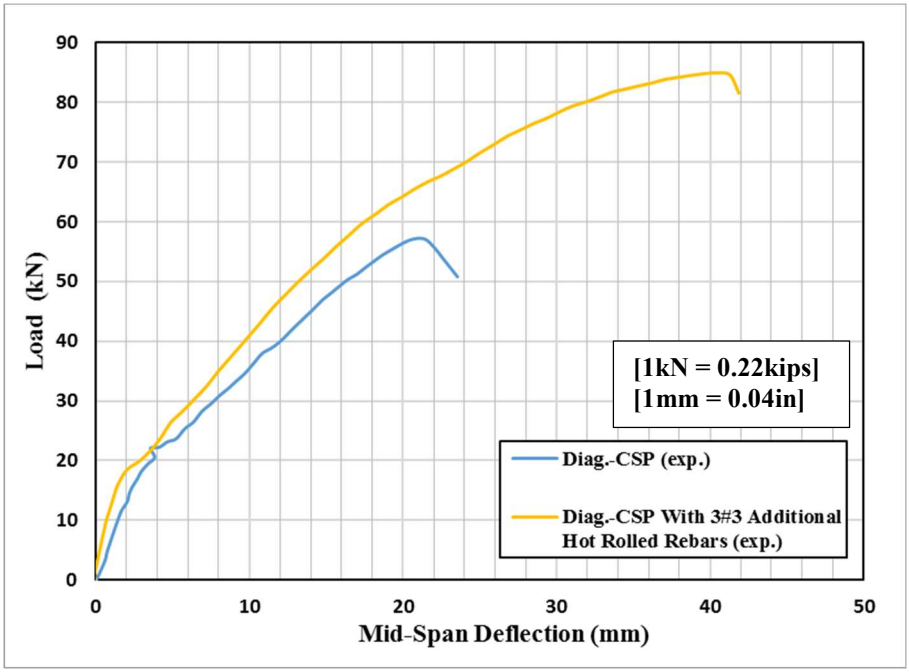

Figure (4.12): Comparison of Load Displacement Curve for Diagonal CSP

4.4. Finite Element Analysis Methodology for CSP

In this section, the numerical finite element model used in analysis of Diagonal-CSP is discussed. The finite element models were developed using finite element program MSC MENTAT and MARC 2016 general purpose finite element analysis program which was also used in the optimization process in the previous section. The CSP constituted of two steel wire mesh faces connected with transversal steel truss wires, a foam core and mortar skins with the wire mesh steel grids embedded in the mortar. The element and material properties selected for modeling of mortar and different types of steel reinforcement of the wall specimens are explained. The boundary conditions applied at the connections or supports of the model are described in this section as well as constraints within the model

that determine the behavior of materials in contact with each other. The loading method applied to the model and its subsequent behavior is determined. The results obtained from the numerical analysis of test specimens are presented and comparisons between the numerical and experiment results are discussed.

4.4.1. Element Types

4.4.1.1. *Shell elements*

In order to model the cementitious skins of the CSP, a 3D Shell element with four (4) nodes, with three (3) translation and three (3) rotational degrees of freedom at each node was selected for modeling of the cementitious mortar which is the same element used for modeling concrete. Figure (4.13) shows the shell element used to model the mortar.

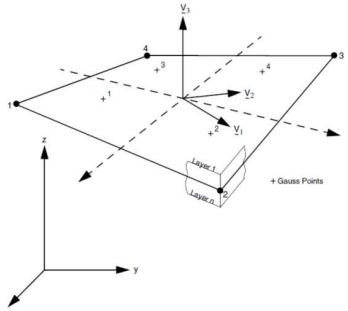

Figure (4.13): Element 75, Four Node 3D Shell Element (MARC) [32]

4.4.1.2. *Beam elements*

A truss-dimensional truss element with two (2) nodes and three (3) translation degrees of freedom at each node was selected for modeling of steel wire mesh, transversal wire (Shear Connectors) and rebars. This is a straight beam in space which includes transverse

shear effects with linear elastic material response as its standard material response; however, it also allows nonlinear elastic and inelastic material response.

4.4.2. Material Properties

4.4.2.1. *Cementitious Mortar*

Mortar is perfect example of low tension material where the behavior of material in compression is different from the behavior of material in tension. In compression, Mortar behavior is represented as linearly elastic until the initial yield stress is reached. Then it passes to the plastic zone with a strain hardening prior to the ultimate compressive stress followed by strain softening. The program computes the cementitious mortar compressive stress-strain curve based on the input of stress versus inelastic strain. In tension, initial behavior is linear elastic until cracking is initiated. A tensile strain softening response is assumed in the post cracking region. In MARC material definition module, the low tension material parameters are defined by two sets of parameters, ″plasticity″ for compressive behavior and ″Damage Effect″ for Tensile behavior using terms such as Critical Stress, Softening Modulus and Crush Strain which are illustrated in Figure (4.14). Using cylindrical test compression strength of Mortar before each test was measured as explained in previous chapters. Using the Chapter 14.8 in ACI 318, the modulus of rapture for concrete is calculated.

Yielding Criteria for Mortar is set to Parabolic Mohr-Coulomb Material model (normally called Drucker-Prager in literature) which is hydrostatic stress dependence and can handle different stress yielding limits in tension and compression. As shown in Figure (4.15), the material model has envelope for plastic yielding criteria in tension. It follows a pressure

dependence plastic flow rule where material gets stronger in compression and has instantaneous failure in tension beyond the defined yielding surface. Drucker–Prager model in MSC Marc is defined using Uniaxial asymmetry ratio (β). It is the different uniaxial yield stresses in tension and in compression and defines the slope of Drucker Prager Yield surface in principal stress diagram.

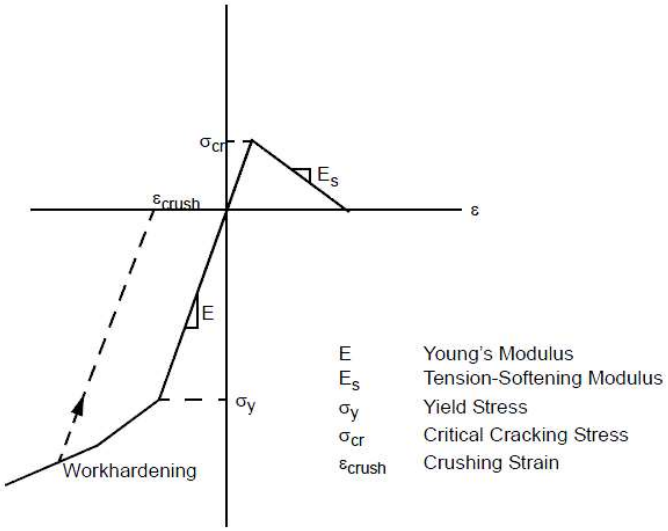

Figure (4.14): Uniaxial Stress-Strain Diagram used for Low Tension Material in MARC.

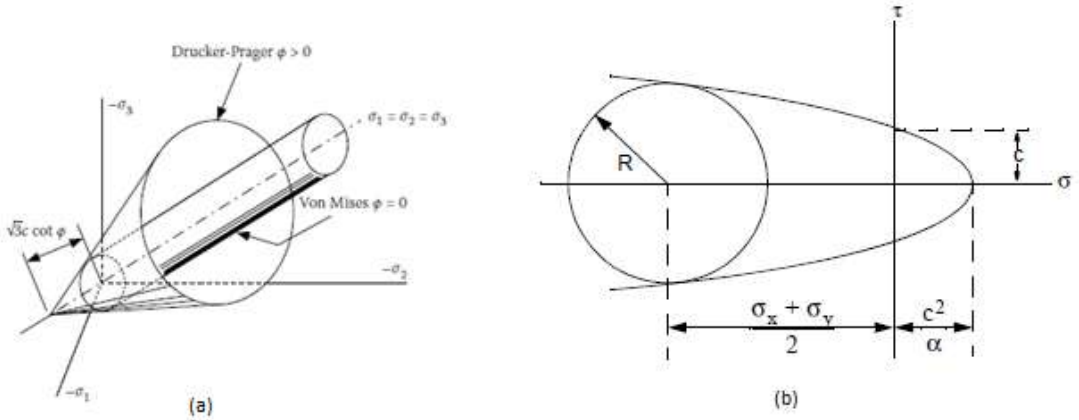

Figure (4.15): Drucker-Prager Material Model in Principal Stress Space (a) 3D (b): 2D [41]

4.4.2.2. *Steel Reinforcements*

The elastic-plastic bi-linear material model in MARC was used for all steel reinforcement in all CSP models. The stress-strain curve depicting the behavior of all steel elements used in the FEM. Due to the presence of different steel types, each had its own modulus of elasticity (E_s). The poisson's ratio of all steel was taken to be the same (ν) = 0.3, which are summarized in Table (3.1).

4.4.2.3. *CSP Foam Core*

The CSP foam core has very low density and no structural importance for the wall except for its use as a spacer in the core section. R. M. Bajracharya (2011) explains that EPS core has a very low modulus of elasticity and does not make any difference on the model results as the value is very low compared to Mortar and steel. Therefore, in order to save time in analysis and reduce complexity it was considered as a void space. [33]

4.4.3. Summary of all Material Properties

The FEM developed on MENTAT comprised of different material properties and dimensions. Each Part was initially drawn according to their realistic geometric dimensions and properties. Then the properties of each of the different material types were selected according to the materials used and their behavior in the Materials tab of MENTAT. The material types were then allocated to the designated geometrical dimensions of the parts drawn in the Geometric tab part of MENTAT. Table (4.1) shows the material properties entered for all the different materials used when forming the CSP sandwich panel model

during the linear elastic phase. The non-linear behavior of each material was then entered separately. Step by step of modeling in MENTAT process is illustrated in Appendix A.

Table (4.1): Material Properties Entered into MENTAT

Material Model	Modulus of Elasticity GPa (ksi)	Poisson's Ratio	Yield Stress MPa (ksi) (Compression)	Yield Stress MPa (ksi) (Tension)
Mortar	21 (3,100)	0.15	$f'_c = 20$ (3)	$f_r = 3$ (0.45)
Steel Wire (Cold Rolled)	200 (29,000)	0.3	$f_y = 500$ (72)	$f_y = 500$ (72)
Steel Rebars (Hot Rolled)	200 (29000)	0.3	$f_y = 431$ (60)	$f_y = 431$ (60)

4.4.4. Model Geometry and Mesh Sizes.

The model geometry created to simulate experimental CSP and then it was discredited into a number of finite elements FEM Analysis. As the mesh density increases, the accuracy of a finite element model generally increases and converges to a numerically correct solution. Therefore, it is necessary to have a fine mesh to obtain the appropriate solution. The accuracy of the model is compared with the experimental results. In order to obtain accurate results from the FE model, the size of the element meshing was set to 25mm (1″) for all the Parts that constituted the model. All the elements in the model are assigned the same mesh size to ensure that corresponding nodes exist at the same location on the element connected using the above mention constraints. The size of the element mesh of 25mm (1″), was believed to be reasonable enough to obtain accurate results while not making the model too large so as not to increase the time of computation too much. The type of the mesh is selected in the model as structured to ensure minimum transition in the mesh and consistent element size throughout the model. Figure (4.16) and Figure (4.17) show the mesh of both the mortar and steel wire mesh.

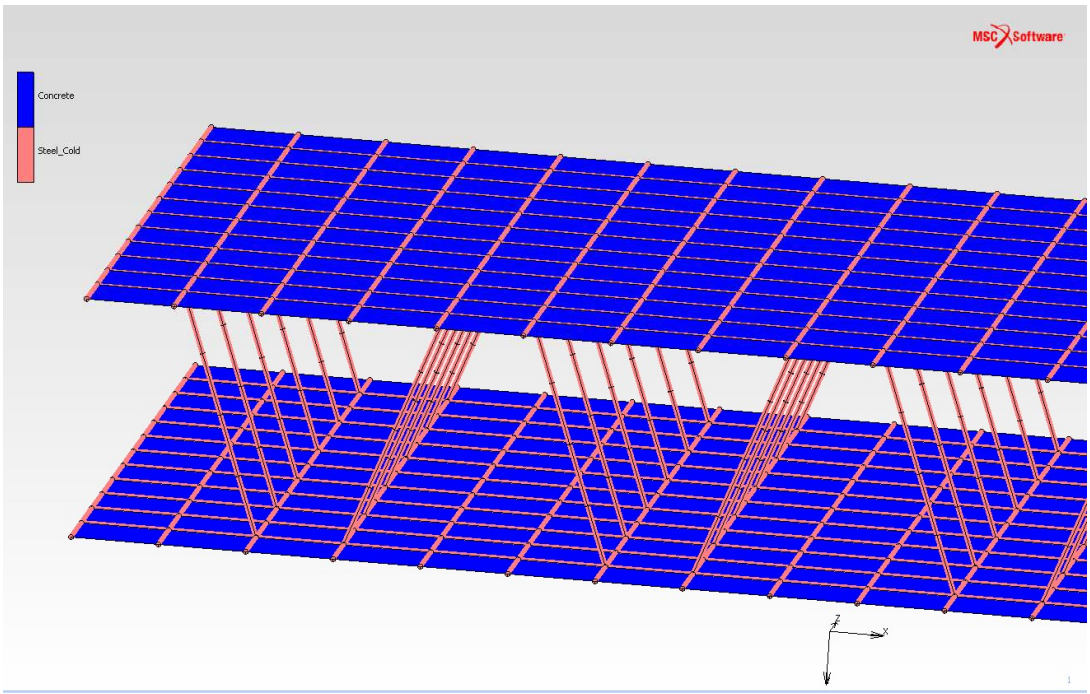

Figure (4.16): Use Quad Shell Elements Mesh for Concrete Wythe Diagonal-CSP

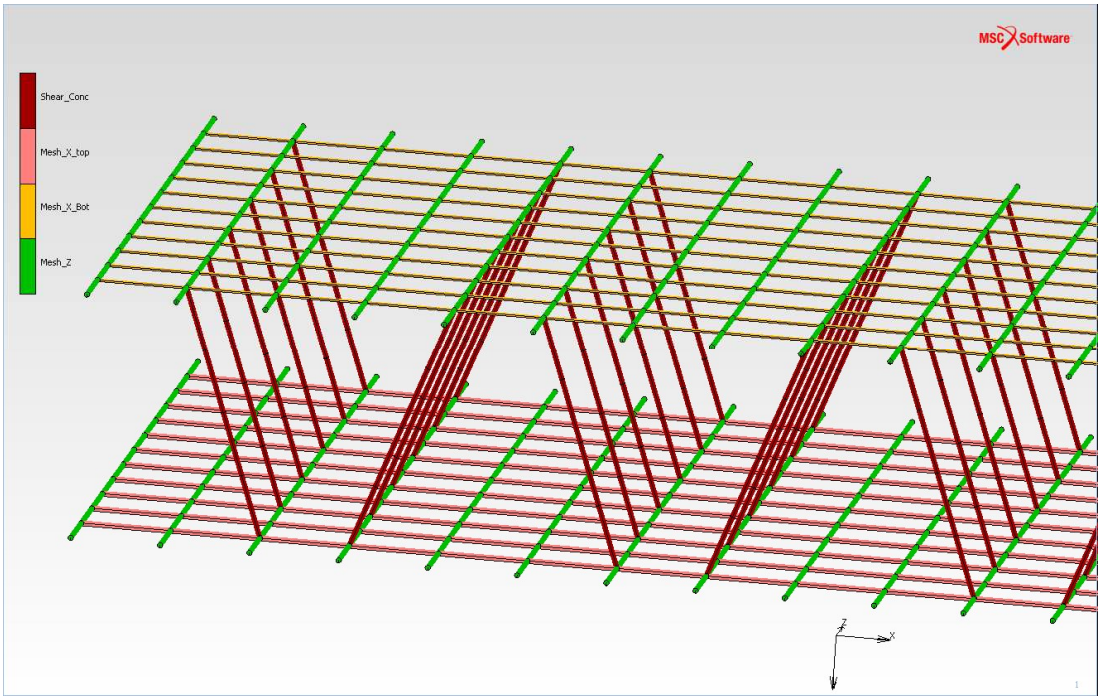

Figure (4.17): Use of 1D Beam Elements for Steel Wire Mesh and Shear Connectors

4.4.5. Loads and Boundary Conditions

As mentioned previously, one of the important step in numerical modeling of an experiment is defining the correct boundary condition representing the actual test. In the experiment, each slab specimen had 6 inches of foam burnt from each side and connected with rebars that would act as hooks that would enable the slabs to be mobilized using cranes on the test date as seen in Figure (4.18). Later each side was filled with mortar left to cure in order to allow the rebars to be firmly fixated to the specimens as seen in Figure (4.19). The specimens also had 2 inches of foam burnt along the length of the specimens and mortar applied to these areas. The reason for burning the foam and applying the mortar to these sections was in order to produce a volume between those areas that would be suitable for the mortar application. [11]

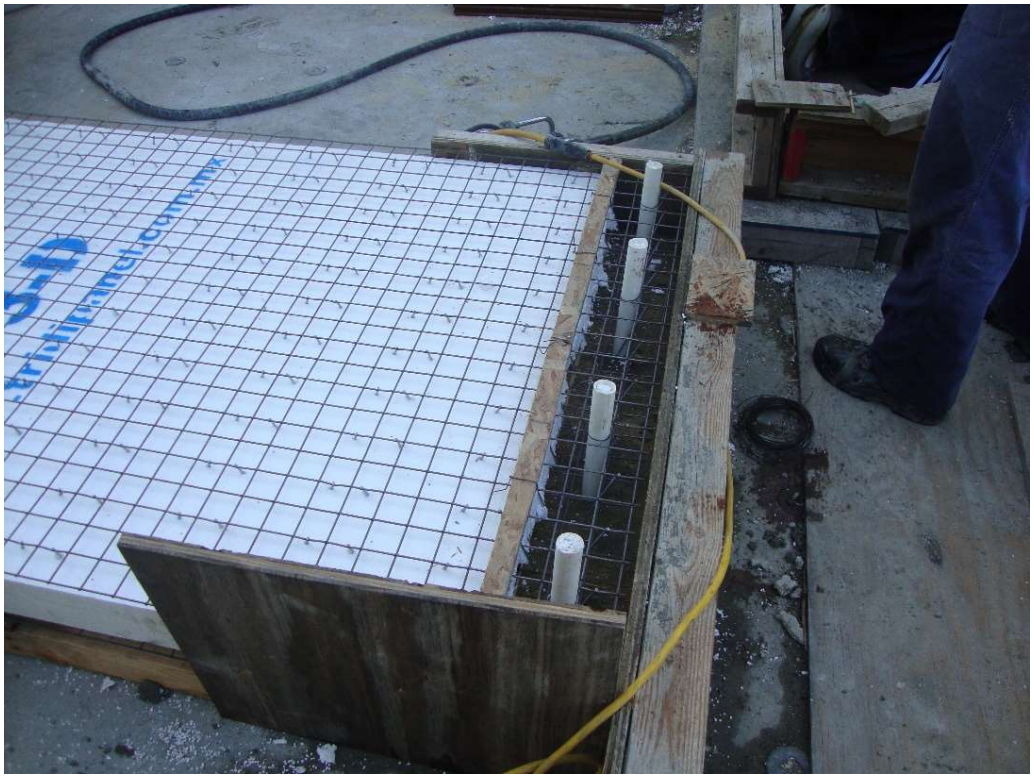

Figure (4.18): The Fixated Part on Each side of Diagonal-CSP

Figure (4.19): Each Side of Diagonal-CSP was filled with Mortar

These relative rigid parts on each side of the panel, although they were created for mobilization of the panels but they have an important effect on the interaction between the two layers of the panel on each side. It acts as a rigid surface connecting the two layers on each side. As a result, both layers will move and rotate together on each side. The influence of this effect is observed at the failure of the specimen in Figure (4.20). Similarly, in the FEM model, a rigid link called RBE2 (Rigid Beam Element) in MARC is used to link the 6 degrees of freedom (3 rotational and 3 translational) of the nodes at the end of the specimen with a single master node. As shown in Figure (4.20) each end of the specimen was rested on steel supports to simulate simple supported slab. However, it should be noted that each end of the slab can be lifted and rotated as the load is being applied in the setup of the experiment in the lab. As it can also be seen at failure in Figure (4.20), the ends of the panel had rotated in the direction of the load that was applied. Therefore, in the FEM, to accurately simulate this support system, rigid surfaces were used that were in contact

with the panel. The interaction between the support and the panel was set to ″Touching″ only to accurately simulate the experiment. This means, preventing elements on top of rigid surface from moving downward only, and allowing them to separate and rotate freely.

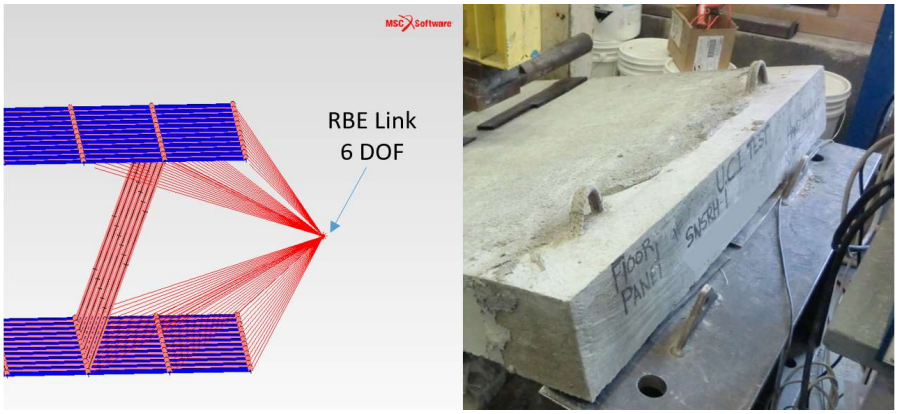

Figure (4.20): Simulating the fixation at each end using RBR Link.

In the experiment, the monotonic unidirectional load was applied, via a steel transfer beam connected to two steel cylinders applying the load to the specimen 380mm (15″) away from the center of specimen as seen in Figure (4.21). In order to accurately model the loading, a rigid surface is used in FEM, at the location of cylinders to move in the direction of application of the load, in displacement controlled method.

In this experiment cracking of the mortar and buckling of steel shear connectors cause sudden drops of stiffness. Since Displacement Control Method can capture the sudden drops of stiffness under application of load it was used rather than Force Control Method for the above analysis. Force control method does not converge numerically in the above situation. The advantage of force control method is in simulations where the load should follow the deformed body. In this experiment since the loads are applied through a rigid body there is no advantage of using force control method.

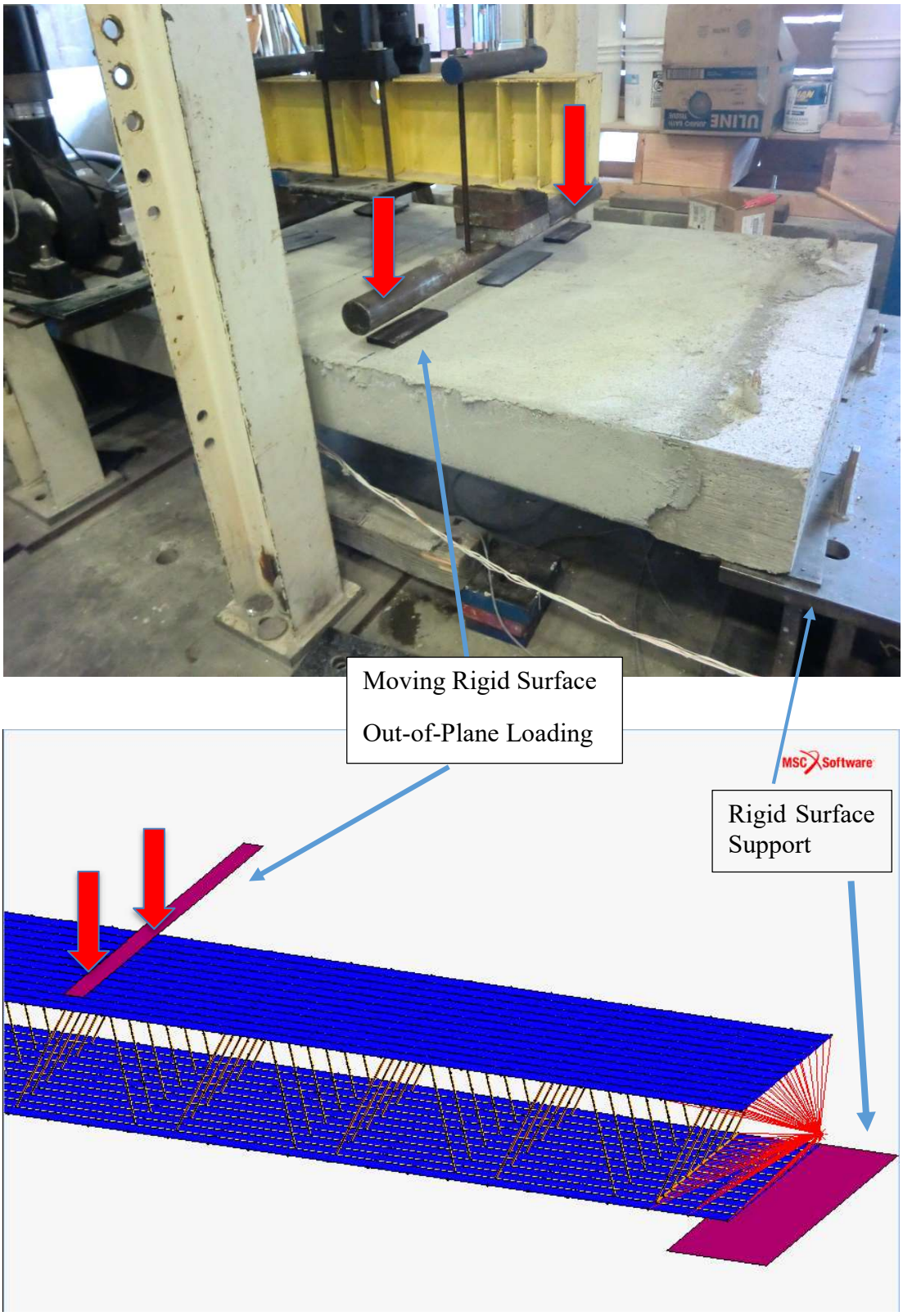

Figure (4.21): Setup of Support and Load for The Experiment and Numerical Modeling

4.4.5.1. *Symmetric Boundary Condition*

Since there are two planes of symmetry in the setup of this experiment along X-Axis and Z-Axis as shown in Figure (4.22), only one quarter of the specimen is modeled in the simulation CSP. This helps to decrease the analysis time dramatically. The symmetric boundary condition is defined along the axis of symmetry. Since the nodes of quadrilateral elements have 6 DOF, the X-Axis symmetry boundary condition limits the X-axis displacement and rotation about Z-axis for the nodes in the symmetric plane. Likewise, the Z-axis boundary condition, limits the displacement along the Z-axis direction, rotation about X-axis for the nodes along Z-plane symmetric boundary condition.

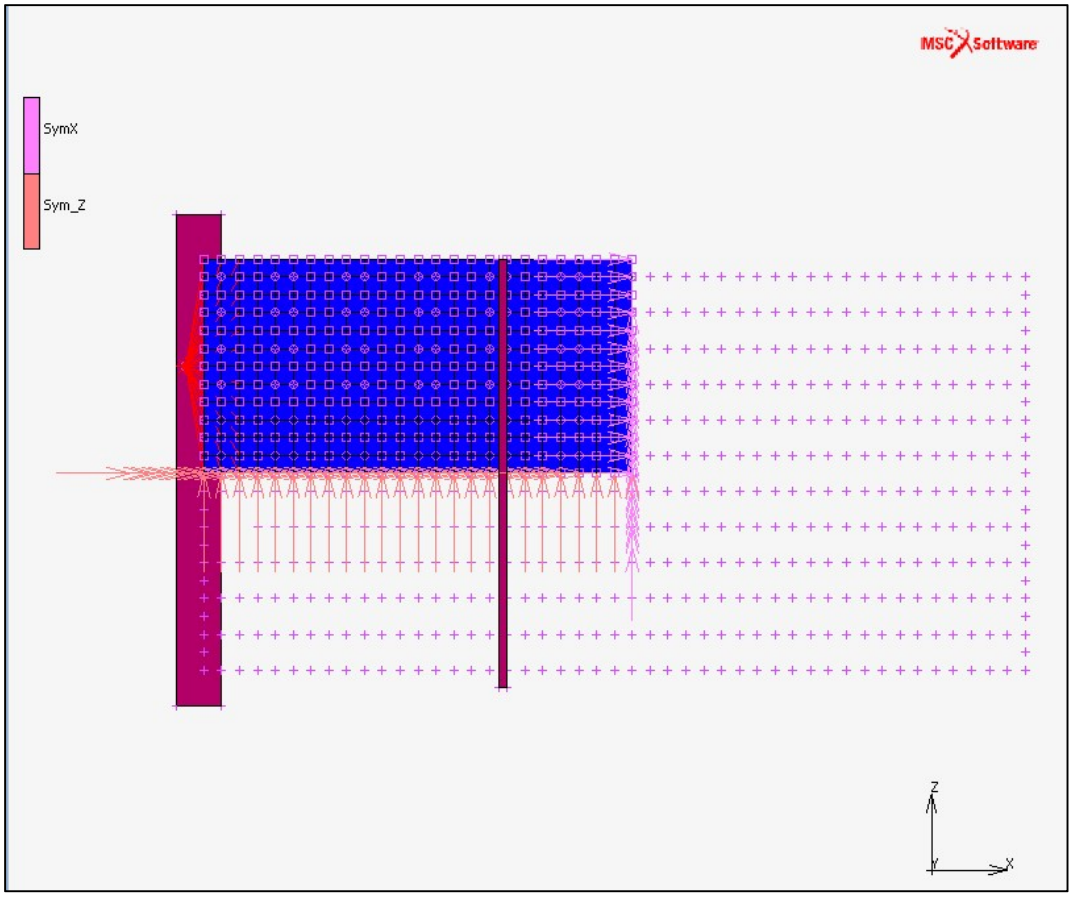

Figure (4.22): Modeling One Quarter of the Specimen using Symmetric BCs

4.4.6. Define Loadcase and Analysis Setup

In order to run the Finite Element Analysis (FEA) a loadcase should be defined for the simulation. Since the loading was monotonic in the experiment, a quasi-static analysis is defined to run the simulation for duration of 1 unit. An adaptive time step setting (Multi-Criteria) is utilized due to nonlinearity of the material and geometry of the model. Initial time step of 0.001 is defined with minimum fraction of loadcase time of 1e-5 and maximum fraction of time step 0.1. However, later this maximum fraction of time step was decreased to 0.05 since there were many drops of stiffness in the initial result of the analysis. In order to have smoother and more accurate load displacement curve, the maximum fraction of time step was decreased to 0.05 to limit the step sizes in the quasi static analysis. Input of these settings can be seen in Figure (4.23) which is used in analysis of this simulation.

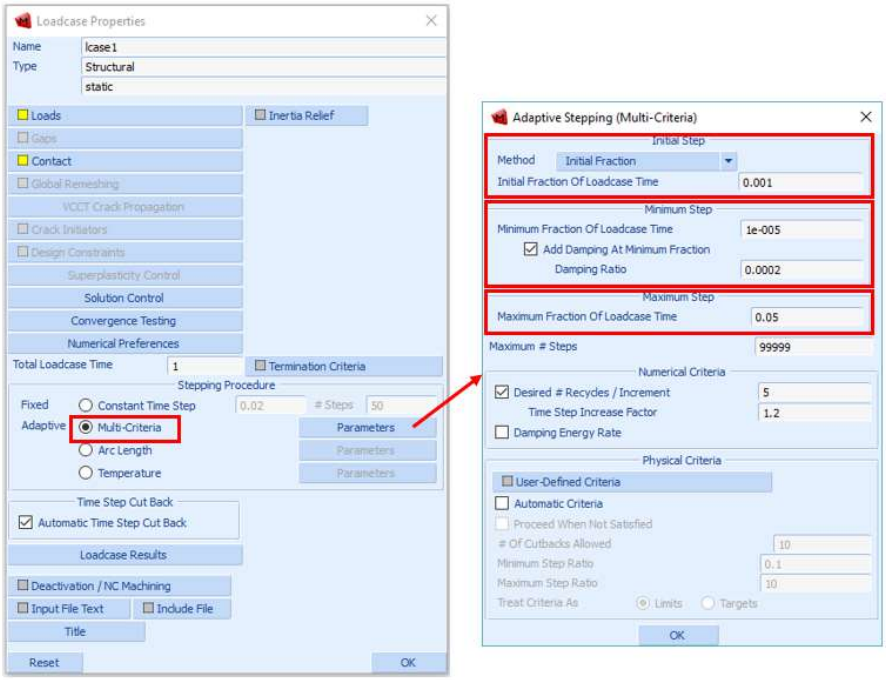

Figure (4.23): Define Loadcase as Adaptive Stepping in MENTAT

4.4.6.1. *Results and Comparison to Experimental Results*

4.4.6.2. *Cracking of the Mortar*

The result from post processing the FEM analysis are compared to results from experiment photos and data from actuator. Looking at the Equivalent cracking strain at the failure of the specimen in simulation, a combination of shear failure at location where the load is being applied and flexural failure in the middle of tension side, where the moment is maximum. These cracking locations from FEA results are comparable to the cracking location observed in the experiment as seen in Figure (4.24)

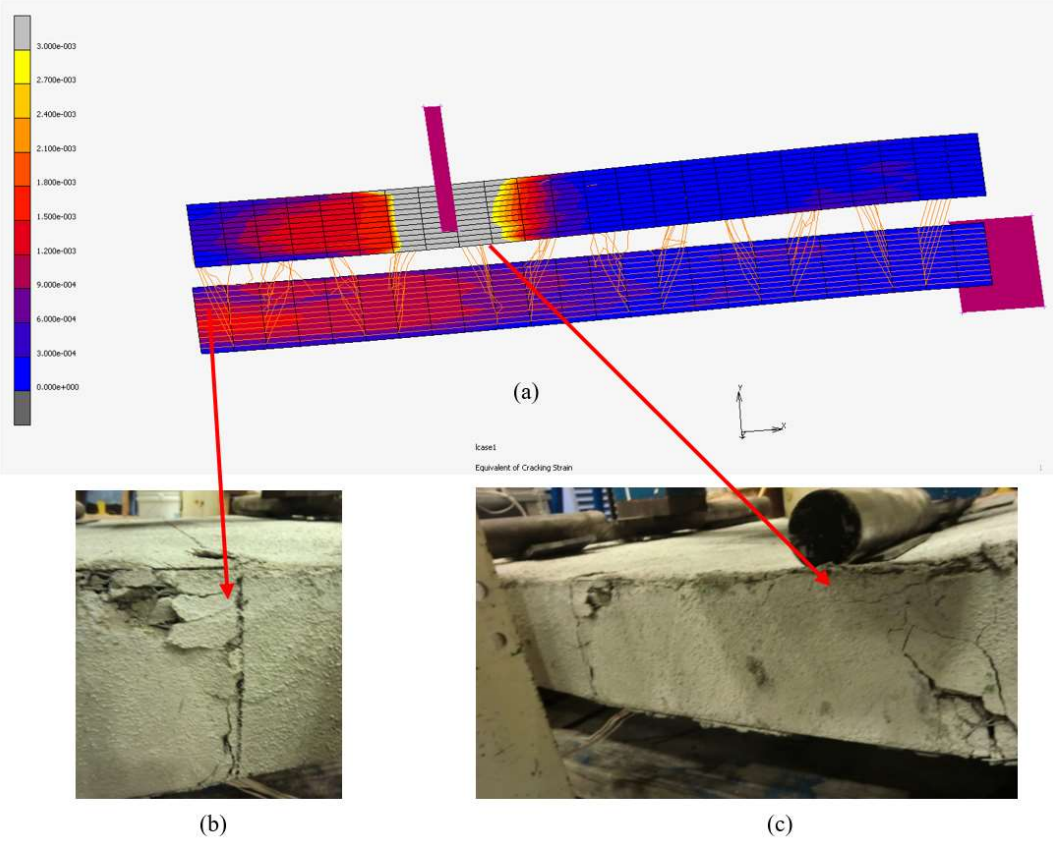

Figure (4.24): Comparing Numerical Modeling Results to Actual Experiment at Ultimate Load. (a) Results of Equivalent Cracking Strain of FEM on One Quarter of Full Specimen (b) Location of Flexural Cracking at Center of the Specimen. (c) Location of Shear Cracking at 45° Degree.

4.4.6.3. *Buckling of the Steel Shear Connectors*

In addition to the experiment, the result of numerical modeling shows that the steel shear connectors are buckling under the load along with the cracking of concrete elements. The buckling of is shear connectors is due to axial compression load resisted by these members. The axial load is induced due to resisting the vertical shear load but also due to resisting he conjugate shear load in plane of the CSP. As the sandwich panel undergo out of plane loading, a conjugate shear force (secondary shear force) is generated due to the applied load as shown in Figure (4.25). This load is resisted by the shear connectors as half of the connectors resisting this load in compression and other half in tension. As a result, the members in compression are prone to buckling. Until the failure of steel shear connectors, the CSP is working in full composite action, where top layer is in tension and bottom layer is in compression. After the buckling of steel shear connectors, there is sudden drop in resistance due unstably of the structure. The displacement-controlled Loading analysis used in FEM analysis captures this failure but analysis continues as the shear connectors snaps through a stable configuration and the analysis continues. However, after this failure the CSP is not in full composite action mode anymore and has lost its initial stiffness and the slope of the Load-displacement curve decreases as it is shown in Figure (4.26). After this point the CSP is working in partially or non-composite action. At the ultimate load, 2164 kgf/m^2 (443 psf).

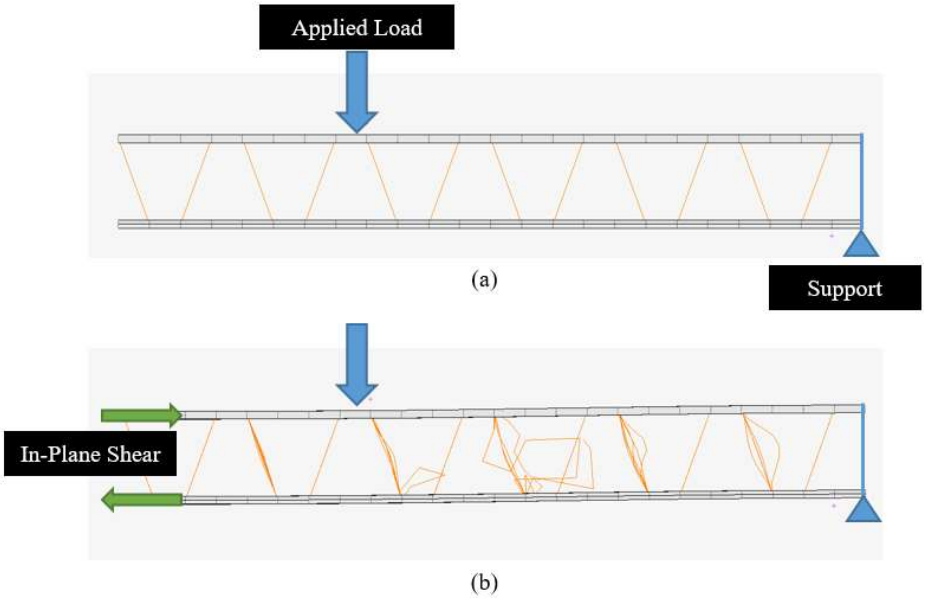

Figure (4.25): (a) Initial Setup (b) Buckling of Steel Shear Connectors due to Horizontal Shear Load (Conjugate Shear)

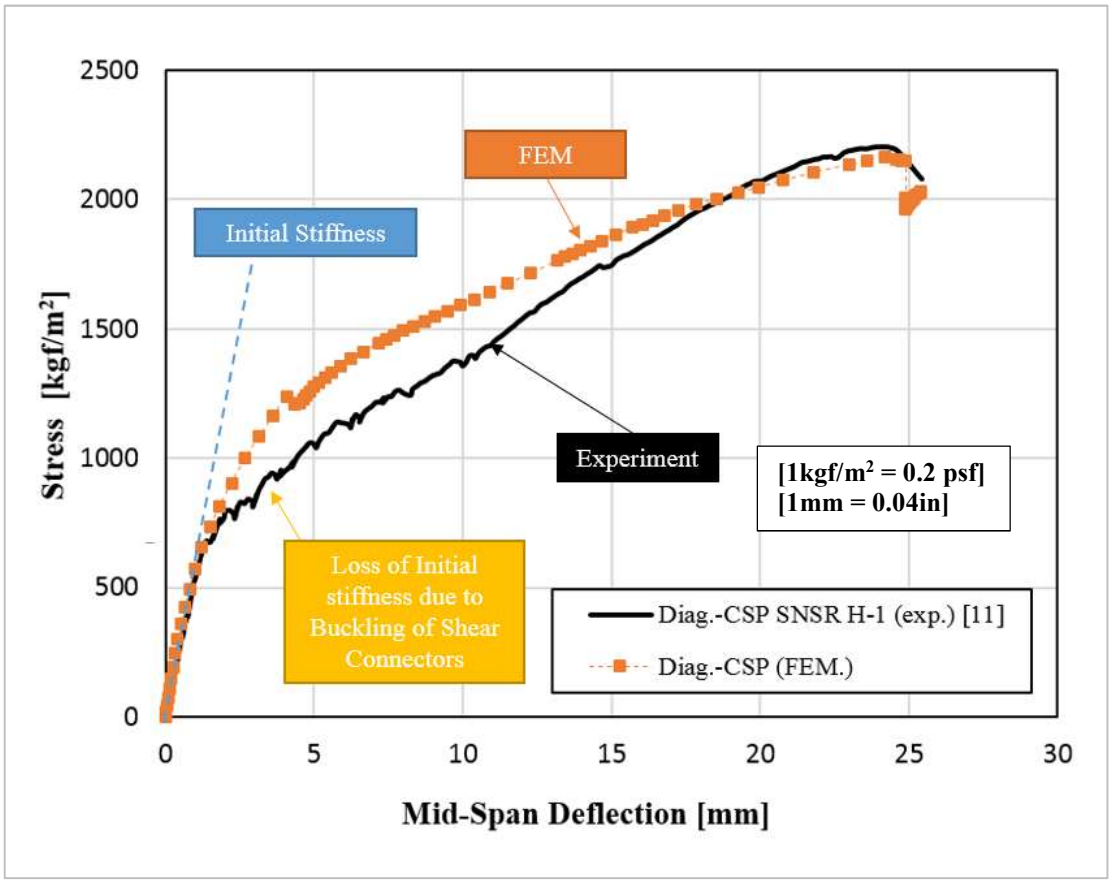

Figure (4.26): Load-Displacement of FEM and Experiment for Diagonal-CSP

4.5. Performance Evaluation of Optimized-CSP using Numerical Modeling

Based on the result of the previous chapter on optimization of CSP using genetic algorithm, an example of light weight and energy efficient design configuration of CSP is identified that meets the limits defined by the structural engineering's codes. In order to evaluate the performance of Optimized-CSP to commercially available CSP in the market that was previously tested at UCI, a panel with similar dimensions of Diagonal-CSP is designed using the shear connector configuration obtained from optimization in Chapter 3 hereby called "Optimized-CSP" This new design of CSP, is optimized under out of plane loading in four-point loading system where the cost of panel (Cost of Material and Cost of Energy Loss) is minimized while meeting the deflection limit defined by ACI-318 Table 24.2.2 Code. (The linear calculation and other design checks have been performed in Appendix D). Finally, in order to compare the performance of optimized design of shear connectors in the design of Optimized-CSP to previously tested specimen, similar thickness of mortar is used on top and bottom layer. A 50mm (2″) of mortar on top, 38mm (1.5″) mortar on the bottom. The final design for Optimized-CSP is shown in the Figure (4.27).

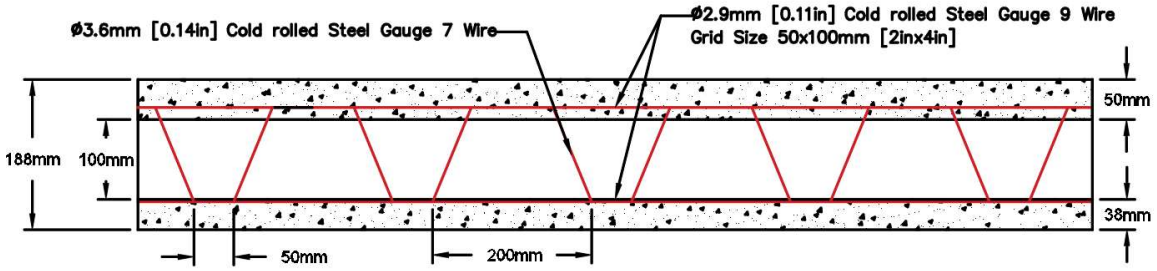

Figure (4.27): Dimension and Cold Rolled Steel Reinforcement used for Optimized-CSP

Using the numerical modeling methodology for CSP that explained in the previous section a quarter of Optimized-CSP is modeled with the exact geometric, material properties and

similar boundary condition as Diagonal-CSP in MSC MENTAT as shown in the Figure (4.28). Next it was analyzed using MSC MARC, cracking location have been identified Figure (4.29). The load displacement curve is obtained and compared with Parallel-CSP and Diagonal-CSP in Figure (4.30).

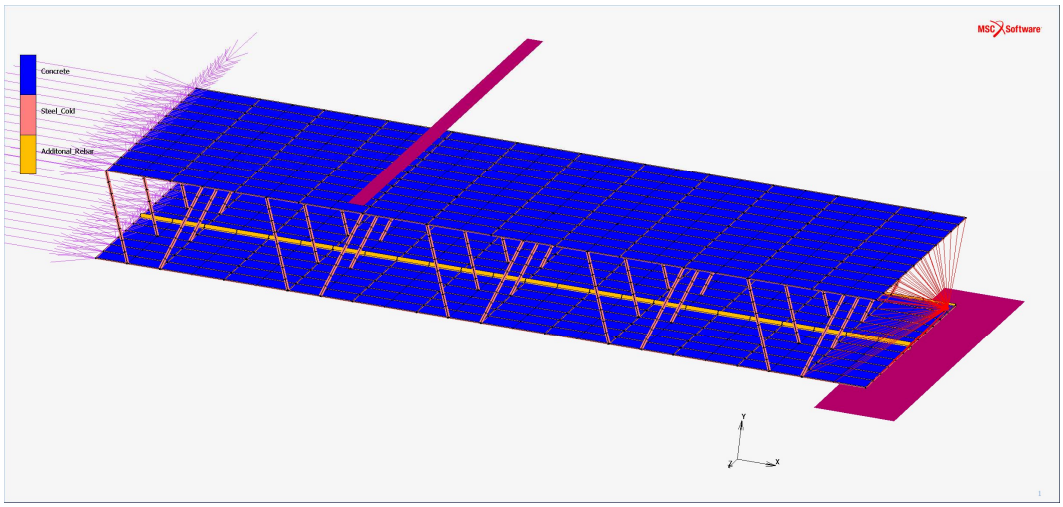

Figure (4.28): Numerical Model of Optimized-CSP with Defined BCs

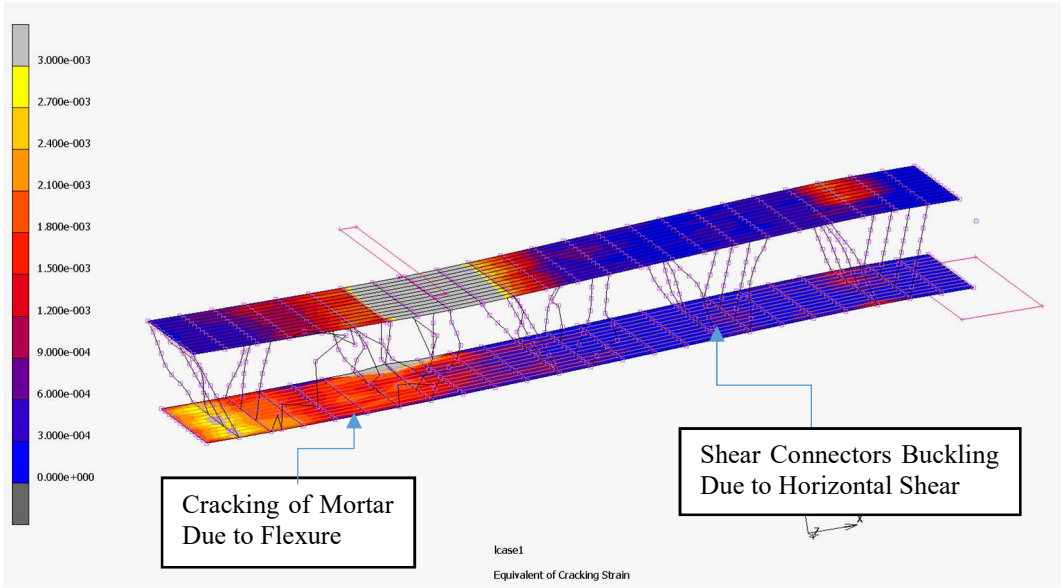

Figure (4.29): Cracking Strain Locations and Buckling of Shear connectors in Results of FEA of Optimized CSP at Ultimate Load

In evaluating the performance of Optimized-CSP, cracking of mortar due to flexure at the middle of span is observed, and there is also buckling of shear connectors due to both horizontal and vertical shear, as seen in Figure (4.29). Similar type of failures are observed in both Diagonal-CSP and Optimized-CSP, where both failed in the middle due to flexure. This translates into proper transfer of shear from the top to the bottom panel in both designs, even though, fewer shear connectors have been used in the Optimized-CSP. In the design of Optimized-CSP 48 shear connectors per m^2 of wire gauge 7 with diameter of 3.5mm [0.11in] is used that results in 1.8 kg [4.09 lbs] while in the design of Diagonal-CSP, 100 shear connectors per m^2 of wire gauge 9 with diameter of 2.9mm [0.09in] was used that results in 2.2kg [4.88lbs]. Comparison of the two designs yields that Optimized-CSP uses 18% less sheer connectors. Consequently, the thermal resistance of Optimized-CSP has improved by 15.78% compared to Diagonal-CSP. In the design of Parallel-CSP, there are only 23 shear connectors per m^2 of wire gauge 9, with diameter of 2.9mm [0.11in] is used that results in 0.72 kg [1.60 lbs] of steel which provides 80% better thermal resistance in comparison to Optimized-CSP, however, as it is seen in Figure (4.30), it has much lower capacity and stiffness compare to the other two designs due to its parallel shear connectors and lack of shear transfer and composite action as it was mentioned in section 4.2. Furthermore, the design of Parallel-CSP has 16.0cm [6.3in] foam insulation, compare to 10.0cm [4.0in] foam used in the design of Optimized-CSP, which reflective on total required depth of panel and total cost of the panel. As it is detailed in Table (4.2) the cost of the insulation foam is approximately 50% of total cost of the panel and 16.0cm [6.3in] foam cost 47% more expensive than 10.0cm [4.0in] with the same density.

The load-displacement curve in Figure (4.30), shows that initial stiffness of Optimized-CSP was held up to loading stress of 1950 kgf/m^2 [390 psf] corresponding to 8.0mm [0.3in] deflection before stiffness of the panel drops. In comparison in Diagonal-CSP, where the initial stiffness was held up to 1250 kgf/m^2 [250psf] corresponding to 4mm [0.15in] deflection before stiffness of the panel drops. The stiffness of the panel is important when the design is checked by the code for serviceability of floor or pounding effecting in roof according to ACI Table 24.2.2.

Another important design evaluation factor that is extracted from the Figure (4.30) is the relative modulus of the toughness. The area under the load-displacement curve is directly proportional to the modulus toughness. Comparing the areas under the three curves in Figure (4.30), shows that the modulus of toughness for the Optimized-CSP is 40% higher than Diagonal-CSP, and 800% higher than Parallel-CSP design. This value corresponds to the maximum amount of strain energy per unit volume the specimen can absorb. Certainly, modulus of toughness becomes an important factor when designing robust sandwich panels that should sustain accidental overload, earthquake or similar events.

Finally, illustrated in Figure (4.30) and detailed in Table (4.2), the Optimized-CSP ultimate loading capacity is 30.2% higher than Diagonal-CSP, and more than 7times higher than Parallel-CSP design. This is achieved by efficiently distributing the shear connectors using thicker wires with larger spacing that was obtained from the optimization process, the shear strength of the panel has improved. Additionally, reducing the number of lateral steel wires via utilizing larger the spacing between lateral steel wires, while increasing the longitudinal steel wire volume has improved the flexural strength. Furthermore, the combination of

above improvements not only improved the design performance but also reduced the total cost by 1.7% compared to Diagonal-CSP and 16.46% compared to Parallel-CSP.

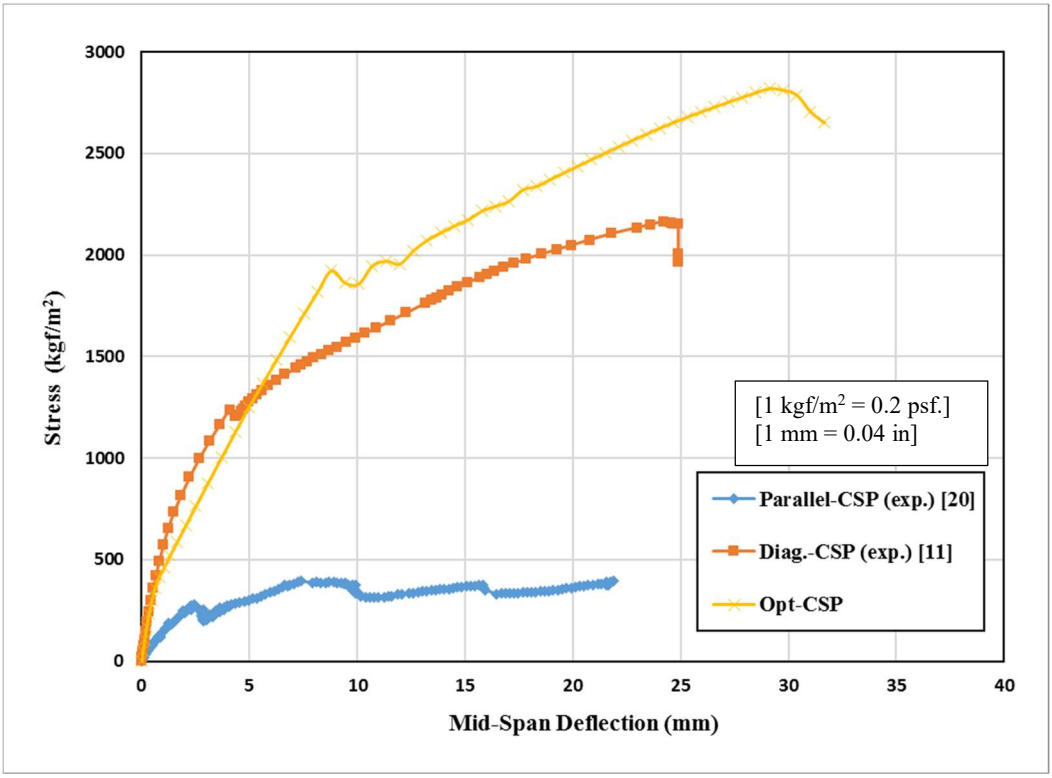

Figure (4.30): Comparison of Parallel-CSP, Diag.-CSP and Opt.-CSP

Table (4.2): Design Specification Comparison of Parallel-CSP, Diag.-CSP and Opt.-CSP

Material	Unit	Diag.-CSP	Opt.-CSP	Parallel-CSP
Steel Shear Connector Weight	**kg [lb]**	2.2 [4.88]	1.84 [4.09]	0.72 [1.60]
Steel Mesh Weight	**kg [lb]**	7.33 [16.29]	7.16 [15.90]	8.13 [18.06]
Total Steel Weight	**kg [lb]**	9.53 [21.18]	9.00 [19.99]	8.85 [19.66]
Concrete Weight	**kg [lb]**	631.1 [1391.1]	631.1 [1391.1]	631.1 [1391.1]
Foam Thickness*	**cm [in]**	10.16 [4.00]	10.16 [4.00]	16.00 [6.30]
Cost of Material	**$**	67.11	65.30	64.79
Cost of Insulation	**$**	36.56	36.56	53.84
Total Cost*	**$**	103.67	101.86	118.63
Ultimate Capacity	**kgf/m2 [psf]**	2164.0 [443.2]	2818.0 [577]	394.0 [80.7]
R-Value (Thermal Resistance)	**K.m²/W**	1.9 [10.7]	2.2 [12.8]	4.0 [22]

(1 kg = 2.2 lbs.), (1 m² K.m²/W [RSI] = 5.67 h.ft².ºF /BTU [R-Value])

* Total Cost is approximation based on the current market value, 3.4 $/kg for Steel and 0.055 $/kg for Concrete. Estimate cost of EPS foam is based 1.21m x 2.43m [48"x98"] sheet foam with 0.90 kg [1lb] density from www.usafoam.com. For 10.1cm [4.0″] and 15.2cm [6.0″] thick foam estimated prices are 36.56$/sheet and 53.84$/sheet respectively in the current US market.

4.6. Performance Evaluation of CSP Walls under In-plane Compression Loading

4.6.1. Parallel-CSP under In-Plane Compression Loading

In 2014 a series of 6 CSP wall specimens with horizontal shear connectors were fabricated and tested in UCI Structural Engineering Testing Hall (SETH) lab. [31] The purpose of that structural evaluation test program was to assess the compression performance of CSP wall panel systems. Two different wall dimensions were evaluated. 1.20m X 2.29m X 15.24 cm (4′ X 7.5′ X 6″) (*L X H X T)* and 1.20m X 4.11m X 15.24 cm (4′ X 13.5′ X 6″) (*L X H X T).*

All wall specimens tested in the evaluation program utilized a foam core with a thickness of 80mm (3.15″). A clear spacing or gap of 15mm (0.60″) was maintained between the wire mesh surface and the exterior surface of the foam core on both side of the panel. A constant thickness of 2.54cm (1”) mortar was applied on both side of the CSP panel. After application of the cementitious mortar, the total thickness of the various wall specimens was 15cm (6″).

In-plane axial loading was applied at a constant rate on top of the wall using hydraulic jacks until failure occurred. As shown in Figure (4.31), the load was applied across the capital at the center of the wall specimen. More detail of the experiments is available in the report published by Bottelo et al. in 2015. [34].

The results from experiment of testing Parallel-CSP is used to develop a reliable numerical modeling methodology that accurately mimics the experimental behavior of CSP and is able to predict the failure criteria comparable to the experimental results in finding strength

and cracking locations. Using similar boundary condition, the Optimized-CSP is modeled and its performance is compared to CSP panels tested at UCI.

4.6.1.1. *FEM Loads and Boundary Conditions*

In the experiment, as shown in Figure (4.31), the load was applied across the capital at the center of the wall specimen. Similarly, in the FEM model, a rigid link called RBE2 in MARC is used to transfer the load to the nodes at the top of the wall simulate the experiment. A master node at the center location of the wall and reaction and displacement were read off from that location. These rigid links are shown in red in Figure (4.31)

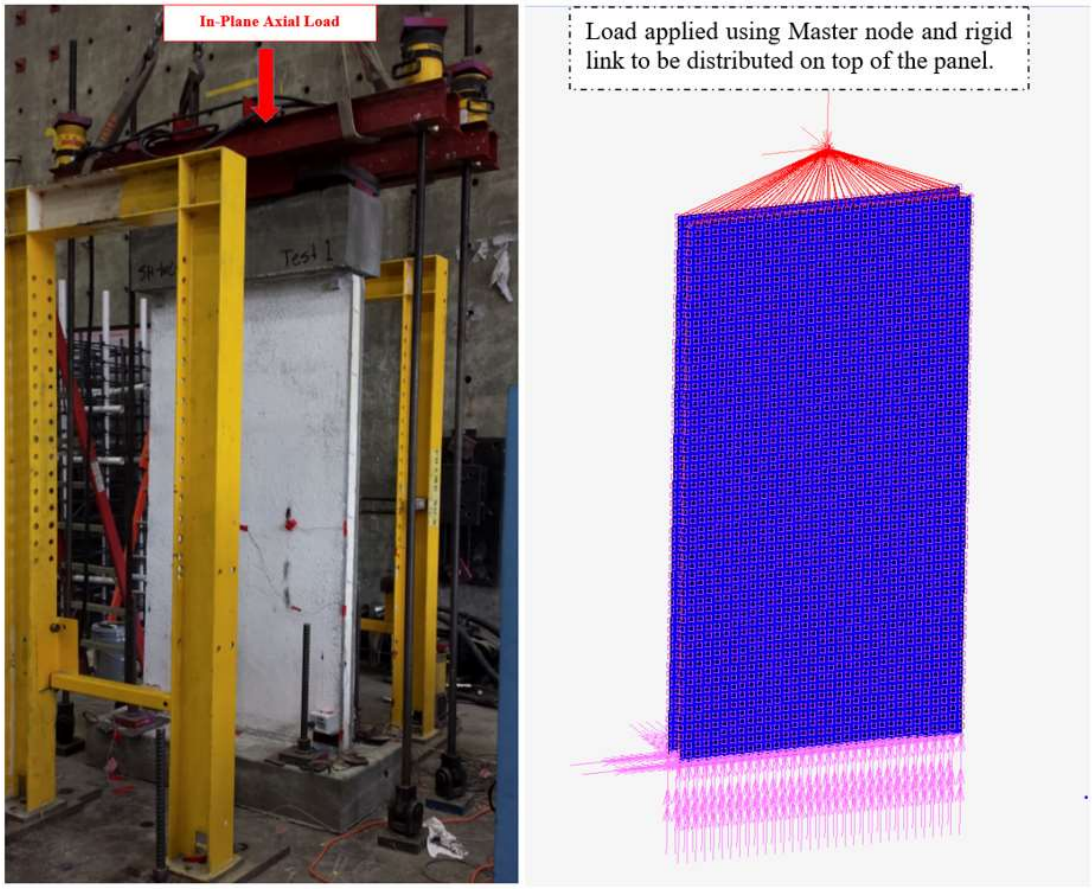

Figure (4.31): Left: Typical Wall Test Setup under In-Plane Axial Loading at UCI, Right: FEM Test setup using MSC MENTAT and MARC.

This master node was also restricted to move in other translational direction and however free to rotate in three rotational degrees of freedom. A 25mm (1.00”) eccentricity equivalent to one-sixth of the CSP thickness is used for applying to in-plane axial load according to Benayoune et al. in evaluating CSP panel subjected to in-plane axial loading. [35] The bottom nodes of the panel were fixed in both translational and rotational degrees of freedom. The loading the FEM model is displacement controlled up-to failure to have better stability and convergent in the analysis. Due to the cracking of the mortar, the model would lose its stability under force controlled boundary condition.

4.6.1.2. *Results and Comparison to Experimental Results*

The results from post processing the FEM analysis are compared to results from experiment photos and data from actuators. According to the observation of experiment of Parallel-CSP done at UCI by Botello et al. [36], the failure of the specimen was sudden with no apparent cracks before complete failure of the wall. Figure (4.32) on right shows the specimen after failure had occurred. The result of FEA in Figure (4.32) on left shows distribution of cracks obtained from the numerical models as compared the actual cracks pattern observed during the experiment for the 8-foot walls. As shown in this figure, a well correlation between the numerical and the experimental results has been achieved. The numerical load-displacement curve obtained from the numerical model is plotted against the three experimental load-displacement curves for the three 8-foot walls that were evaluated in this phase (refer to Figure (4.33)). The difference in the results of three experiment may be due to the This difference may be due to the unintended eccentricity occurring in the experimental.

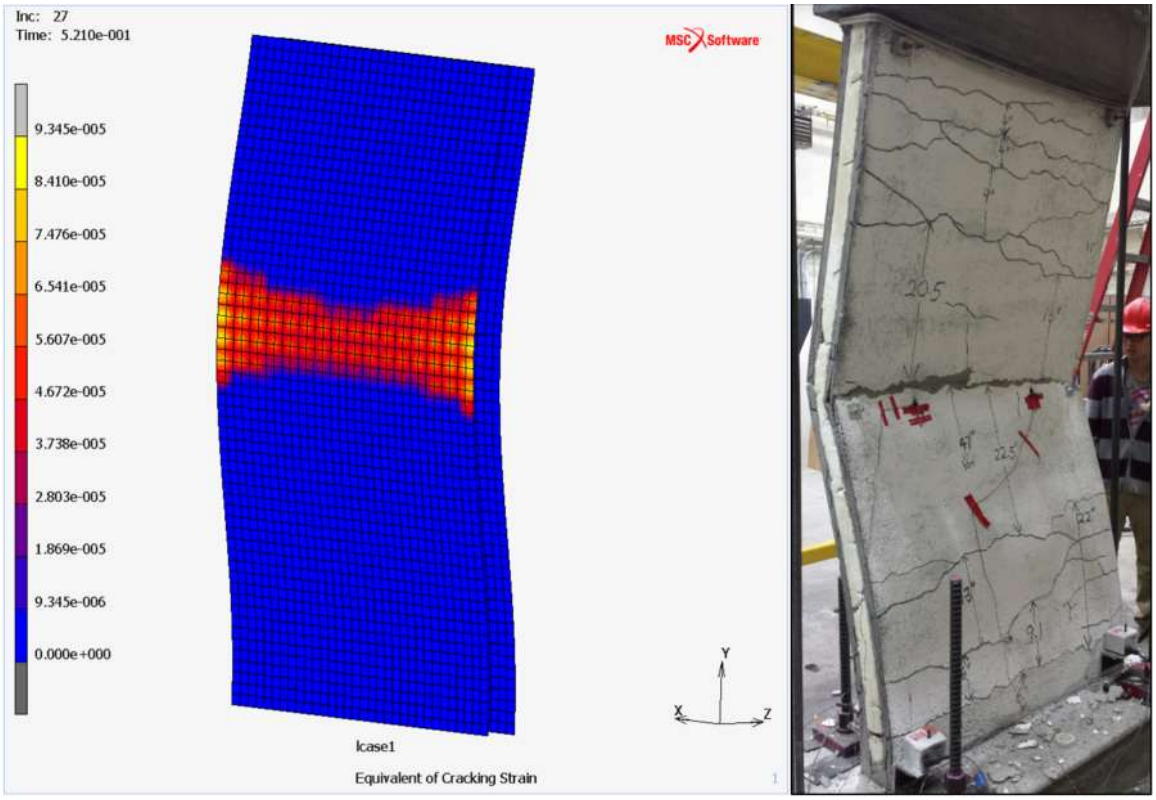

Figure (4.32): Cracking Strain location in FEM Analysis (MSC.Marc) Matches the Location of Failures for the 2.45m (8 foot) Walls in Experiments

The result FEM shows a linear behavior up to cracking and suddenly in increment 23, there is a sudden drop in the load resisted on the wall. Figure (4.32) is a screenshot from this increment. This step was captured by the FEA analysis since the loading was set to displacement control. In the next increment the numerical result of the FEA analysis did not converge and the analysis stops. Similar behavior was published in the observations of the experiment that failure was sudden with no apparent cracks before complete failure of the wall. [36]. Furthermore, in the observation report published by Botello et al. at UCI, before the collapse of Parallel-CSP specimen, right before buckling, a loud sound of

separation of welding between the horizontal shear connectors and the two wire mesh faces was heard.

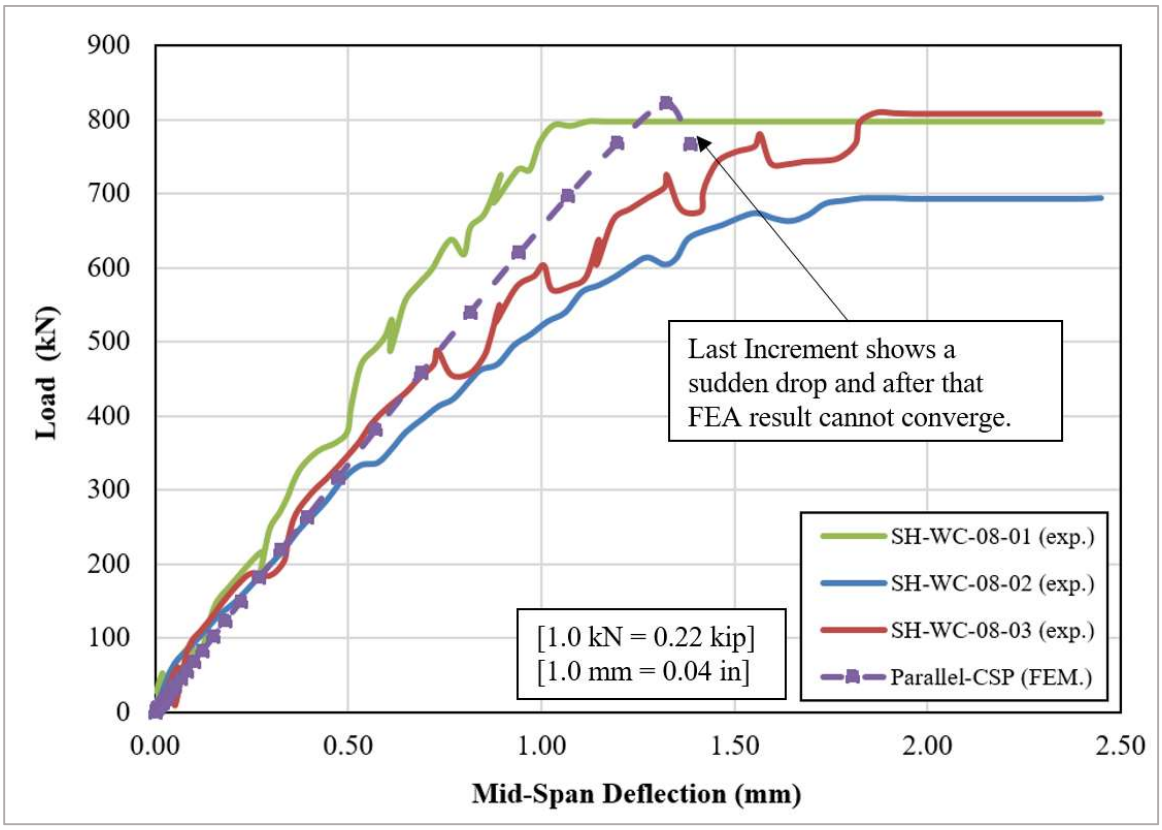

Figure (4.33): Numerical Analysis (FEM) Complies with Experimental Results Extracted in Load vs. Displacement Plot for 8-Foot Wall Specimens

Upon separation of horizontal shear connector from two wire mesh faces, the composite action in Parallel-CSP is lost. As a result, each face of the sandwich panel works independently and reduce drastically the capacity of wall. After the composite action was missing the load on the panels was already way above their buckling capacity and as a result a sudden failure of the wall was observed. Using structural analysis calculation, the failure of the horizontal shear connectors is justified during the experiment. the similar behavior of the wall is expected. Due to the unintended eccentricity occurring in the

experimental, a moment is applied to the wall in the same time as applying the in-plane axial loading. This moment creates horizontal shear across the two panel as shown in Figure (4.34). The eccentricity that resulted in failing of shear connectors is analytically calculated in Appendix D. The result is 12.55m [0.5in] which is within the range of allowable maximum eccentricity which is one-sixth of the thickness of the wall. [35]

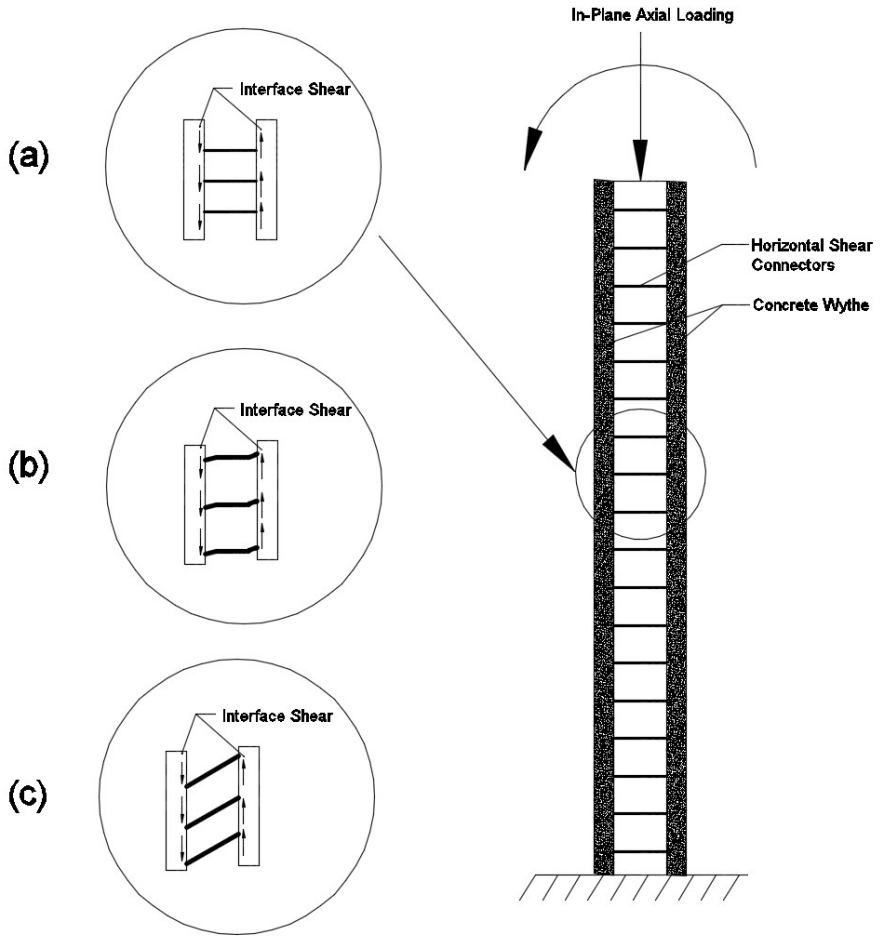

Figure (4.34): Behavior of Horizontal Shear connectors under In-Plane Axial Loading. (a) Horizontal Shear Connectors Before application of Load. (b) Horizontal Shear Connectors as Beam Element Resisting Bending. (c) Horizontal Shear Connectors as Link element resisting shear before failure.

In structural evaluation of Parallel CSP by Mosallam et al. (2015) the capacity of steel horizontal shear connector in Parallel-CSP is calculated using Maximum Distortion Energy Theory (von Mises' Yield Criterion) for combined Moment and shear as in Eq. 13. The bending and shear stress for wires is calculated using Eq 14 and Eq. 15 accordingly and inserted into Eq. 13. Using the yielding strength of Cold rolled steel wires used in Parallel-CSP, the capacity of each steel wires is calculated. The calculation is detailed in Appendix D.

$$\boldsymbol{\sigma} = \sqrt{\boldsymbol{\sigma_x^2} + \boldsymbol{3\tau_{xy}^2}} \qquad \text{Eq. 13}$$

$$\boldsymbol{\sigma_x} = \frac{\boldsymbol{MY}}{\boldsymbol{I_{wire}}} = \frac{\boldsymbol{0.5\,F1\,l_{wire}\,Y}}{\boldsymbol{I_{wire}}} \qquad \text{Eq. 14}$$

$$\boldsymbol{\tau_{xy}} = \frac{\boldsymbol{4\,F1}}{\boldsymbol{3\,A}} \qquad \text{Eq. 15}$$

However, since the bending stiffness of these wires are small and the wires can be easily deformed, therefore wires work more as a link element between the two faces of the panel as shown in case (c) in Figure (4.34). Therefore, the capacity of the wires is calculated using its shear capacity only.

$$\boldsymbol{\sigma} = \sqrt{\boldsymbol{3\tau_{xy}^2}} \qquad \text{Eq. 16}$$

The result of analytical study in Appendix D, further justifies the failure of shear connectors in Parallel-CSP and early loss of composite action, as it was observed in the full-scale experiment. As a result, the panel failed at 800kN [180kips], where through full composite action of wall, the panel should have sustained 2606 kN [586 kips]. On the other extreme situation, if there were no composite action and calculating with assumption of two

separate walls with similar dimensions, the capacity of would reduce to 293 kN [66 kips]. Figure (4.35) shows the capacity of Parallel-CSP wall in different failure modes.

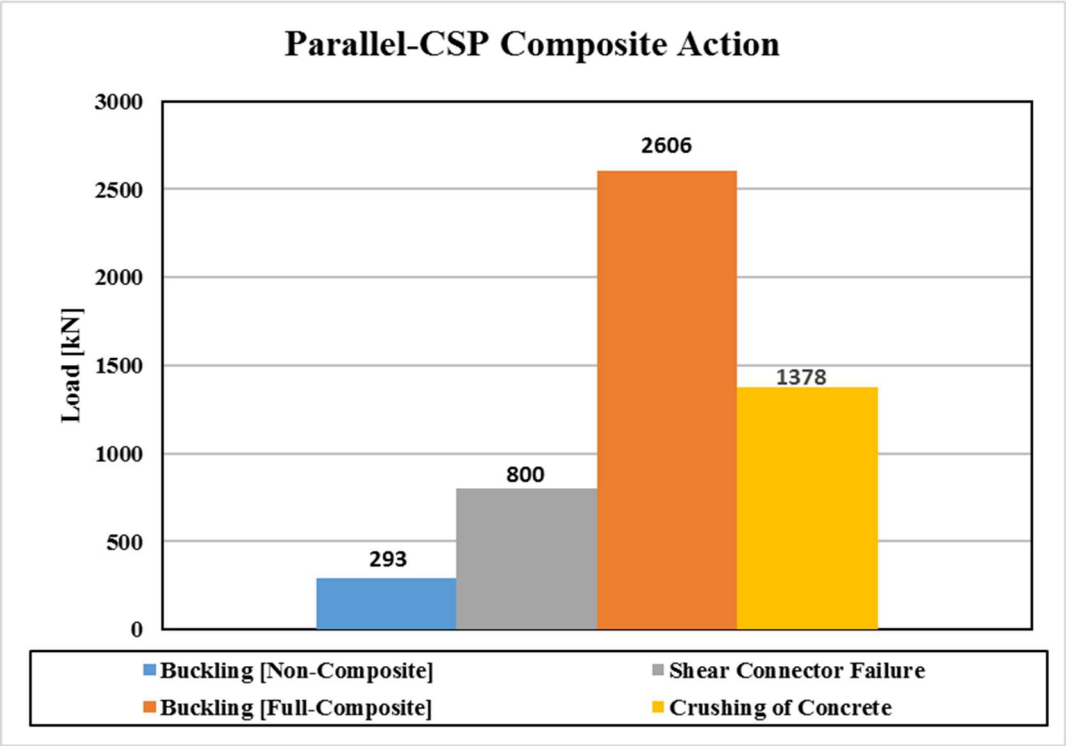

*[1 kN = 0.22 kips]

Figure (4.35): Different Failure Modes of Parallel-CSP Wall under In-Plane Axial Load

As both result of full-scale experiment at UCI and numerical modeling predicted, the Parallel-CSP wall failed due to buckling at about 800kN [180 kips]. As it was observed in the experiment and further investigated in analytical calculation in Appendix D, the Parallel-CSP wall initially sustains the load up to 800kN [180 kips] without any major crack. This shows a partial composite action between the two wythe of the panel as the load has passed the 293 kN [66 kips] Non-composite capacity limit. However, at 800kN [180 kips] a loud sound was heard during the experiment and the horizontal shear connector failed. This has been further investigated in Appendix D, that this is the load that shear

connector could handle before yielding. Since the horizontal shear connectors are made from brittle cold rolled steel, loud sound and sudden failure of the wire is justified.

The failure of shear connector is due to moment exerted on the wall due to unintended eccentricity during the experiment. In Appendix D, the result indicates that only 12.5mm [0.5in] eccentricity at 800kN [180 kips] would exert enough bending on the wall that would pass the capacity of the horizontal shear connectors using (Eq. 16). This amount of unintended eccentricity is well within the code (ACI-318 11.5.3.1) which allows the one-sixth of the wall thickness eccentricity for axial loading. Upon failure of the shear connectors, the panel would work as non-composite and the capacity of the wall under in-plane axial load would drop to 293 kN [66 kips]. After the composite action was missing each face experience sufficient buckling to fail.

4.6.2. Shear Interface Strength of Diagonal Shear Connectors

A similar size of panel is analyzed in this section with Diagonal-CSP and Optimized-CSP using same boundary condition and loading that was used in the full-scale experiment of Parallel-CSP that was tested at UCI. Upon evaluation of the strength and failure modes of this panel, the result is compared to the strength of other CSP panels designs.

As it was discussed in the previous section, one important factor that controls the strength of the sandwich panel under in-plane axial loading is the strength of shear connectors and composite action between the two wythe of the panel. In order to evaluate the shear capacity of diagonal shear connectors within the sandwich panel which have been utilized in both design of Diagonal-CSP and Optimized-CSP Nihawan [37], has proposed the following equation.

$F_h = A_s N \cos(\theta) (f_{st} + f_{sc})/2$ *Eq. 17*

where, F_h = *Interface Shear Load;*

A_s = area of shear connectors;

N = total number of truss members;

θ = angle in degrees between web member and horizontal plane ;

f_{st} = allowable stress in tension member;

f_{sc} = allowable stress in compression member

As it was discussed in the previous section, the CSP under in-plane axial loading should sustain allowable unintended eccentricity while it is resisting the axial loading. The allowable unintended eccentricity by (ACI 318 11.5.3.1) is one-sixth of the panel thickness. However, in order to compare the result of analysis in this section for Diagonal-CSP with the Parallel-CSP that was presented in the previous section, exact similar 12.5mm [0.5in] eccentricity is considered during axial loading the Diagonal-CSP Panel.

In Appendix D, strength of both design of Diagonal-CSP and Optimized-CSP is evaluated using procedure explained above. The summary of results is shown in Figure (4.36) for comparison. As shown in the Figure (4.36), the strength of the sandwich panel has greatly improved upon improving the strength of shear connectors. As it was mentioned in the previous section, The total interface shear force is resisted by both the tension and compression shear connectors members. Since in the design of Optimized-CSP as it is shown in Figure (4.27) a thicker shear connector have been used vs. design of Diagonal-

CSP, the strength of shear connectors is higher by 25%. In another word, a better composite action has been achieved through using larger diameter shear connectors with larger spacing as in the design of Optimized-CSP.

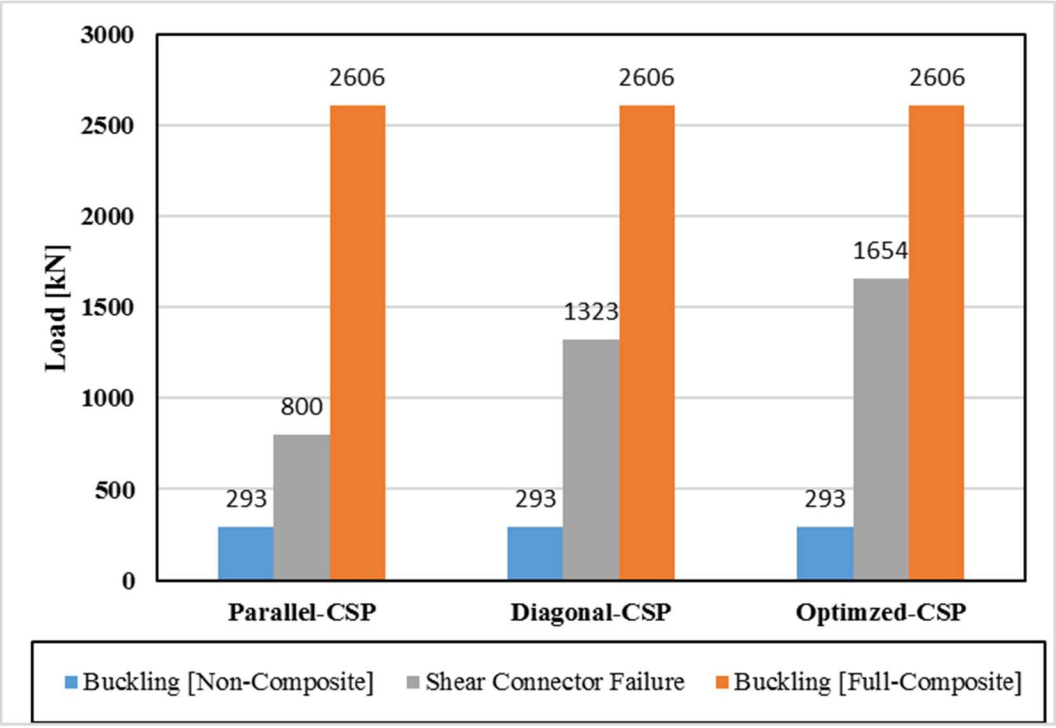

Figure (4.36): CSP Walls Under In-Plane Axial Load Strength Comparison

In the design of Diagonal-CSP in the dimension of CSP wall that was subjected to in-plane axial loading, 156 shear connector of Gauge 9 wire with diameter of 3.0mm (0.11in) have been used. This gives a total surface area of 11.35 cm^2 [1.76 in^2] of steel. On the hand, in the design of Optimized CSP, 108 shear connectors of Gauge 7 with diameter of 3.6 (0.14in) have been used. This gives a total surface area of 10.7 cm^2 [1.66 in^2] of steel. Therefore, in the Optimized-CSP design a lower volume of steel have achieved a better composite action between the two wythe of the panel under in-plane axial loading.

CHAPTER 5

CONCLUSIONS AND RECOMMENDATIONS

This research focused on accomplishing for the first time a reliable and numerically tested optimization, design procedures for an optimal orthotropic cementitious sandwich panel composite system that meets all the performance targets of the designer and it is aligned with building codes. The previously published literatures have evaluated the flaws, and the benefits of the current cementitious sandwich panels' design. However, such studies did not focus on of optimizing the current commercially-produced panels. For the first time, this research introduced a reliable numerical modeling methodology that accurately mimics the experimental behavior and is able to predict the failure criteria comparable to the experimental results in finding strength and cracking locations. Following the maturity of the reliable numerical model, for the first time an optimization methodology is defined that incorporates a combination of mathematical and numerical optimization methods to identify the optimum cementitious sandwich panel design. In addition, this study utilized the state-of-the-art nonlinear finite element analysis software MSC-MARC in parallel to parametric optimization procedure using the Taguchi statistical method for quality control. The numerical models are based on several full-scale tests that were performed on different types of sandwich panels under different loading scenarios at UCI structural lab. Additionally, for the first time, the genetic algorithm is used in optimization of cementitious sandwich panel as a second approach for optimization.

The optimization results introduced an improved panel design that meets the minimum code requirement for any specific design criteria. The optimized panels developed in this

study are lighter, economic (use less steel) and have a better installation performance as described earlier in Chapter 4.

The results of the parametric study, that employed the Taguchi method, identified the effect of each design factor on the improvement of the panel performance and improved thermal insulation properties that was included in the objective function. Furthermore, the result of genetic algorithm optimization converged to a model that cost of material has been reduced by 45% and cost of energy by 28% compare to the base model. This is achieved by increasing the thermal resistance of the CSP from 2.06 [m^2.K/W] (R-12) to 2.89 [m^2.K/W] (R-16) achieved by model 47. Using Pareto-frontier, other optimum solutions have been identified. For example, if the cost of material is the priority, while meeting the design requirement, designer can choose model 50 where the cost of material has been reduced by 48% with 35.6% increase in the thermal resistance value; or if the insulation is the priority while meeting the design requirement, designer can choose model 47 where the thermal resistance value has been increased by 40% while the cost of material has been decreased only by 38%.

In Chapter 4, the performance of the optimized CSP panel obtained from optimization process in this study is compared to the off-the-shelf commercially produced panels that have been extensively studied at UCI in previous years thought full-scale experiments. A numerical modeling methodology is identified where the boundary condition reflect the experiment setup used to test the panels at UCI. The similar setup was used to evaluate the performance of the optimized model and result was used to compare its performance to commercially produced panels. Details of the performance evaluation and comparison was detailed in section 4.4 of this research.

In the following paragraphs, conclusions are drawn from both sensitivity analysis using Taguchi method, and optimization of cost function using genetic algorithm done in this study.

5.1. Conclusions and Recommendations

Based on the results of CSP Optimization illustrated in Chapter 3, and comparison with off-the-shelf commercially produced panels described in Chapter 4, and in order to reduce the cost of the CSP and in the same time improve its thermal insulation, the following adjustments can be made to the commercially available CSPs:

- The optimized design is based on minimum load requirements of ASCE 7-10. As a results of optimization material cost lowered by 34% while thermal Insulation is improved by 41%. Additional reinforcement can be added for specific buildings design requirements.
- Diagonal members of CSP are prone to buckling under both horizontal and vertical shear loads. In order to improve the transfer of shear forces, larger diameter wires are recommended instead of series of smaller diameter steel wires. This provides better stiffness, and improves the composite action in sandwich panel.
- By relying on the larger diameter of the diagonal steel wires, optimization converged in the numerical analysis models with lower volume of shear connectors connecting the two face wire mesh layers. Accordingly, a reduction on both thermal bridging and cost of the panel is resulted. A ratio of 1:5 between the shear connectors and steel mesh placed on each face is recommended.

- Steel wires on compression can be reduced to meet the minimum requirement of shrinkage reinforcement according to ACI 318-14, Table 7.6.1.1. However, the local buckling of the main wire reinforcement should be considered when the CSP member is under compression.

- It is recommended that the thickness of the concrete or mortar layer applied at the compression side to be at least 2″ (50mm) as it is very efficient in improving the strength of the CSP and also it contributes to the thermal insulation of the panel.

- Currently all exterior steel meshes used for commercially produced CSP panels uses a ratio of 1:1, although the lateral steel wires do not contribute to the panel stiffness since these panels are made for one way slabs. Therefore, it is recommended to use 1:2 wire mesh ratio to reduce the cost of the panel.

- In locations where temperature fluctuation is higher (i.e. thermal insulation maters,) the designer should rely on the exterior concrete or mortar face and the longitudinal reinforcement to resist the load, such as in the case described in model 47 presented earlier in this study. In this case, a ratio of 1:5.5 between the shear connectors and steel mesh on each face is recommended.

5.2. Recommendations for Future Research

Using the optimization procedure for CSP developed in this study and using the observed behavior of various elements of the panel, the following recommendations for future research are identified:

- Although this optimization procedure in this study was used for optimization of cementations sandwich panels, it can further be used for optimization of other structural insulated panels, such as double panel sandwich structures, where two layers of foam cores with three layer of cementations wythes; one at the center and two wythes at the exterior side of the panel be used.
- Other parameters can be added or be replaced in the optimization function following the procedures described in this study. These parameters can be added to the actual cost of panel such as labor, manufacturing cost or other materials variations to be implemented in producing such panel system. Other performance requirements such as: sounds insulation or humidity insulation etc. can also be included in the optimization process.
- Further research on optimizing panel performance under asymmetric loading, curved or inclined panels where different boundary conditions are applied is needed.
- The quality of wires welds and probability of failure of welds during manufacturing can be considered in future studies in order to highlight the importance of the manufacturing process and its effect on the panel structural performance.
- Future research on the use of different materials for the panel core such as foam concrete, rockwall panels, rice husk, liquid foam and recycle materials etc. is recommended. For example, using foam concrete can possibly help in stabilizing the shear connectors (preventing early buckling) and improve the composite action between the two steel mesh wire layers. However, modeling interaction between

the shear connectors and the foam concrete is complex and requires further testing of the actual samples and data for adjusting the numerical model behavior.

- Future studies may also include analysis of panels made of monotonic foam concrete and stronger steel truss system instead of conventional sandwich panels with an insulating core surrounded by upper and lower mesh. This system may have potential applications for certain applications like floors or roof panels.
- This study focused on improving the composite action in sandwich panel under flexural loading and does not influence the strength of the panel under in-plane shear loading. In order to improve the strength of the panel under in-plane shear loading, a different approach for designing CSP is required. A new design where either additional shear connectors in the direction of in-plane shear loading or improving the boundary elements in the design of CSP need to be verified both experimentally and analytically in future research.

BIBLIOGRAPHY

[1] R. Mark De Souza and J. S. Williams, ″Population, Health and the Environment,″ The Population Reference Bureau, 2003.

[2] B. Botello, A. Mosallam and E. Mirnateghi, ″Structural Evaluation of Schnell™ Home S.R.L. Expanded Polystyrene (EPS) Sandwich Panels Slabs Subjected to Out-of-Plane Flexural Loads,″ University of California Irvine, Irvine, 2014.

[3] A. Einea, ″State-of-the-art of precast concrete Sandwich panels,″ PCI J, vol. 36, no. 6, pp. 78-98, 1991.

[4] ″Sustainable Buildings and Construction Program,″ United Nation Environmnet Program,

[5] B. Lawson, ″The NSW Good Wood Guide,″ School of Architecture, Uni of New South Wales, Sydney.

[6] R. Seifert, ″Alaska Residential Building Manual.Cooperative Extension Service,″ University of Alaska Fairbanks, 2007.

[7] S. Brzev and T. Guevara-Perez, , Precast Concrete Construction, Canada: British Columbia Institute of Technology, Canada., 2010.

[8] ″CATI Tech Notes,″ Computer Aided Technology, [Online].

[9] D. Zenkert, ″An introduction to Sandwich Construction.,″ Department of Lightweight Structures, Royal Institute of Technology, Stockholm, Sweden, 1993.

[10] M. M. Mashal, ″Quantification Of Seismic Performance Factors For Buildings Incorporating Three-Dimensional Construction System,″ State University Of New York At Buffalo, 2011.

[11] I. El Demerdash, ″Structural Evaluation of Sustainable Orthotropoic Three-Dimensional Sandwich Panel System,″ University of California, Irvine, 2013.

[12] M. Schlotter, A Comparison of Core Materials for Sandwich Composite Constructions, 2002.

[13] C. T. Salmon, ″Full Scale Testing of Precast Concrete Sandwich Panels,″ ACI Journal, vol. 94, pp. 354-362, 1997.

[14] K. Branner, ″Capacity and Lifetime of Foam Core Sandwich Structures,″ Technical University of Denmark, Department of Naval Architecture and Offshore Engineering, 1995.

[15] D.L. Durfree, ″Structural Foam-Core Panels in Northwest HUD-Code Manufactured Housing: A Preliminary Assessment of Opportunities and Obstacles,″ July 1993.

[16] M. Baginski, ″Sustainable Structures″.

[17] EVG-3D®, ″″A Brief Introduction into the EV-3D® Panel Construction System″,″ [Online]. Available: http://evgaustralia.com.

[18] Hadrian, ″A New Innovative Panel Building System,″ Tri-D Systems, [Online]. Available: www.tridipanel.com.

[19] M. Kabir, ″Structural Performance of 3D Sandwich Panels under Shear and Flexural Loading,″ Scientia Iranica, vol. 12, no. 4, pp. 402-408, 2005.

[20] Bush and Stine, ″Flexural behavior of composite precast concrete sandwich panels with continuous truss elements.,″ PCI, Vols. (March -April), pp. 112-121, 1994.

[21] G. Carbonari, ″Flexural behaviour of light-weight sandwich panels composed by concrete and EPS,″ Construction and Building Materials, vol. 35, pp. 792-799, 2012.

[22] G. G. a. L. W. S. Goble, ″Optimum design of prestressed beams,″ ACI, vol. 68, no. 9, pp. 712-718, 1971.

[23] J. S. Arora, Introduction to optimum design, New York, N.Y.: McGraw-Hili, Inc.,, 1989.

[24] U. Kirsch, ″Optimum design of prestressed beams,″ Camp. and Struct, vol. 2, no. 4, pp. 573-583, 1972.

[25] L. L. Friel, ″Optimum singly reinforced concrete sections,″ ACI, vol. 71, no. 11, pp. 556-558, 1974.

[26] R. H. Brown, ″Minimum cost selection of one-way slab thickness,″ J. Struct. Div., ASCE, vol. 101, no. 12, pp. 2585-2590, 1975.

[27] A. E. Naaman, ″Minimum cost versus minimum weight of prestressed slabs,″ J. Struct. Div., ASCE, vol. 102, no. 7, pp. 1493-1505, 1976.

[28] H. Barbosa, A. Lemonage and L. Fonseca, ″A genetic algorithm for the design of space framed structures.,″ XXIV CILAMCE – Iberian Latin-American Congress on Computational Methods in Engineering, Ouro Preto, Brasil, 2003.

[29] ″MSC MARC, Volume B: Element Library,″ MSC Software, Newport Beach, CA, USA, 2014.

[30] R. M. Bajracharya, ″Structural Evaluation of Concrete Expanded Polystyrene Sandwich Panels for Slab Applications,″ Centre of Excellence in Engineered Fibre Composites, Faculty of Engineering, Surveying, University of Southern Queensland., Civil & Environmental Engineering Department, University of California Irvine, 2011.

[31] A. Mosallam, B. Botello, E. Mirnateghi and I. Rabie, ″Structural Evaluation of Schnell Home S.R.L. Expanded Polystyrene (EPS) Sandwich Wall Panels Subjected to In-Plane Axial Compression Loading.,″ UCI, Irvine, CA, 2015.

[32] A. Mosallam, B. Botello and E. Mirnateghi, ″Structural Evaluation of Schnell Home S.R.L. Expanded Polystyrene (EPS) Sandwich Panels Slabs Subjected to Out-of-Plane Flexural Loads.,″ UCI, Irvine, CA, 2014.

[33] A. Mosallam, B. Botello, E. Mirnateghi and I. Rabie, ″Structural Evaluation of Schnell Home S.R.L. Expanded Polystyrene (EPS) Sandwich Wall Panels Subjected to Monotonic and full-reversal cyclic in-plane shear loading combined with simulated gravity loads,″ UCI, Irvine, 2015.

[34] G. Christopher and D. Johnston, Oxford Dictionary of Construction, Surveying, and Civil Engineering, Oxford: Oxford: Oxford UP, 2012.

[35] M. Abdolhosseini Qomi MJ, ″Data analytics for simplifying thermal efficiency planning in cities,″ The Royal Society, no. 13, 2016.

[36] A. S. Mosallam and N. Bedwei, ″Design Optimization of FRP Universal Connectors,″ Polymers and Polymer Composites, vol. 2, no. 2, p. 115, 1994.

[37] J. C. Nihawan, Insulated Wall Panels - Interface Shear Transfer, Omaha, Nebraska: PCI Journal, 1996.

[38] ″MSC MARC, Volume A: Theory and User Information,″ MSC Software, Newport Beach, CA, USA, 2014.

[39] S. Rajeev and C. S. Krishnamoorthy, ″Discrete Optimization Of Structures Using Genetic Algorithms,″ J. Struct. Eng., vol. 118, no. 5, pp. 1233-1250, 1992.

[40] A. Benayoune, ″Flexural behaviour of pre-cast concrete sandwich composite panel – Experimental and theoretical investigations,″ ScienceDirect, pp. 580-592, 2008.

[41] K. Byun, ″Development Of Structural Lightweight Foamed Concrete Using Polymer Foam Agent,″ Department of Civil Engineering, Yonsei Univ., Seoul, Korea,

[42] Zienkiewicz, O C 1977. Finite Element Method, 3rd ed. Maidenhead, UK: McGraw-Hill

APPENDIX A

Step by Step of Modeling and Analysis in MSC MENTAT and MARC

The following illustrate the pre-processing procedure used to model CSP in MSC MENTAT.

Step 1: Create Geometry:

Under the Geometry tab, in Basic Manipulation group, select Geometry and Mesh.

Next using basic CAD skills, geometry of CSP is created. Top and Bottom Concrete wythe is defined using 2D Surface (Quad) Steel wire Mesh on top and bottom are defined using 1D Line (Curve) Shear Connector are defined using 1D line (Curve)

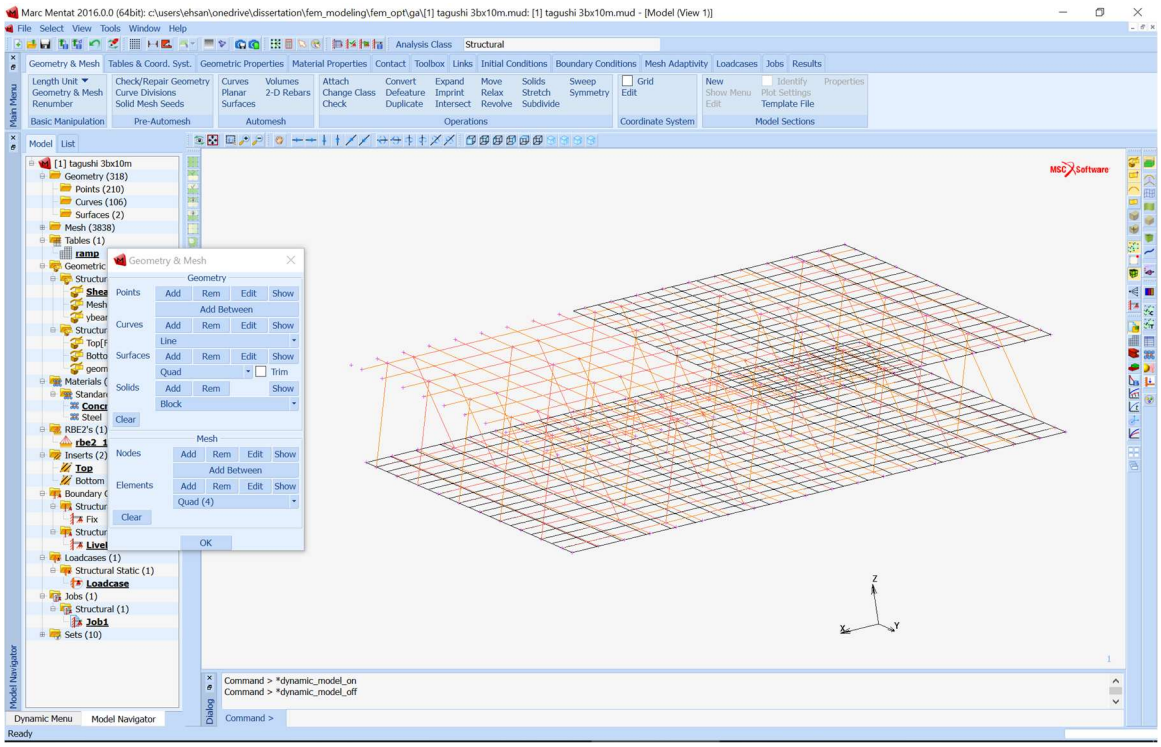

Figure (A.1): Create Geometry in MSC MENTAT

Step 2: Create Mesh

Using convert tool, 2D surface (Concrete top and bottom layer) can be converted to quadratic elements. In this study, the 40″ by 40″ concrete layers were meshed into 1:1″ elements.

Convert Steel Wire elements into 1D Elements using the Convert tool in the Operation group. In this study, maximum size of 1D element were set to 1″. This can be achieved by dividing each wire according to its length.

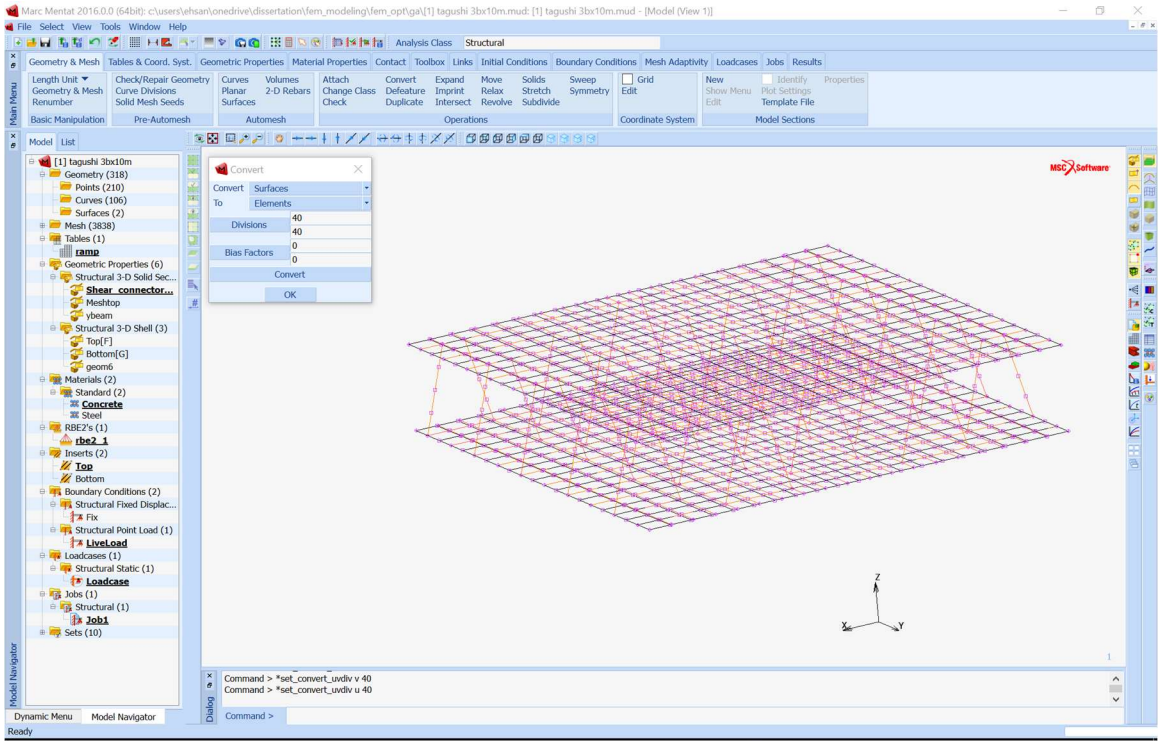

Figure (A.2): Convert Geometry into Mesh Element

Step 3: Assign Geometric Property:

Under the Geometry tab, in the Geometric Properties menu, by pulling down New (Structural), different geometric properties available in MENTAT are shown.

In this study, Concrete elements are assigned as Shell Elements. Pull down New (Structural) > 3-D > Shell; In the Geometric properties window, insert concrete shell thickness in Constant Element Thickness. Name of the Concrete shell can also be defined in the Name section. (Top); Next by selecting Add Elements, the geometric property can be applied to the concrete elements meshed in the previous step.

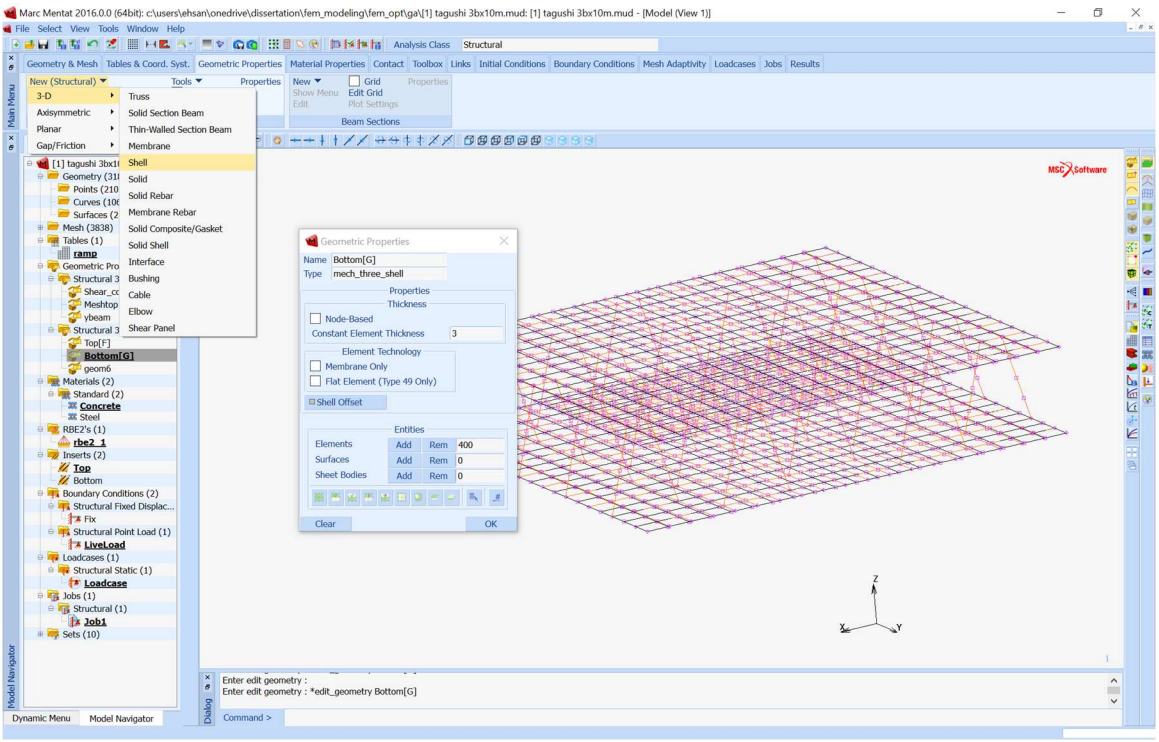

Figure (A.3): Define Shell property for Concrete wythe Elements

Similarly, by repeating the previous step, geometric property of bottom elements can be defined and applied to the elements meshed in the previous step.

Next Beam element property will be defined for steel wire elements. For each wire diameter a different geometric property should be created. Pulling down New Structural > 3-D > Solid Section Beam. Beam elements property will open. Enter Name (i.e Shear_connector) Set Cross section: Circular. Enter diameter); It is important to define the local axis of each element property appropriately perpendicular to its direction. For example, wire steel Mesh on each face which is defined X-Y plane. The local axis should be defined using <0 0 1> Z-Axis.

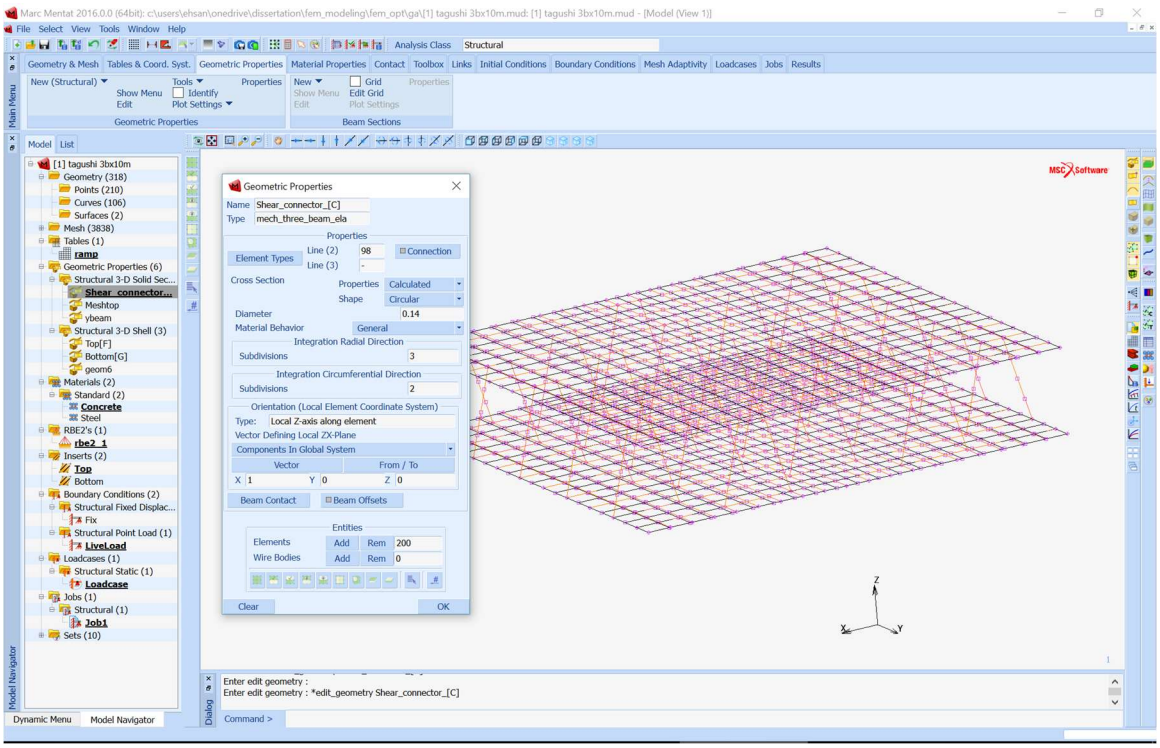

Figure (A.4): Define Beam Elements property for Steel Wires

Step 4: Assign Material Property:

Under the Material Properties tab, In Material Properties group, pull down New > Finite Stiffness region > Standard to open Material Properties Menu

Enter Name (i.e: Concrete), Enter Young Modulus (i.e 3000ksi) Poisson Ratio (0.15).

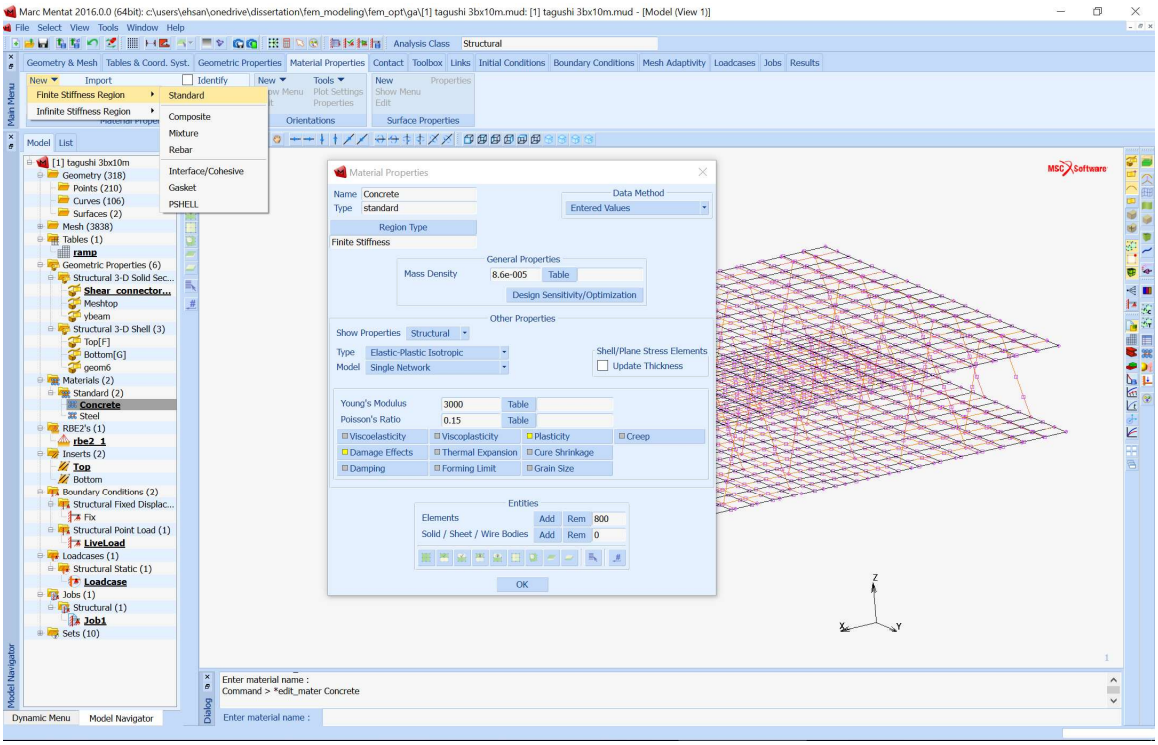

Figure (A.5): Define Concrete Material Property for Concrete Elements

Next select Plasticity to plasticity material property. For Concrete in this study the Yield Criterion was set to Parabolic Mohr-Columb (normally called Drucker-Prager in literature). Concrete compression strength is entered in Yield Stress. Beta Factor of Parabolic Mohr-Columb is the Uniaxial asymmetry ratio of the model which can be defined by the user. It is the ratio of $\sigma c/\sigma t$.

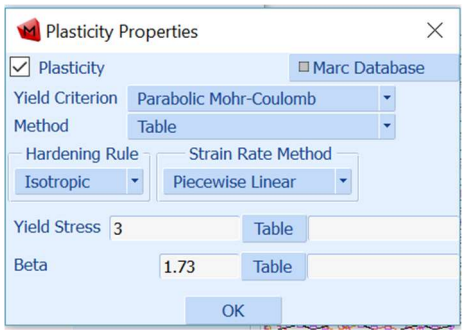

Figure (A.6): Define Material Plasticity for Concrete

Next Concrete behavior in Tension is defined using Damage Effects in Material Properties Menu. Concrete Critical Stress, softening modulus is entered in this menu. The low softening modulus will help the analysis to converge faster. However, the actual behavior of concrete in tension is a sudden brake and higher softening modulus will converge to more accurate result. Therefore, start with low softening modulus and increase it up to 10% of Elastic modulus defined previously.

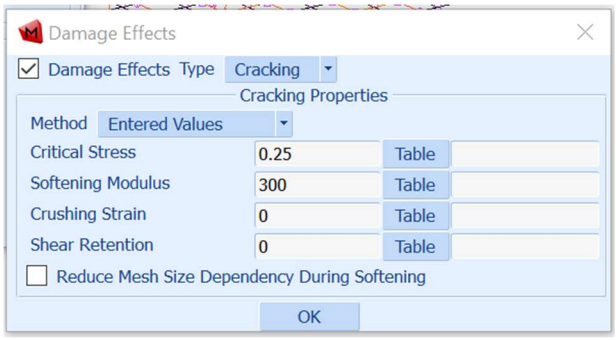

Figure (A.7): Define Damage Effect for Concrete Element in Tension

Next define Material Property for Steel. Pull down New > Finite Stiffness region > Standard to open Material Properties Menu; Enter Name (i.e Steel), Enter Young Modulus (i.e 29000ksi) Poisson Ratio (0.3); Enter Plastic property in the plasticity menu. In this study. Elastic-perfect plastic material model was defined for Steel elements. Enter Yield Stress 80ksi for cold wires. This material property is applied to all steel wire elements in the model.

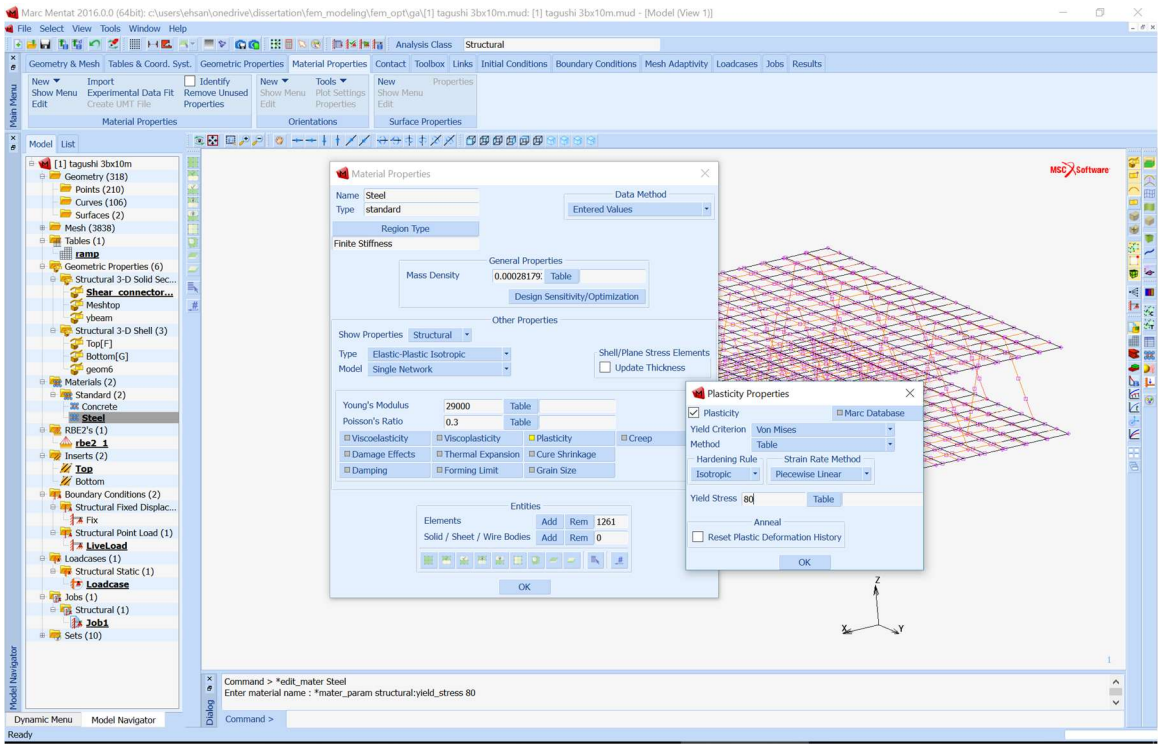

Figure (A.8): Define Steel Material Property

Step 5: Embedding Steel Mesh wires into Concrete Elements.

In order for steel Mesh elements to work with Concrete shell elements (reinforce them), Mentat has a tool (Insert) under the Links Tab. Pull down Insert > New to define this link.

Two different links should be defined independently for top and bottom face. Add Concrete shell elements as Host Entities and Add Steel Wire Mesh as Embedded Entity from the model.

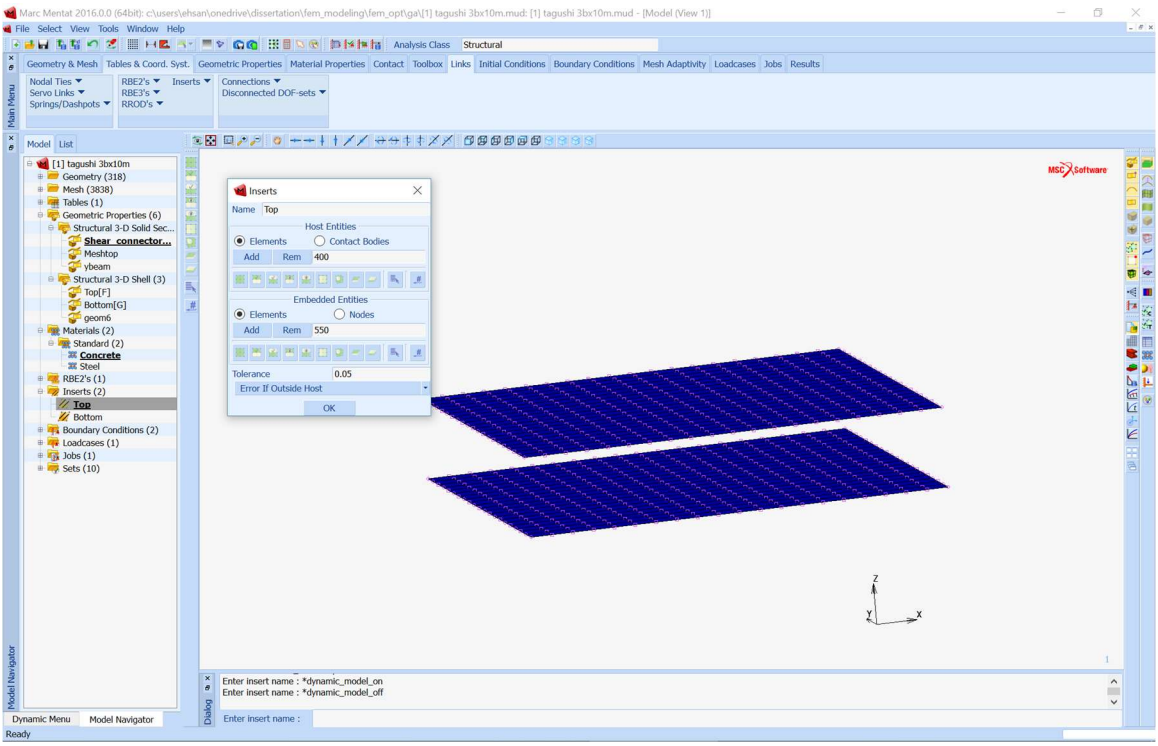

Figure (A.9): Embed Steel Mesh Elements into Concrete Elements.

Step 6: Add Boundary Condition

The CSP unit is boundary condition set to Pin-pin for a four-point bending test. Under the Boundary Conditions tab, Fix Displacement is selected. Translation direction constrained and applied to the nodes on each side of CSP accordingly.

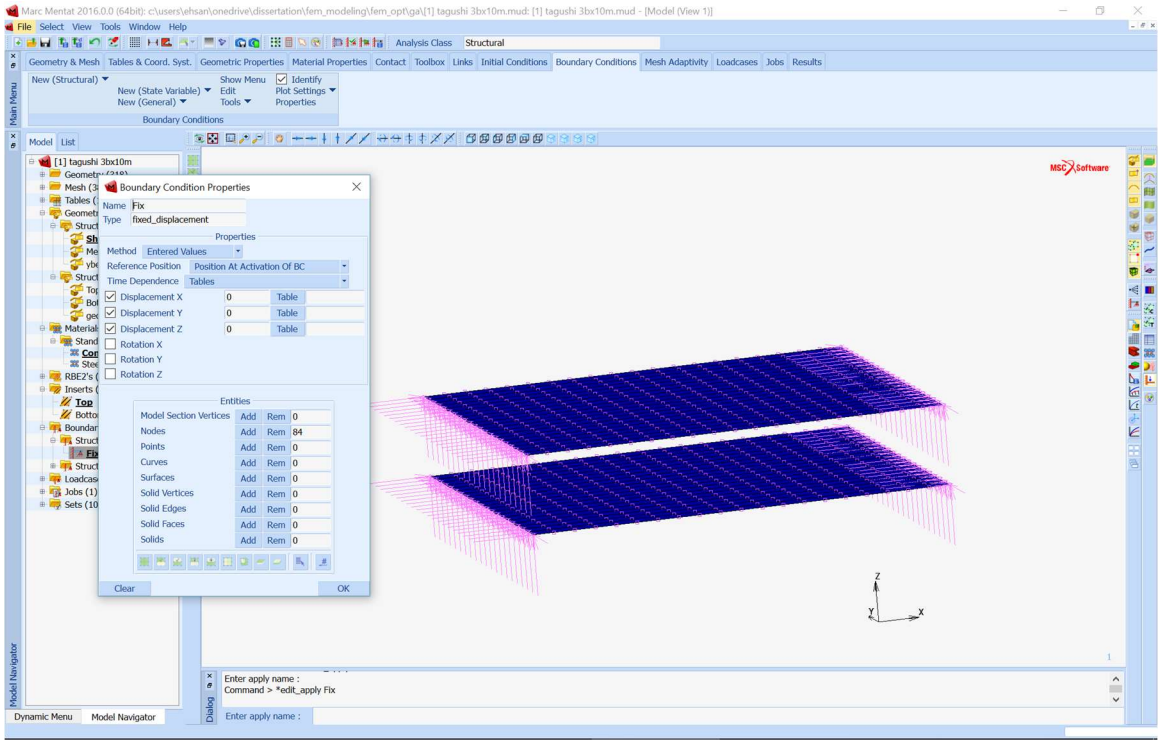

Figure (A.10): Define Pin-Pin Boundary Condition for the Model

Next in order to apply the load on top of the panel according to four-point Loading protocol, a reference node is defined. This helps in post processing to read the total reaction load of one node rather all the nodes that load is being applied. An RBE2 Rigid link can be used to link the reference node to the nodes that loads needs to be applied.

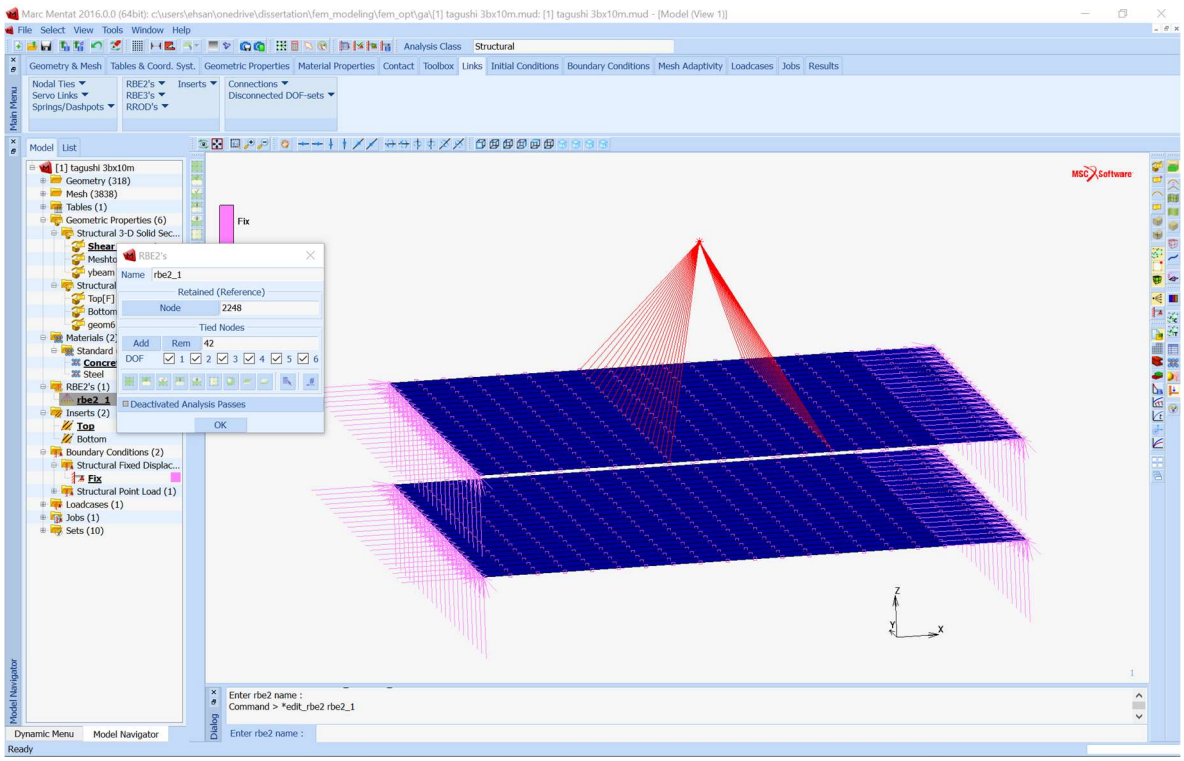

Figure (A.11): Define Rigid Link Between Reference Node and Boundary Nodes

A point Load is defined and applied to reference node defined in the previous step. First, in order to have incremental results, a ramp function is used from 0 – 1 for the point load. This ramp function can be defined under Tables tab.

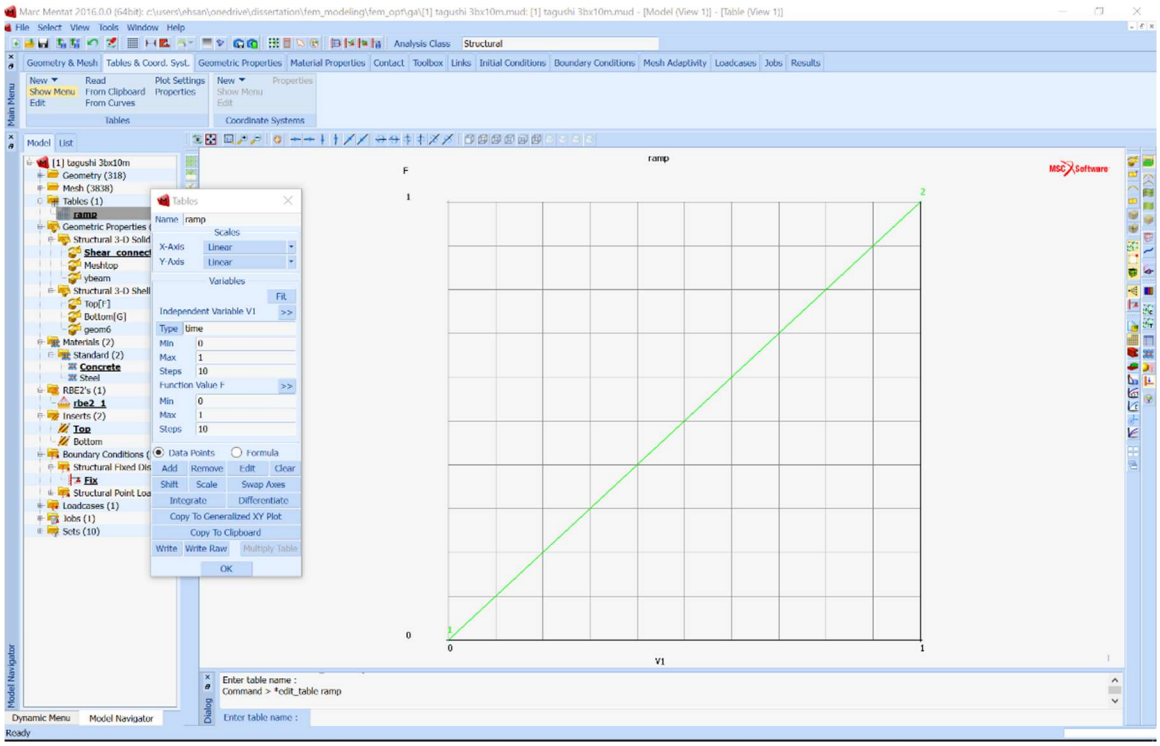

Figure (A.12): Define ramp function using Tables

Next the point Load can be defined. The magnitude of the force is calculated for each model separately. It is equal to Live Load + Self weight of the panel. The Live load is defined as 40psf * (40/12) *(40/12) + Self weight which is calculated for each model separately.

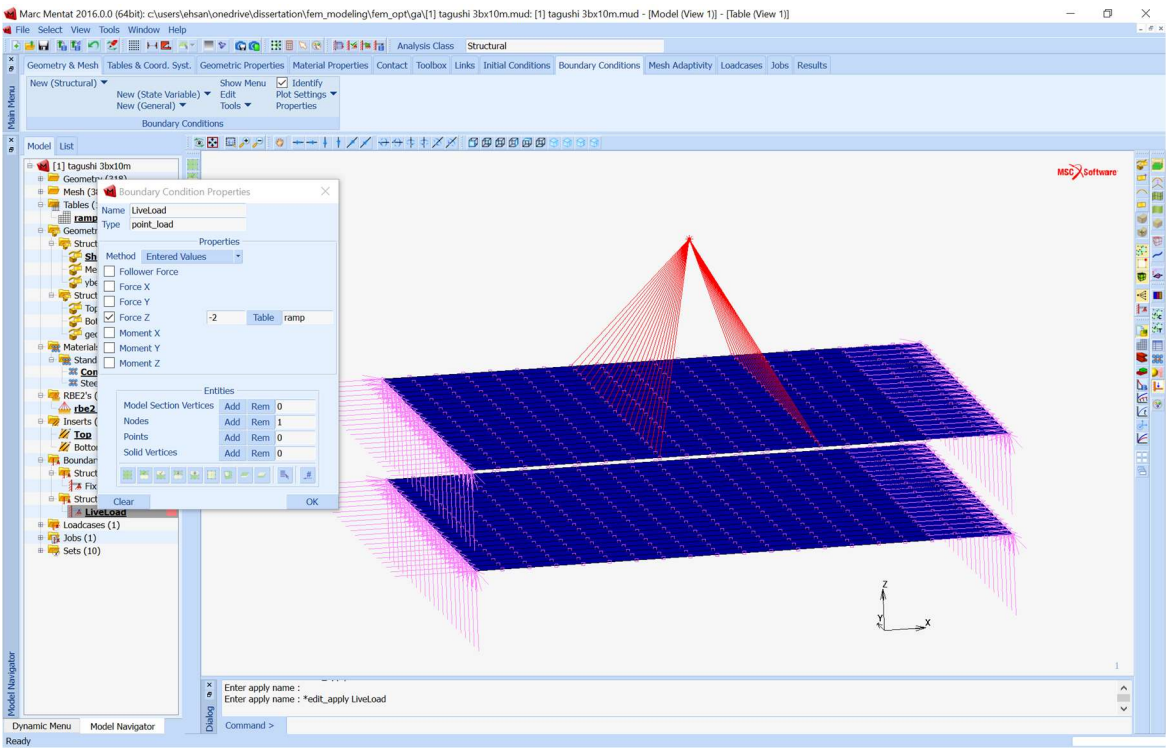

Figure (A.13): Define Point Load with Ramp function

Step 7: Define a Load Case:

The loadcase in this simulation is defined as Multi-Criteria (It is called Adaptive-Stepping in other FEA software) since there is material nonlinearly defined. The parameters of stepping function are defined accordingly.

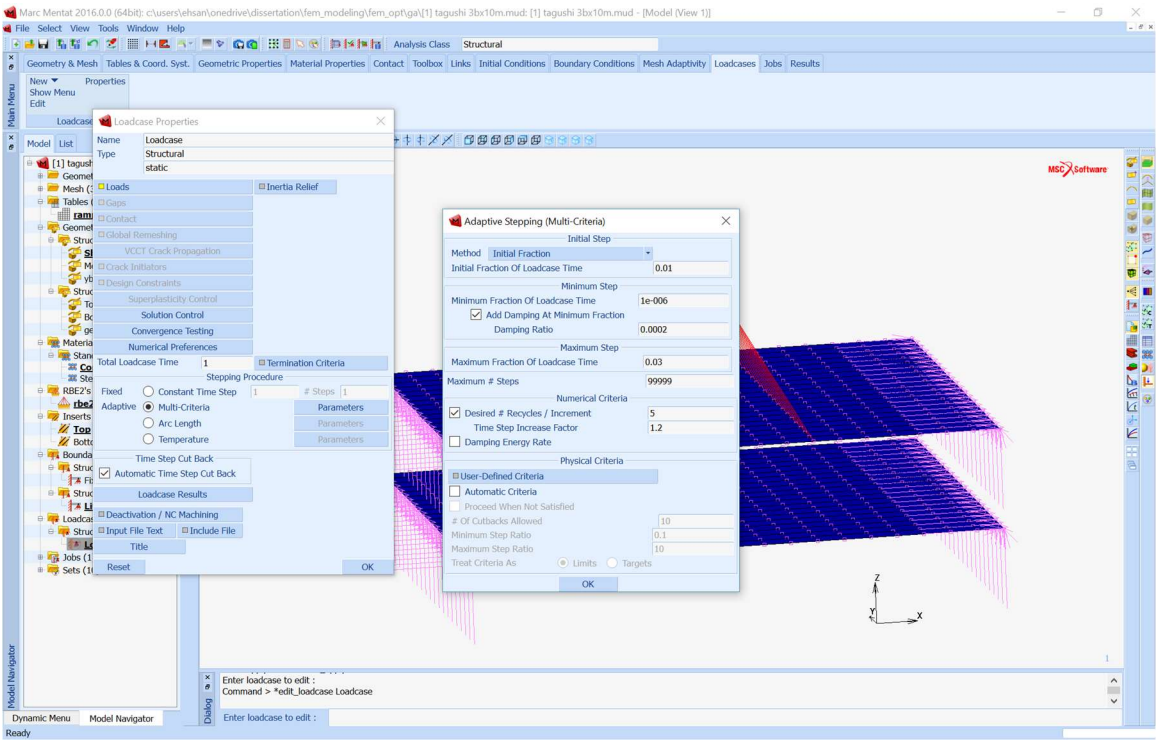

Figure (A.14): Define an Adaptive Load case

Step 8: Define Job and Run Analysis

Since this Analysis has both material nonlinearity and geometry nonlinearity in 3D, for more accurate results, Nonlinear procedure is set to Large Strain.

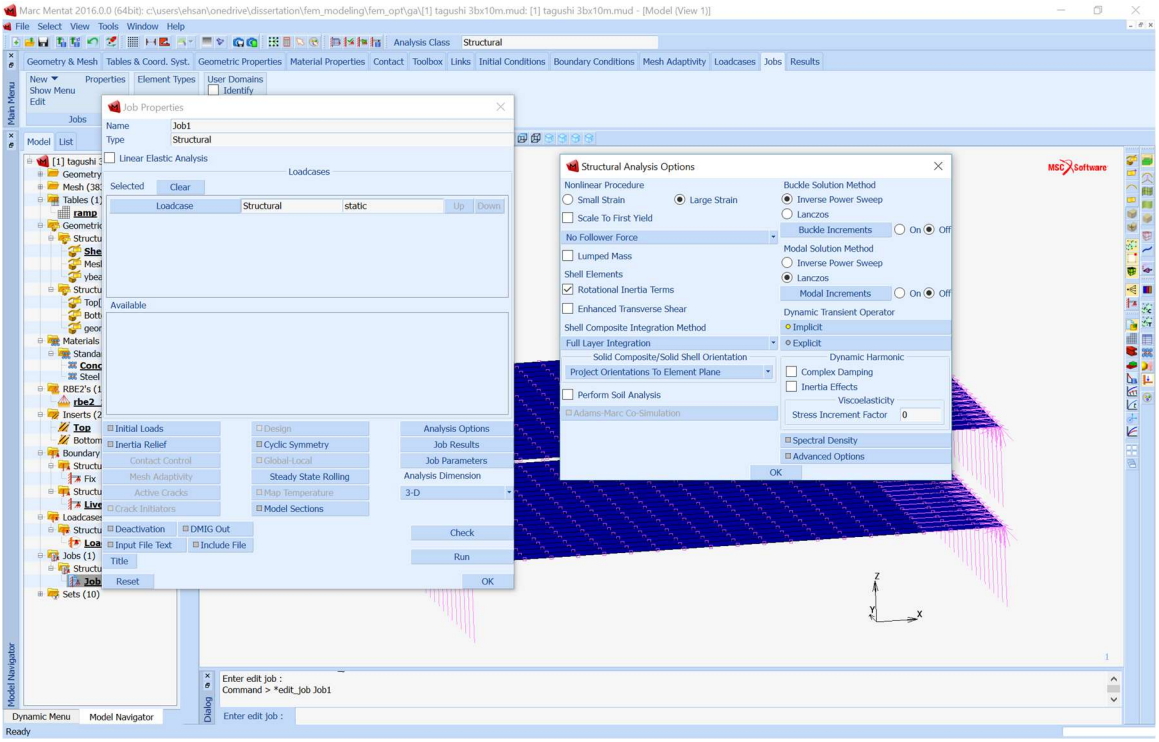

Figure (A.15): Define a Nonlinear Job with Large Strain

Under the Job results, Beam Axial forces, Total Strain, Stresses and Cracking strain is requested for post processing.

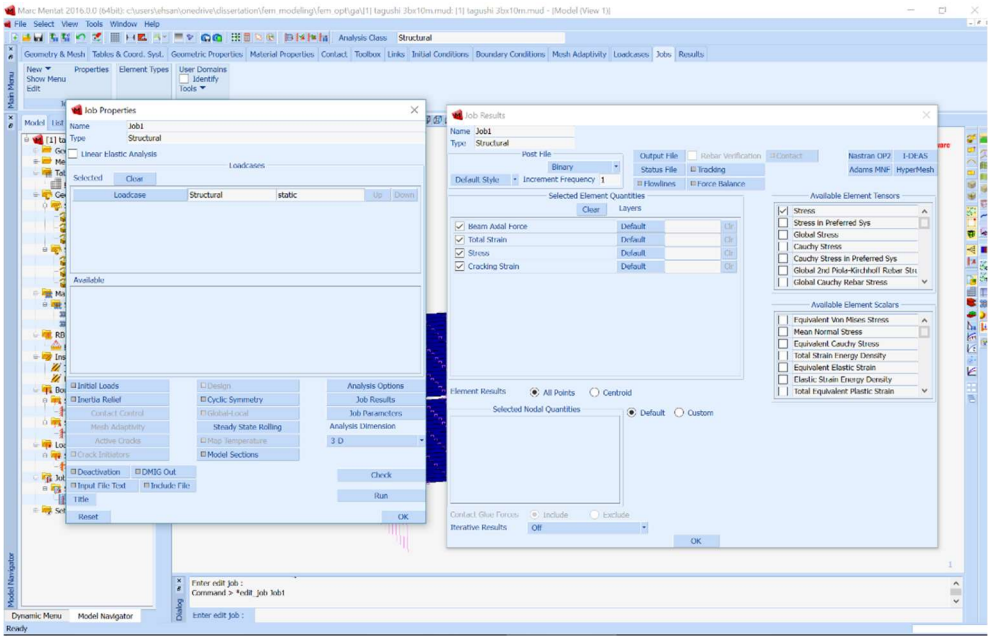

Figure (A.16): Define Job Result Request

Next we can run the analysis. Exit number 3004 analysis has converged without an error. Otherwise, Exit Numbers should troubleshoot accordingly.

Figure (A.17): Verify Successful Analysis

APPENDIX B

Detailed Results of Genetic Algorithm, Generations by Generation.

In the following tables, each row is obtained according to the steps below:

Row 1: Assigning unique Individual number for each model.

Row 2: For the 1st generation, the models is generated randomly according the design criteria boundary limits. For the 2nd generations and later, Row 2 is obtained from row 24 of its previous table.

Row 3: Volume of Steel is obtained from each model directly.

Row 4: Weight of Steel is obtained from Row 3 x Steel Density. Density of Steel is assumed to be $\rho_s = 0.284$ lb/in^3 in this study.

Row 5: Normalized Steel Weight is calculated for Optimization function. Steel Weight obtained from Row 4 is divided by Steel weight from specified CSP with Minimum value from all the design variable limits defined in this study.

Row 6: Volume of Mortar is obtained from each model directly.

Row 7: Weight of Mortar is obtained from Row 6 x Mortar Density. Density of Mortar is assumed to be $\rho_m = 0.087$ lb/in^3 in this study.

Row 8: Normalized Mortar Weight is calculated for optimization function. Mortar Weight obtained from Row 4 is divided by Mortar weight from specified CSP with Minimum value from all the design variable limits defined in this study.

Row 9: Total Weight is the sum of row 4 and row 5.

Row 10: Self weight from Row 9 is added to maximum live load of 100 psf converted into point load for 40″ X 40″ (approximately 1 m^2) sample used in the optimization analysis. This is done only for FEA analysis so that the design of the CSP is controlled by deflection under service load. However, for ultimate factored load accordingly LRFD design CSP, the 40psf ASCE is used is used to check the capacity of this CSP and compare it to the Base Model.

Row 11: The point load from Row 10 is converted to Surface load by dividing it by 40″x40″ and convert the load to psf.

Row 12: The Thermal Resistance capacity of CSP is calculated according to section: 3.4.2.

Row 13: Normalized Energy loss is calculated by taking the ratio of Thermal Resistance calculated from Row 12 to specific Thermal Resistance from specified CSP with Minimum value from all the design variable limits defined in this study.

Row 14: Maximum Deflection is measured from FEA analysis using MSC Marc.

Row 15: Maximum Deflection from Row 14 is normalized by the deflation limit from ACI code L/360 as described in section 3.3. If this value is positive this means that the design did not pass the deflection limit control and will penalized in the optimization function.

Row 16: Stiffness is calculated from dividing the Row 15 by Row 10.

Row 17: Objective Function is calculated using the Objective function equation described in section 3.4.

Row 18: Fitness Function is calculated according to Eq. (12) of Part 4 in section 3.6.

Row 19: Fitness factor is calculated from dividing Fitness function calculated in Row 18 by average fitness function of each generation.

Row 20: The two highest fitness factor ratio calculated in Row 19, Survival factor 2 is assigned. For the next two ratios, survival factor 1 is assigned. For the model with the lowest fitness factor ratio, Survival factor 0 is assigned which means this design is not fit to continue for the future generation of CSP. This step represent confirms the Darwinian principle of survival of the fittest.

Row 21: Mates are assigned according to the Survival Factor Grade in Row 20.

Row 22: Starting Crossover parameter is assigned randomly for each pair of mates.

Row 23: Ending Crossover parameters is assigned randomly for each pair of mates as long as they do not have common design member.

Row 24: The crossover is applied and the new generation of models is created. Instead of the model that was not fit to continue, a new model within the design criteria is included in the new generation. If the new model that is added to the generation from outside is a strong candidate in the new generation, the GA will converge faster.

This process is repeated until the objective function converges to certain value. The last generation is the most optimized generation obtained in this process.

Table (B.1): 1st to 2nd Generation of CSP Results.

1	Individual Number		1	2	3	4	5
2	1st Generation		13322132	13322131	32321222	12111333	11111113
3	Volume of Steel	(in^3)	26.5	34	33	13.6	13.1
4	Weight of Steel	(lb)	7.53	9.66	9.37	3.86	3.72
5	W_s/W_{sp}	Ratio	2.02	2.60	2.52	1.04	1.00
6	Volume of Mortar	(in^3)	6400	6400	8000	9600	3200
7	Weight of Mortar	(lb)	556.80	556.80	696.00	835.20	278.4
8	W_c/W_{cs}	Ratio	2.00	2.00	2.50	3.00	1.00
9	Total Weight	(lb)	564.33	566.46	705.37	839.06	282.12
10	Live + Self Weight	(kips)	1.67	1.68	1.82	1.95	1.39
11	Live + Self Weight	psf	151	151	164	176	126
12	R_t	(K/W)	2.89	2.89	2.29	4.23	4.26
13	Et/Eb	Ratio	0.44	0.44	0.56	0.18	0.18
14	u_{FEA}	(in)	0.0051	0.0052	0.0046	0.0025	0.1300
15	$u_{FEA} / u_{max} - 1$	Ratio	-0.95	-0.95	-0.96	-0.98	0.18
16	Stiffness	(kips/in)	328.30	322.40	394.65	779.62	10.71
17	Objective Function Φ(X)		20.81	26.54	25.92	10.68	28.42
18	Fitness function Fi		**18.29**	**12.56**	**13.18**	**28.42**	**10.68**
19	Fi/F		1.10	0.76	0.79	1.71	0.64
20	Survival of Fittest		2	1	1	2	0
21	Mates		4	3	2	1	0
22	Crossover 1		2	3	3	2	0
23	Crossover 2		4	5	5	4	0
24	2nd Generation	#	12112132	13321131	32322222	13321333	13111131

(1 in = 25.4 mm) , (1 in3 = 16.3 cm3) , (1 lb = 0.45 kg)

(1 m2.K/W [RSI] = 5.67 h.ft2.oF /BTU [R-Value])

Table (B.2): Developing the 3rd Generation of CSP using GA

1	Individual Number		6	7	8	9	10
2	2nd Generation		12112132	13111131	32111222	13321333	13111131
3	Volume of Steel	(in^3)	26.5	34	33	13.6	13.1
4	Weight of Steel	(lb)	7.53	9.66	9.37	3.86	3.7204
5	W_s/W_{sp}	Ratio	2.02	2.60	2.40	1.04	1.00
6	Volume of Mortar	(in^3)	6400	6400	6400	9600	3200
7	Weight of Mortar	(lb)	556.80	556.80	556.80	835.20	278.4
8	W_c/W_{cs}	Ratio	2.00	2.00	2.00	3.00	1.00
9	Total Weight	(lb)	564.33	566.46	566.17	839.06	282.12
10	Live + Self Weight	(kips)	1.67	1.68	1.68	1.95	1.39
11	Live + Self Weight	psf	151	151	151	176	126
12	R_t	(K/W)	2.26	2.26	1.86	3.09	3.02
13	Et/Eb	Ratio	0.91	0.91	1.10	0.67	0.68
14	u_{FEA}	(in)	0.0051	0.0052	0.0046	0.0025	0.1300
15	$u_{FEA} / u_{max} - 1$	Ratio	-0.95	-0.95	-0.96	-0.98	0.18
16	Stiffness	(kips/in)	328.30	322.40	364.39	779.62	10.71
17	Objective Function Φ(X)		9.23	13.20	13.13	3.43	5.02
18	Fitness function Fi		**7.40**	**3.43**	**3.51**	**13.20**	**11.62**
19	Fi/F		0.94	0.44	0.45	1.69	1.48
20	Survival of Fittest		1	0	1	2	2
21	Mates		4	0	5	1	3
22	Crossover 1		2	0	3	2	3
23	Crossover 2		4	0	5	4	5
24	3rd Generation		11322132	32111131	13111222	12111132	12111113

(1 in = 25.4 mm) , (1 in^3 = 16.3 cm^3) , (1 lb = 0.45 kg)

(1 m^2.K/W [RSI] = 5.67 $h.ft^2.{}^oF$ /BTU [R-Value])

Table (B.3): Developing the 4th Generation of CSP using GA

1	Individual Number		11	12	13	14	15
2	3rd Generation		11322132	32111131	13111222	12111132	12111113
3	Volume of Steel	(in^3)	17.76	18.5	18.2	21.8	18.8
4	Weight of Steel	(lb)	5.04	5.25	5.17	5.74	5.34
5	W_s/W_{sp}	Ratio	1.36	1.41	1.39	1.54	1.44
6	Volume of Mortar	(in^3)	6400	6400	6400	9600	3200
7	Weight of Mortar	(lb)	556.80	556.80	556.80	696.00	278.40
8	W_c/W_{cs}	Ratio	2.00	2.00	2.00	2.50	1.00
9	Total Weight	(lb)	561.84	562.05	561.97	701.74	283.74
10	Live + Self Weight	(kips)	1.67	1.67	1.67	1.81	1.39
11	Live + Self Weight	psf	151	151	151	163	126
12	R_t	(K/W)	2.99	2.87	2.57	2.36	2.54
13	Et/Eb	Ratio	0.69	0.72	0.80	0.87	0.81
14	u_{FEA}	(in)	0.0080	0.0075	0.0067	0.0021	0.0075
15	$u_{FEA} / u_{max} - 1$	Ratio	-0.93	-0.93	-0.94	-0.98	-0.93
16	Stiffness	(kips/in)	208.98	222.94	249.55	862.73	185.83
17	Objective Function Φ(X)		2.08	2.17	2.13	2.38	2.18
18	Fitness function Fi		4.56	4.94	5.30	6.46	5.48
19	Fi/F		**6.46**	**6.09**	**5.73**	**4.56**	**5.55**
20	Survival of Fittest		1.14	1.07	1.01	0.80	0.98
21	Mates		2	1	1	0	2
22	Crossover 1		10	8	7	0	6
23	Crossover 2		2	1	1	0	2
24	4th Generation	#	11221113	12111131	12111222	13111132	32111113

(1 in = 25.4 mm) , (1 in3 = 16.3 cm3) , (1 lb = 0.45 kg)

(1 m2.K/W [RSI] = 5.67 h.ft2.oF /BTU [R-Value])

Table (B.4): Developing the 5th Generation of CSP using GA

1	**Individual Number**	#	16	17	18	19	20
2	**4th Generation**	#	11221113	12111131	12111222	13111132	32111113
3	**Volume of Steel**	**(in^3)**	24.8	18.5	13.9	16.2	13.6
4	**Weight of Steel**	**(lb)**	7.04	5.25	3.95	4.60	3.86
5	**W_s/W_{sp}**	**Ratio**	1.89	1.41	1.06	1.24	1.04
6	**Volume of Mortar**	**(in^3)**	6400	6400	6400	6400	3200
7	**Weight of Mortar**	**(lb)**	556.80	556.80	556.80	556.80	278.40
8	**W_c/W_{cs}**	**Ratio**	2.00	2.00	2.00	2.00	1.00
9	**Total Weight**	**(lb)**	563.84	562.05	560.75	561.40	282.26
10	**Live + Self Weight**	**(kips)**	1.67	1.67	1.67	1.67	1.39
11	**Live + Self Weight**	**psf**	151	151	151	151	126
12	**R_t**	**(K/W)**	2.64	2.87	2.87	2.99	2.89
13	**Et/Eb**	**Ratio**	0.78	0.72	0.72	0.69	0.71
14	**u_{FEA}**	**(in)**	0.0080	0.0022	0.0020	0.0065	0.0083
15	**$u_{FEA} / u_{max} - 1$**	**Ratio**	-0.93	-0.98	-0.98	-0.94	-0.92
16	**Stiffness**	**(kips/in)**	209.23	760.02	836.27	257.31	167.74
17	**Objective Function Φ(X)**		7.66	4.94	3.63	4.10	3.47
18	**Fitness function Fi**		**1.76**	**2.52**	**2.32**	**2.34**	**3.27**
19	**Fi/F**		0.72	1.03	0.95	0.96	1.34
20	**Survival of Fittest**		0	2	1	1	2
21	**Mates**		0	15	14	13	12
22	**Crossover 1**		0	1	2	2	1
23	**Crossover 2**		0	3	4	4	3
24	**5th Generation**	#	12121113	22111213	11211222	13111113	32111132

(1 in = 25.4 mm) , (1 in3 = 16.3 cm3) , (1 lb = 0.45 kg)

(1 m2.K/W [RSI] = 5.67 h.ft2.oF /BTU [R-Value])

Table (B.5): Developing the 6th Generation of CSP using GA

1	Individual Number	#	21	22	23	24	25
2	5th Generation	#	12121113	22111213	11211222	13111113	32111132
3	Volume of Steel	(in^3)	17.4	20.8	16.2	13.9	16.2
4	Weight of Steel	(lb)	4.94	5.91	4.60	3.95	4.60
5	W_s/W_{sp}	Ratio	1.33	1.59	1.24	1.06	1.24
6	Volume of Mortar	(in^3)	3200	6400	6400	6400	3200
7	Weight of Mortar	(lb)	278.40	556.80	556.80	556.80	278.40
8	W_c/W_{cs}	Ratio	1.00	2.00	2.00	2.00	1.00
9	Total Weight	(lb)	283.34	562.71	561.40	560.75	283.00
10	Live + Self Weight	(kips)	1.39	1.67	1.67	1.67	1.39
11	Live + Self Weight	psf	126	151	151	151	126
12	R_t	(K/W)	2.83	2.99	2.99	2.87	2.47
13	Et/Eb	Ratio	0.73	0.69	0.69	0.72	0.83
14	u_{FEA}	(in)	0.0590	0.0080	0.0070	0.0080	0.0240
15	$u_{FEA} / u_{max} - 1$	Ratio	-0.46	-0.93	-0.94	-0.93	-0.78
16	Stiffness	(kips/in)	23.62	209.09	238.77	208.84	58.04
17	Objective Function Φ(X)		4.57	5.59	4.10	3.63	4.82
18	Fitness function Fi		4.65	3.63	5.12	5.59	4.40
19	Fi/F		0.99	0.78	1.09	1.19	0.94
20	Survival of Fittest		1	0	1	2	2
21	Mates		18	0	16	20	19
22	Crossover 1		1	0	1	4	4
23	Crossover 2		3	0	3	8	8
24	6th Generation	#	11221113	22111113	12111222	13111213	32111113

(1 in = 25.4 mm) , (1 in3 = 16.3 cm3) , (1 lb = 0.45 kg)

(1 m2.K/W [RSI] = 5.67 h.ft2.oF /BTU [R-Value])

Table (B.6): Developing the 7th Generation of CSP using GA

1	Individual Number	#	26	27	28	29	30
2	6th Generation	#	11221113	22111113	12111222	13111213	32111113
3	Volume of Steel	(in^3)	17.2	15.3	16.4	11.9	18.2
4	Weight of Steel	(lb)	4.88	4.35	4.66	3.38	5.17
5	W_s/W_{sp}	Ratio	1.31	1.17	1.25	0.91	1.39
6	Volume of Mortar	(in^3)	3200	4800	6400	3200	6400
7	Weight of Mortar	(lb)	278.40	417.60	556.80	278.40	556.80
8	W_c/W_{cs}	Ratio	1.00	1.50	2.00	1.00	2.00
9	Total Weight	(lb)	283.28	421.95	561.46	281.78	561.97
10	Live + Self Weight	(kips)	1.39	1.53	1.67	1.39	1.67
11	Live + Self Weight	psf	126	138	151	126	151
12	R_t	(K/W)	2.89	2.67	2.93	2.77	2.57
13	Et/Eb	Ratio	0.71	0.77	0.70	0.74	0.80
14	u_{FEA}	(in)	0.110	0.008	0.006	0.065	0.007
15	$u_{FEA} / u_{max} - 1$	Ratio	0.00	-0.93	-0.95	-0.41	-0.94
16	Stiffness	(kips/in)	12.67	191.49	278.58	21.41	238.85
17	Objective Function Φ(X)		4.44	4.23	4.22	3.25	5.30
18	Fitness function Fi		**4.11**	**4.31**	**4.32**	**5.30**	**3.25**
19	Fi/F		0.97	1.01	1.02	1.24	0.76
20	Survival of Fittest		1	2	1	2	0
21	Mates		23	24	21	22	0
22	Crossover 1		1	4	1	4	0
23	Crossover 2		3	8	3	8	0
24	7th Generation	#	12121113	21112213	11211222	13111113	32111213

(1 in = 25.4 mm) , (1 in3 = 16.3 cm3) , (1 lb = 0.45 kg)

(1 m2.K/W [RSI] = 5.67 h.ft2.oF /BTU [R-Value])

Table (B.7): Developing the 8th Generation of CSP using GA

1	Individual Number	#	31	32	33	34	35
2	7th Generation	#	12121113	21112213	11211222	13111113	32111213
3	Volume of Steel	(in^3)	17.21	17.6	16.4	11.9	16.17
4	Weight of Steel	(lb)	4.89	5.00	4.66	3.38	4.59
5	W_s/W_{sp}	Ratio	1.31	1.34	1.25	0.91	1.23
6	Volume of Mortar	(in^3)	3200	4800	6400	3200	4800
7	Weight of Mortar	(lb)	278.40	417.60	556.80	278.40	417.60
8	W_c/W_{cs}	Ratio	1.00	1.50	2.00	1.00	1.50
9	Total Weight	(lb)	283.29	422.60	561.46	281.78	422.19
10	Live + Self Weight	(kips)	1.39	1.53	1.67	1.39	1.53
11	Live + Self Weight	psf	126	138	151	126	138
12	R_t	(K/W)	2.89	2.84	2.93	2.77	2.52
13	Et/Eb	Ratio	0.71	0.72	0.70	0.74	0.82
14	u_{FEA}	(in)	0.117	0.008	0.006	0.065	0.007
15	$u_{FEA} / u_{max} - 1$	Ratio	0.06	-0.93	-0.95	-0.41	-0.94
16	Stiffness	(kips/in)	11.91	196.49	278.58	21.41	218.88
17	Objective Function Φ(X)		5.08	4.65	4.22	3.25	4.74
18	Fitness function Fi		**3.25**	**3.68**	**4.10**	**5.08**	**3.58**
19	Fi/F		0.82	0.93	1.04	1.29	0.91
20	Survival of Fittest		0	1	1	2	2
21	Mates		0	33	32	35	34
22	Crossover 1		0	1	1	4	4
23	Crossover 2		0	3	3	8	8
24	8th Generation	#	12111213	11212213	21111222	13111213	32111113

(1 in = 25.4 mm) , (1 in3 = 16.3 cm3) , (1 lb = 0.45 kg)

(1 m2.K/W [RSI] = 5.67 h.ft2.oF /BTU [R-Value])

Table (B.8): Developing the 9th Generation of CSP using GA

1	Individual Number	#	36	37	38	39	40
2	8th Generation	#	12111213	11212213	21111222	13111213	32111113
3	Volume of Steel	(in^3)	14.19	17.45	16.5	12.21	16.17
4	Weight of Steel	(lb)	4.03	4.96	4.69	3.47	4.59
5	W_s/W_{sp}	Ratio	1.08	1.33	1.26	0.93	1.23
6	Volume of Mortar	(in^3)	4800	4800	6400	4800	3200
7	Weight of Mortar	(lb)	417.60	417.60	556.80	417.60	278.40
8	W_c/W_{cs}	Ratio	1.50	1.50	2.00	1.50	1.00
9	Total Weight	(lb)	421.63	422.56	561.49	421.07	282.99
10	Live + Self Weight	(kips)	1.53	1.53	1.67	1.53	1.39
11	Live + Self Weight	psf	138	138	151	138	126
12	R_t	(K/W)	2.94	2.88	2.90	2.82	2.47
13	Et/Eb	Ratio	0.70	0.71	0.71	0.73	0.83
14	u_{FEA}	(in)	0.008	0.008	0.006	0.008	0.024
15	$u_{FEA} / u_{max} - 1$	Ratio	-0.93	-0.93	-0.95	-0.93	-0.78
16	Stiffness	(kips/in)	191.45	191.57	278.58	191.38	58.04
17	Objective Function Φ(X)		3.58	4.55	4.30	3.27	4.81
18	Fitness function Fi		**4.50**	**3.53**	**3.78**	**4.81**	**3.27**
19	Fi/F		1.13	0.89	0.95	1.21	0.82
20	Survival of Fittest		2	0	1	2	1
21	Mates		39	0	40	36	38
22	Crossover 1		4	1	1	4	1
23	Crossover 2		8	3	3	8	3
24	9th Generation	#	12111213	11212113	32111222	13111213	21111113

(1 in = 25.4 mm) , (1 in3 = 16.3 cm3) , (1 lb = 0.45 kg)

(1 m2.K/W [RSI] = 5.67 h.ft2.oF /BTU [R-Value])

Table (B.9): Developing the 10th Generation of CSP using GA

1	Individual Number	#	41	42	43	44	45
2	9th Generation	#	12111213	11212113	32111222	13111213	21111113
3	Volume of Steel	(in^3)	14.19	17.45	18.21	12.21	14.59
4	Weight of Steel	(lb)	4.03	4.96	5.17	3.47	4.14
5	W_s/W_{sp}	Ratio	1.08	1.33	1.39	0.93	1.11
6	Volume of Mortar	(in^3)	4800	3200	6400	4800	3200
7	Weight of Mortar	(lb)	417.60	278.40	556.80	417.60	278.40
8	W_c/W_{cs}	Ratio	1.50	1.00	2.00	1.50	1.00
9	Total Weight	(lb)	421.63	283.36	561.97	421.07	282.54
10	Live + Self Weight	(kips)	1.53	1.39	1.67	1.53	1.39
11	Live + Self Weight	psf	138	126	151	138	126
12	R_t	(K/W)	2.94	2.83	2.57	2.82	2.79
13	Et/Eb	Ratio	0.70	0.73	0.80	0.73	0.74
14	u_{FEA}	(in)	0.008	0.043	0.006	0.008	0.059
15	$u_{FEA} / u_{max} - 1$	Ratio	-0.93	-0.61	-0.95	-0.93	-0.46
16	Stiffness	(kips/in)	191.45	32.40	278.66	191.38	23.60
17	Objective Function Φ(X)		3.58	4.59	5.30	3.27	3.84
18	Fitness function Fi		**4.99**	**3.99**	**3.27**	**5.30**	**4.74**
19	Fi/F		1.12	0.89	0.73	1.19	1.06
20	Survival of Fittest		1	1	0	2	2
21	Mates		42	41	0	45	44
22	Crossover 1		1	1	0	4	4
23	Crossover 2		3	3	0	8	8
24	10th Generation	#	11211213	12112213	32111113	13111213	21111113

(1 in = 25.4 mm) , (1 in3 = 16.3 cm3) , (1 lb = 0.45 kg)

(1 m2.K/W [RSI] = 5.67 h.ft2.oF /BTU [R-Value])

Table (B.10): Analysis of the 10th Generation of CSP.

1	**Individual Number**	#	46	47	48	49	50
2	**10th Generation**	#	11211213	12112213	32111113	13111213	21111113
3	**Volume of Steel**	**(in^3)**	14.43	17.2	16.17	14.69	14.59
4	**Weight of Steel**	**(lb)**	4.10	4.88	4.59	4.17	4.14
5	**W_s/W_{sp}**	**Ratio**	1.10	1.31	1.23	1.12	1.11
6	**Volume of Mortar**	**(in^3)**	4800	4800	3200	4800	3200
7	**Weight of Mortar**	**(lb)**	417.60	417.60	278.40	417.60	278.40
8	**W_c/W_{cs}**	**Ratio**	1.50	1.5	1.00	1.5	1.00
9	**Total Weight**	**(lb)**	421.70	422.48	282.99	422.48	282.54
10	**Live + Self Weight**	**(kips)**	1.53	1.53	1.39	1.53	1.39
11	**Live + Self Weight**	**psf**	138	138	126	138	126
12	**R_t**	**(K/W)**	2.88	2.89	2.47	2.82	2.79
13	**Et/Eb**	**Ratio**	0.71	0.71	0.83	0.72	0.74
14	**u_{FEA}**	**(in)**	0.12	0.051	0.024	0.086	0.059
15	**$u_{FEA} / u_{max} - 1$**	**Ratio**	0.09	-0.54	-0.78	-0.22	-0.46
16	**Stiffness**	**(kips/in)**	12.76	27.32	58.04	16.19	23.60
17	**Objective Function Φ(X)**		4.62	4.44	4.81	3.89	3.84

(1 in = 25.4 mm) , (1 in3 = 16.3 cm3) , (1 lb = 0.45 kg)

(1 m2.K/W [RSI] = 5.67 h.ft2.oF /BTU [R-Value])

APPENDIX C

Analytical Calculation for Slab Design Check

The calculations performed on the different CSP structural elements are primarily based on the same standards used for calculating reinforced concrete elements. The main standard used for the calculations of CSP is the ACI 318 along with ASCE Minimum Loads.

The mortar compression layer is the resisting element to compressive stresses induced within the section of the CSP structural element when subjected to flexure. The steel wire mesh in the tension layer as well as any reinforcing steel bars placed are the elements that resist the tensile forces induced within a CSP section subjected to flexure. Shear stresses are mainly resisted by the diagonal shear connector wires as well as the mortar layers when subjected to out-of-plane bending or shear forces.

Although the calculations performed use the same equations as those used for the same structural elements constructed using reinforced concrete, yet modifications to various factors and particular elements was accomplished due to the different nature of the CSP system as opposed to the reinforced concrete one. Assumptions are described when calculating for the CSP in this section.

In the following, similar sample floor plan and procedure that was used to evaluate the performance of commercially available Base model that was used by El Demerdash [11], is considered to check the flexural capacity, shear capacity as well as deflection limit of the Base Panel as well as the optimized panels.

The following are the assumptions used for analysis of panel.

All the spans simply supported, Length = 8ft (2.43m) (Tested By: El Demerdash [11])

Unit Weight of mortar = 2,100 kg/m^3 = 130 lb/ft^3

f_c' = 3,000 psi

f_y = 60,000 psi (Hot Rolled steel rebars)

f_y = 80,000 psi (Cold Rolled steel wire mesh)

TABLE 9.5(a)—MINIMUM THICKNESS OF NONPRESTRESSED BEAMS OR ONE-WAY SLABS UNLESS DEFLECTIONS ARE CALCULATED

	Minimum thickness, *h*			
	Simply supported	One end continuous	Both ends continuous	Cantilever
Member	Members not supporting or attached to partitions or other construction likely to be damaged by large deflections.			
Solid one-way slabs	$\ell/20$	$\ell/24$	$\ell/28$	$\ell/10$
Beams or ribbed one-way slabs	$\ell/16$	$\ell/18.5$	$\ell/21$	$\ell/8$

Notes:
Values given shall be used directly for members with normalweight concrete (density w_c = 2320 kg/m^3) and Grade 420 reinforcement. For other conditions, the values shall be modified as follows:
a) For structural lightweight concrete having unit density, w_c, in the range 1440-1920 kg/m^3, the values shall be multiplied by $(1.65 - 0.003w_c)$ but not less than 1.09.
b) For f_y other than 420 MPa, the values shall be multiplied by $(0.4 + f_y/700)$.

Figure (C.1): Using following table shown from ACI 318

(Minimum Deflection Thickness)

- *Calculation for Base Model from El Demerdash et al. 2013* [11]

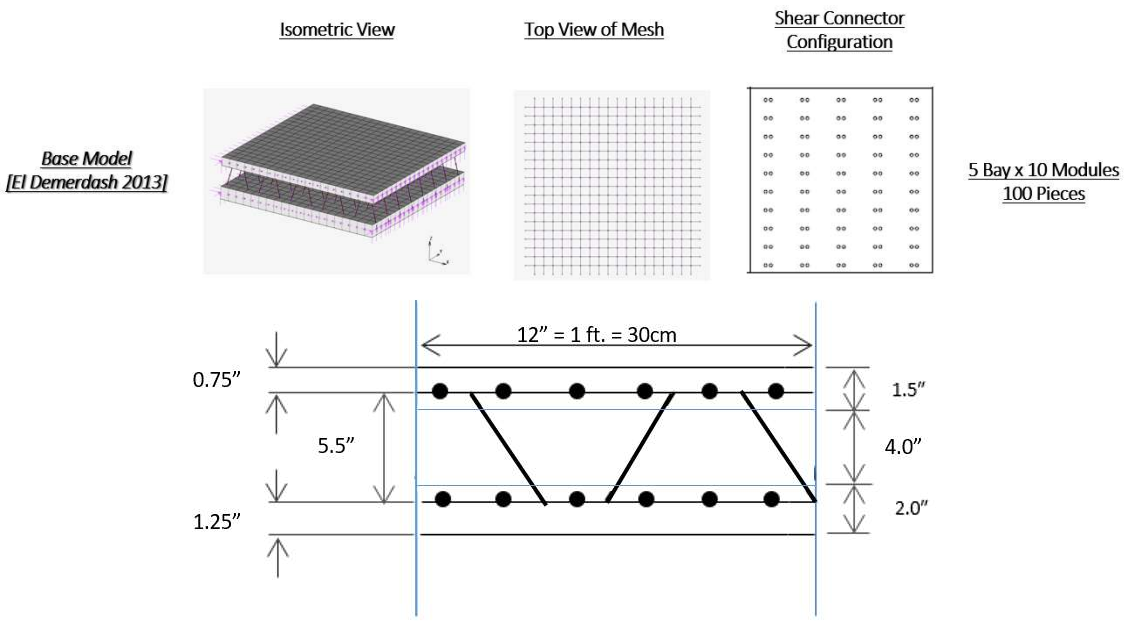

Figure (C.2): Cross Section of Base Model

$h = \frac{\ell}{20}$ Due to assumption of simply supported

$h = \frac{8 \times 12}{20} = 4.8\ in$ (8 ft = 2.45 m this is the span in the floor plan tested by El Demerdash [11]

Actual thickness = $7.5'' > 4.8''$

$d = 7.5'' - 1.25'' = 6.25''$

Self-weight of $12''$ strip:

Self-weight $= \frac{3.5*12}{144} * 130 = 38\ lb/ft$

**where 3.5 is the total mortar thickness *130 is the mortar unit weight*

Loading condition

$U = 1.2\ D.L. + 1.6\ L.L.$

** for residential buildings L.L. usually equals around 40 psf*

**assume additional D.L. tiling etc of 15 psf*

Therefore:

$U = 1.2(38 + 15) + 1.6(40) = 128\ lb/ft$

$M_u = \frac{w\ell^2}{8} = \frac{128 * (8)^2}{8} * 12in \cdot lb = 12288\ in \cdot lb$

Required Nominal Moment $M_n = \frac{M_u}{\emptyset} = \frac{12288}{0.9} = 13653\ in \cdot lb$

$M_n = Tjd$ *where* $jd = 0.9 \times 6.25 = 5.625''$

$M_n = 13653 = A_s \times f_y \times jd = A_s f_y \times (5.625)$

$A_S = 6 * \left[\frac{(0.12)^2\pi}{4}\right] = 6(0.0113) = 0.068in^2$

$[(0.068 \times 80{,}000)] \times 5.625 = 30600\ in.lb\ > 13653\ in.lb$ OK

$\_M_n > \frac{M_u}{\emptyset}$ OK

<u>Maximum Deflection Calculations for simply supported one-way slab:</u>

Based on the previous slab design, an analysis of the serviceability of the slab design with respect to its abidance with the maximum allowable deflection limits will be performed in this section.

$E_c = 57.000\sqrt{f_c'} = 57.000\sqrt{3.000} = 3.12 \times 10^6$ psi (21.525 MPa)

$E_s = 29 * 10^6$ psi (200.000 MPa)

Modular Ratio $n = \frac{E_s}{E_c} = \frac{29*10^6}{3.12*10^6} = 9.3$

Modulus of Rupture = $f_r = 7.5\sqrt{f_c'} = 7.5\sqrt{3.000} = 410.8$ psi

$$I_g = \frac{12 \times (1.5)^3}{12} + \frac{12 \times (2.0)^3}{12} + (12 \times 1.5) \times 2.75^2 + (12 \times 2) \times 3^2 = 363\ in^4$$

For 3D EPS Panels $I_e = I_{eff} = \frac{2}{5} I_g = 145\ in^4$

$M_{cr} = \frac{f_r \times I_g}{y} = \frac{410.8 \times 145}{3.25} = 18.328\ in \cdot lb$

Total Dead Loads = self-weight + finishings = 38 +15 = <u>53 psf</u>

Live Loads = 40 psf

Total Dead and Live Loads = 53 + 40 = <u>93 psf</u>

Cold Rolled ${A_s}/{_{ft}} = 0.068\ in^2$

$$d = h - 1.25 - \frac{d_b}{2} = 7.5 - 1.25 - \frac{0.12}{2} = 6.19\ in$$

$$\frac{bc^2}{2} + nA_s c - nA_s d = 0$$

$$\frac{12c^2}{2} + 9.3 * 0.118c - 9.3 * 0.118 * 6.1 = 0$$

We compute that <u>$c = 0.97\ in$</u>

<u>For Dead Load:</u>

Service load moment $\frac{w\ell^2}{8} = \frac{53*(8)^2}{8} * 12in \cdot lb = 5080\ in \cdot lb$

$5080\ in \cdot lb < M_{cr} = 18.328\ in \cdot lb$

$$\Delta = \frac{5wl_n^4}{384E_cI_e}$$

Therefore $\Delta = \frac{5*53*(8*12)^4}{384*(3.12*10^6)*145} * \frac{1}{12} = 0.011$ in

Deflection under Service Load

Service load moment $\frac{w\ell^2}{8} = \frac{93\times(8)^2}{8} \times 12in \cdot lb = 8920\ in \cdot lb$

$8920\ in \cdot lb < M_{cr} = 18.328in \cdot lb$

$$\Delta_L = \frac{5 * 93 * (8 * 12)^4}{384 * (3.12 * 10^6) * 145} * \frac{1}{12} = 0.227\ in$$

Deflection Requirements:

$\frac{\ell}{360} = \frac{8*12}{360} = 0.267$ in $> \Delta_L$ (Immediate deflection due to Live Loads)

Shear Capacity Check

$V_c = 2\sqrt{f_c'}hd = 2\sqrt{3000} \times 12 \times 3.5/1000 = 4.6\ kip$

$V_s = \frac{A_s f_y d}{s} = \frac{(10\times0.12^2*3.14) \times 80.000 \times 7.5}{4*1000}$ =16.9 kip

$V_n = (V_c + V_s) = 20.5\ kip$

$V_u = {}^{Pu}/_{2} = {}^{128 * 8 * 12}/_{(2 * 1000)} = 6.1\ kip < [0.75 * 20.5 = 16.16kip]$ *OK*

- *Calculation for Optimized CSP Model 50*

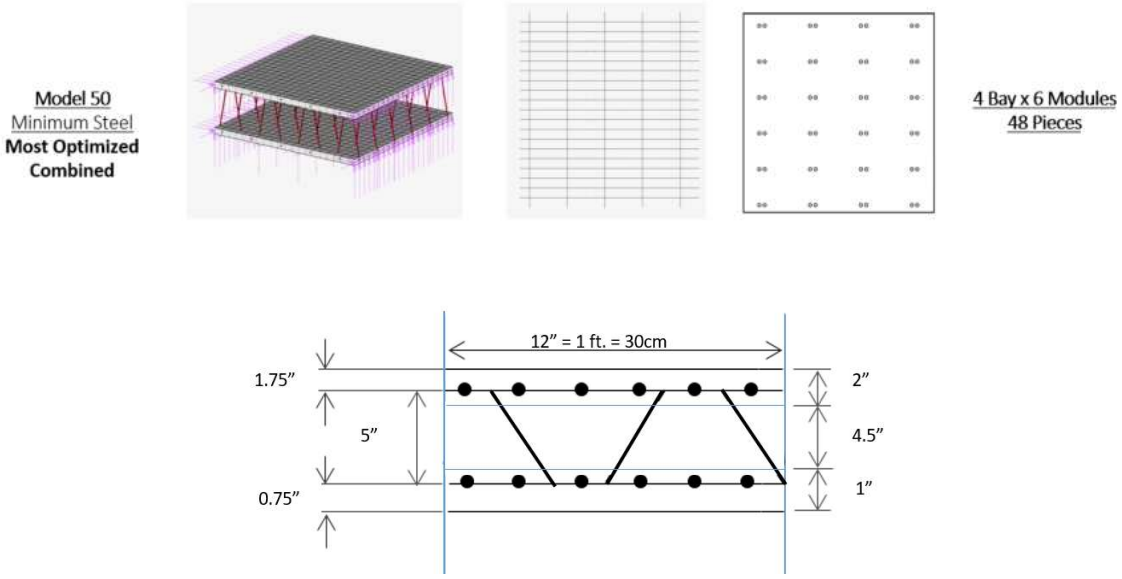

Figure (C.3): Cross Section of Optimized Model 50

$d = 7.5'' - 1.25'' = 6.25''$ (158 mm)

Self-weight of 12″ (30 cm) strip:

Self-weight $= \frac{3*12}{144} * 130 = 33\ lb/ft$ (49 kgf/m)

**where 3.5 is the total mortar thickness *130 is the mortar unit weight*

Loading condition

$U = 1.2\ D.L. + 1.6\ L.L.$

** for residential buildings L.L. usually equals around 40 psf (195 kgf/m^2)*

**assume additional D.L. tiling etc of 15 psf (73 kgf/m^2)*

Therefore:

$U = 1.2(33 + 15) + 1.6(40) = 121\ lb/ft$ (180 kgf/m)

$$M_u = \frac{w\ell^2}{8} = \frac{121 * (8)^2}{8} * 12in \cdot lb = 11616\ in \cdot lb$$

Required Nominal Moment $M_n = \frac{M_u}{\emptyset} = \frac{11616}{0.9} = 12907\ in \cdot lb$

$M_n = Tjd$ *where* $jd = 0.9 \times 6.25 = 5.625''$ (142.8 mm)

$M_n = 12907 = A_s \times f_y \times jd = A_s f_y \times (5.625)$

$A_S = 6 * \left[\frac{(0.09)^2\pi}{4}\right] = 0.038in^2$ (24.5 mm^2)

$[(0.038 \times 80{,}000)] \times 5.625 = 17100\ in.lb\ > 12907\ in.lb$ OK

$\_M_n > \frac{M_u}{\emptyset}$ OK

Maximum Deflection Calculations for simply supported one-way slab:

Based on the previous slab design, an analysis of the serviceability of the slab design with respect to its abidance with the maximum allowable deflection limits will be performed in this section.

$E_c = 57.000\sqrt{f_c'} = 57.000\sqrt{3.000} = 3.12 \times 10^6$ psi (21.525 MPa)

$E_s = 29 * 10^6$ psi (200.000 MPa)

Modular Ratio $n = \frac{E_s}{E_c} = \frac{29*10^6}{3.12*10^6} = 9.3$

Modulus of Rupture = $f_r = 7.5\sqrt{f_c'} = 7.5\sqrt{3.000} = 410.8$ psi (2.8 MPa)

$I_g = \frac{12\times(1)^3}{12} + \frac{12\times(2.0)^3}{12} + (12\times 1)\times 3.25^2 + (12\times 2)\times 2.75^2 = 371\ in^4$ (1.54 x 10^8 mm^4)

For 3D EPS Panels $I_e = I_{eff} = \frac{2}{5} I_g = 126\ in^4$ (5.24 x 10^7) mm^4

$M_{cr} = \frac{f_r \times I_e}{y} = \frac{410.8\times 126}{3.25} = 16040\ in\cdot lb$

Total Dead Loads = self-weight + finishings = 33 +15 = <u>48 psf (234 kgf/m^2)</u>

Live Loads = 40 psf (195 kgf/m^2)

Total Dead and Live Loads = 48 + 40 = <u>88 psf (430 kgf/m^2)</u>

<u>For Dead Load:</u>

Service load moment $\frac{w\ell^2}{8} = \frac{48*(8)^2}{8} * 12in\cdot lb = 4608\ in\cdot lb$

$4608\ in\cdot lb < M_{cr} = 16040\ in\cdot lb$

$\Delta = \frac{5wl_n^4}{384E_cI_e}$

Therefore $\Delta = \frac{5*48*(8*12)^4}{384*(3.12*10^6)*126} * \frac{1}{12} = 0.135$ in (3.4 mm)

<u>Deflection under Service Load</u>

Service load moment $\frac{w\ell^2}{8} = \frac{88\times(8)^2}{8} \times 12in\cdot lb = 8400\ in\cdot lb$

$8400\ in\cdot lb < M_{cr} = 16040\ in\cdot lb$

$\Delta_L = \frac{5*88*(8*12)^4}{384*(3.12*10^6)*126} * \frac{1}{12} = 0.22\ in$ (5mm)

Deflection Requirements:

$\frac{\ell}{360} = \frac{8*12}{360} = 0.267$ in $> \Delta_L$ (Immediate deflection due to Live Loads)

Shear Capacity Check

$V_c = 2\sqrt{f_c'}hd = 2\sqrt{3000} \times 12 \times 3/1000 = 3.97\ kip$ *(1800 kgf)*

$V_s = \frac{A_s f_y d}{s} = \frac{(8 \times 0.12^2 * 3.14) \times 80.000 \times 7.5}{8*1000}$ =5.09 kip *(2308 kgf)*

$V_n = (V_c + V_s) = 9.03\ kip$ *(4082 kgf)*

$V_u = {}^{Pu}/_{2} = {}^{121 * 8 * 12}/_{(2 * 1000)} = 5.81\ kip < 0.75 * 9.03 = 6.77\ kip$ *(3070 kgf) OK*

- **Case Study:**

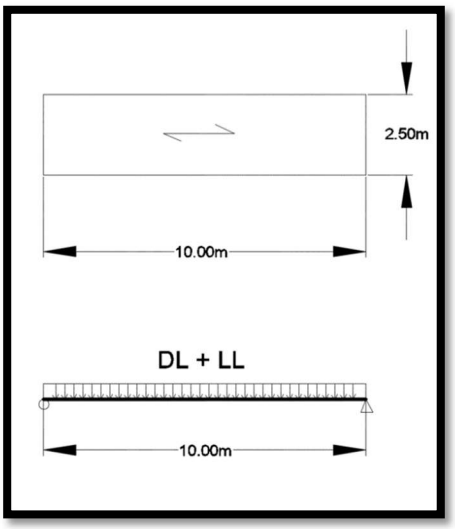

The case requires a design of slab 10m (32.8ft) span x 2.5m (8.2ft) width using a CSP. The thickness of the panel is 25cm (9.8″). The proposed panel cross section is illustrated in the figures below:

This floor is designed according ACI-318 design criteria's and minimum loading according ASCE 7. Additional required hot rolled rebars for flexural strength is calculated so that design meets the ACI-318 flexural requirement which is the critical in this design due to the long span of the panel.

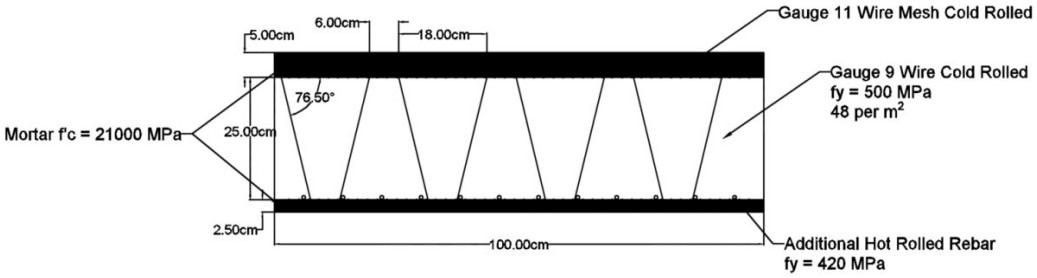

Side View

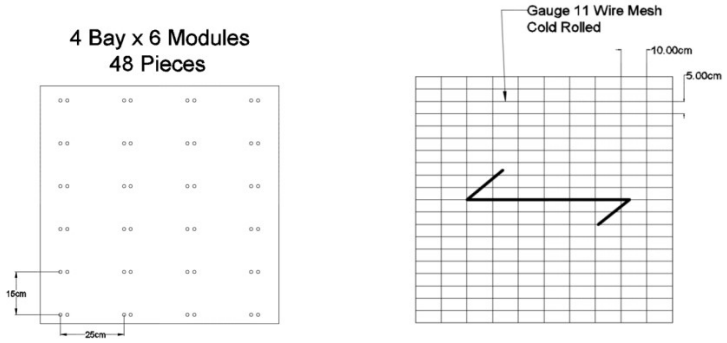

Top View

Loading Assumptions:

Self-weight of 1m (32.8ft) strip:

Self-weight $= \frac{7.5}{100} * 2400 = 180\ kgf/m$ (120 lb/ft)

**where 7.5cm is the total mortar thickness 5cm (2") on top and 2,5cm (1") on bottom.*

**2400 kg/m^3 (150 lb/ft^3) is the assumed mortar unit weight*

Loading conditions

$U = 1.2\ DL\ +\ 1.6\ LL$

** for residential buildings L.L. usually equals around (200 kgf/m^2) (40 psf)*

**assume additional D.L. tiling etc of 70 kgf/m^2 (15 psf)*

Therefore:

$U = 1.2(180 + 70) + 1.6(200) = 620\frac{kgf}{m}$ $(416\ lb/ft)$

$M_u = \frac{w\ell^2}{8} = \frac{620 * (10)^2}{8} = 7750\ kgf.m$

$d = (32.5\ - 2.5) = 30cm$

Required Nominal Moment $M_n = \frac{M_u}{\emptyset} = \frac{7750}{0.9} = 8610\ kg.m$

$M_n = Tjd$ *where* $jd = 0.9 \times 30cm = 27cm$

$M_n = 8610 = A_s \times f_y \times jd = A_s f_y \times (27)$

$A_S = 20 * \left[\frac{(0.23)^2\pi}{4}\right] = 0.83\ cm^2$ (0.12 in^2)

$[0.83 \times 5100] \times 27 = 114291\ kgf.cm\ < 861000\ kg.cm$ Additional Rebars required

$$861000 = [(A_{S1} * 5100) + (A_{S2} * 4200)] * 30cm$$

**where A_{S1} is the Cold rolled wire mesh and A_{S2} is for the Hot rolled rebars*

Therefore:

$$28700 = 0.83 * 5100 + A_{S2} * 4200$$

$A_{S2} = 5.8\ cm^2$ (0.89 in^2)

Since A_S of one 8 mm rebar is equal to 0.50 cm^2 therefore 12 additional 8 mm rebar / m is needed at every 8cm.

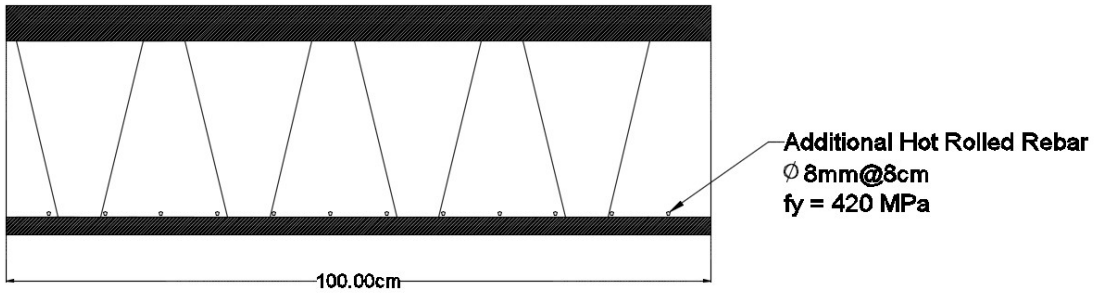

Shear Capacity Check

$$V_c = 0.53\sqrt{f_c'}b_w d = 0.53\sqrt{200} \times 100 \times 5 = 3747\ kgf$$

$V_s = \frac{A_s f_y d}{s} = \frac{(6 \times 0.29^2 * 3.14/4) \times 5100 \times 30}{25}$ =2424 kgf << *3747 Not OK Use Higher Gauge Wire – Gauge 7*

$V_s = \frac{A_s f_y d}{s} = \frac{(6 \times 0.36^2 * 3.14/4) \times 5100 \times 30}{25}$ = *3735 kgf ≈ 3747 kgf OK*

*V_n = 0.75 * (Vc + Vs) = .75 * (3747 + 3735) = 5611 kgf*

$V_u = {}^{Pu}/_{2} = {}^{620 * 1 * 10}/_{2} = 3100\ kgf < Vn = 5611$ *(OK) Pass*

Maximum Deflection Calculations for simply supported one-way slab:

Based on the previous slab design, an analysis of the serviceability of the slab design with respect to its abidance with the maximum allowable deflection limits will be performed in this section.

$E_c = 4700\sqrt{f_c'} = 4700\sqrt{20} = 21000$ MPa

$E_s = 200.000$ MPa $(29 * 10^6)$ psi

Modular Ratio $n = \frac{E_s}{E_c} = \frac{200000}{21000} = 9.52$

Modulus of Rupture = $f_r = 0.62\sqrt{f_c'} = 0.62\sqrt{20} = 2.8$ MPa (28 kg/cm^2) (410.8 psi)

$I_g = \frac{100*(2.5)^3}{12} + \frac{100*(5)^3}{12} + (100 \times 2.5) \times 16^2 + (100 \times 5) \times 12^2 = 1.37\ x\ 10^5$cm^4

For 3D Panels $I_e = I_{eff} = \frac{2}{5} I_g = 54868$ cm^4

$M_{cr} = \frac{f_r \times I_e}{y} = \frac{28 \times 54868}{15} = 36578\ kg.cm$

Total Dead Loads = self-weight + finishing = 180 +70 = <u>230 kgf/m^2</u>

Live Loads = 200 kgf/m^2

Total Dead and Live Loads = 230 + 200 = <u>430 kgf/m^2</u>

Service load moment $\frac{w\ell^2}{8} = \frac{430*(10)^2}{8} = 5375\ kgf.m$ = 537500 *kgf,cm*

$537500\ in \cdot lb > M_{cr} = 36578\ in \cdot lb$

$\Delta = \frac{5wl_n^4}{384E_cI_e}$ Therefore $\Delta = \frac{5*200*(10)^4}{384*(5.5*10^{-4})2.1*10^9} = 0.022$ m (2.2cm)

<u>Deflection Requirements:</u>

$\frac{\ell}{360} = \frac{10*100}{360} = 2.7$ cm $> 2.2\ cm$ (Immediate deflection of due to Live Loads) Pass ACI Table 9.5 (b)

In order to simulate the model a displacement-controlled loading is required, due to softening of the material and possible drop of stiffness due to buckling of shear connectors. Hence, a four-point loading on the 10m (32.8ft) floor is modeled to evaluate the performance of the CSP. 1m (3.2ft) strip of the CSP is modeled following the methodology steps defined in this study for simulating the CSP. The CSP is loaded until failure and failure locations is illustrated in the figures below. Since the CSP is reinforced with additional hot rolled longitudinal rebars, the panel is failing at ultimate load due to mix of buckling of shear connectors and cracking of concrete due to shear.

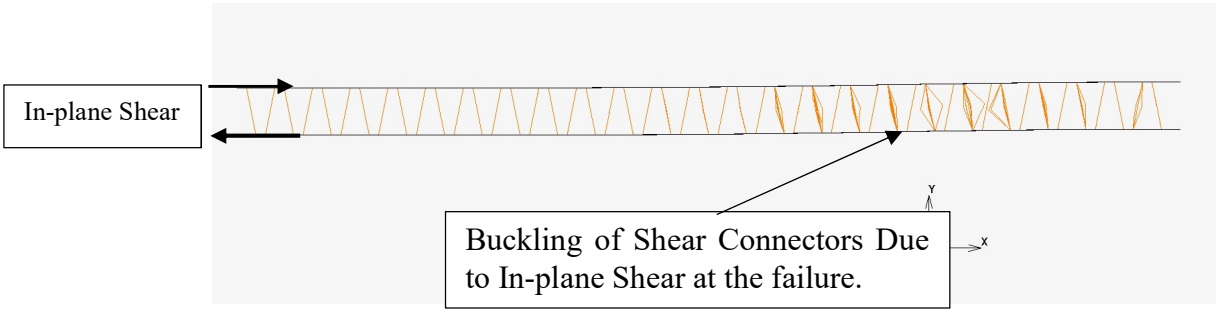

Figure (C.4): Buckling of shear connector at time of Failure Due to In-plane Shear

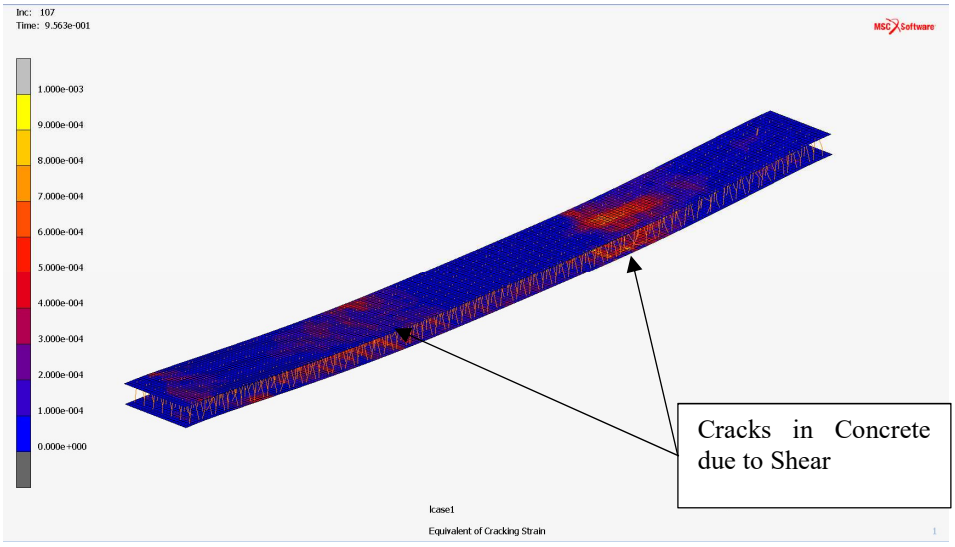

Figure (C.5): Shear Cracks at Ultimate load, since the CSP is reinforced with additional Longitudinal Rebars.

APPENDIX D

Analytical Calculation for CSP under In-Plane Axial Loading

Parallel-CSP Under In-Plane Loading

The following calculation is made for evaluating the capacity of Parallel-CSP under in-plane axial loading. The actual full-scale experiment was done at UCI by Botello et al. in 2015. In the observation of test, a sudden failure the wall was observed. This happened following loud sound, which was due to separation of shear connectors from the steel meshes. As a result, the composite action in the wall was lost and each face resisted the in-plane axial force independently, which reduced the total capacity of the wall drastically. In the following calculation, the behavior of the panel is evaluated.

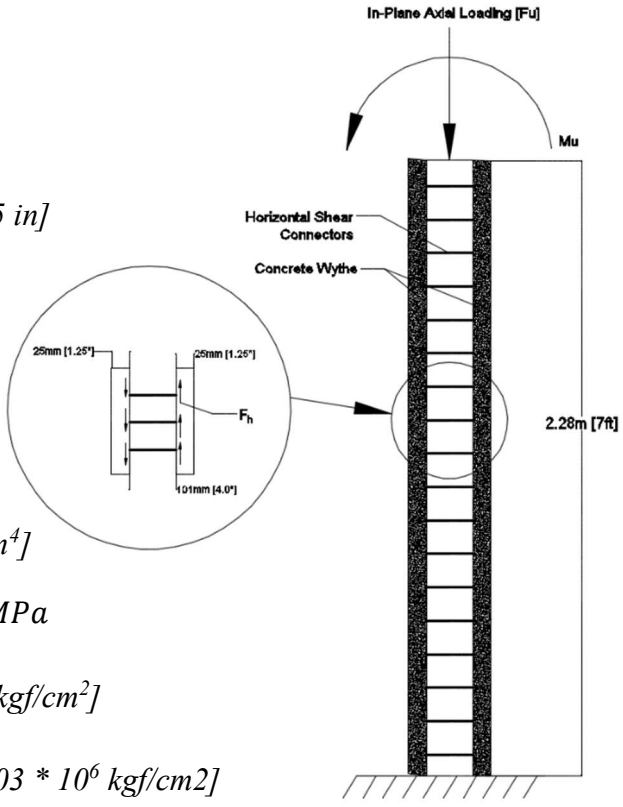

Panel Width = b = 122cm [48 in]

Panel Thickness = h = 15.2cm [6.0in]

Mortar Thickness (avg) t = 3.18cm [1.25 in]

Panel Height l_u = 228cm [90 in]

f'_c = 20.68 MPa [3,000 psi] (28-Day)

$I_g = (1/12(b)(t^3) + (b*t) *(h/2-t/2)^2)*2$

I_g = 28824 cm^4 [692.5 in^4]

$I_e = I_g/5 = 28824/5 = 5765$ cm4 [138.5 in^4]

$E_c = 4700\sqrt{f_c'} = 4700\sqrt{25} = 23500\ MPa$

E_c = 23500 MPa [3408.3 ksi] [2.4 $*$ 10^5 kgf/cm^2]

$E_s = 200.000\ MPa\ [29 * 10^3\ ksi]$ *[2.03 * 10^6 kgf/cm2]*

Buckling Capacity of Wall with composite action.

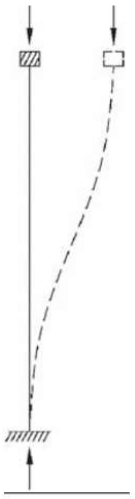

$$P_c = \frac{\pi^2 E I_g}{(k l_u)^2}$$

where:

P_c = Eulers Buckling Load

E = Elastic Modulus of Mortar

k = End Restraint Effective Length

l_u = Effective Length

$$P_c = \frac{\pi^2 E I_e}{(k l_u)^2} = \frac{\pi^2 2.4{*}10^5 {*}\ 5765}{(1{*}228)^2} = 2.62 * 10^5 \text{ kgf } [2576 \text{ kN}] [578 \text{ kip}] \qquad [Eq.D1]$$

Shear Capacity of horizontal shear connectors:

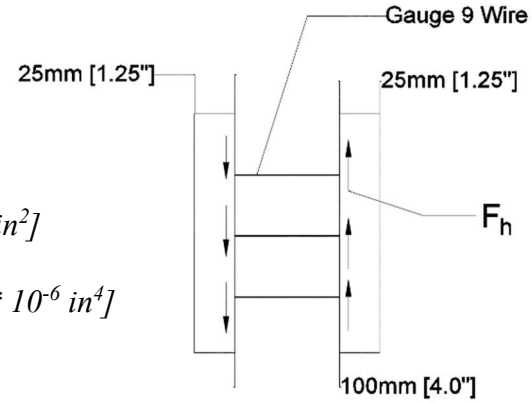

$Ø_{(wire)}$ = 3.0mm [0.114 in]

Wire cross sectional area A_s = 7.0 mm^2 [0.011 in^2]

*Moment of Area for Wire I_w = 3.97 mm^4 [9.55 * 10^{-6} in^4]*

Length of Wire L_w = 101mm [4in]

As explained in the text, since the bending stiffness of wire is very small, and the wire can easily be deformed, the stresses in the wire is mainly controlled by shear stresses

$$\sigma = \sqrt{3\tau_{xy}^2}$$

$$\tau_{xy} = \frac{4\ F_h}{3\ A_w} = 0.20\ F_h$$

$\sigma = 0.35F_h = Yeild\ strenth\ of\ the\ wire = 386$ MPa [56000 psi]

$F_{h\ [max]}$ per Wire = 1103 N [4910 lbs]

Total Number of Shear Connectors Wires in Parallel–CSP Wall = 90

$F_{h\ (max\ total)}$ *= 99.3 kN [22kip]*

$F_h * L_w = M_u$ *(Maximum Moment that shear connectors can handle before failing)*

*99.3 * 101 = 10030.4 kN – mm*

Axial Force * Eccentricity = Induced Moment to the Panel

Induced Moment to the Panel / Axial Force of Panel Before Failing of Shear connectors *in experiment = Eccentricity -> (10030.4 / 802) = 12.47mm [0.49in] O.K.*

This eccentricity is within the allowable maximum eccentricity for in-plane axial loading: t/6 [152mm/6 = 25mm [1.00in]

Upon failing of shear connectors the composite action between the two panel is lost and each panel would work independently which is dramatically lower than buckling capacity when there is composite action between the two layers of the wall.

Buckling capacity of each panel.

$I_g = 1/12(b)(t)^3 = 1/12 * 120 * 25^3 = 156.25\ cm^4$ *[3.75* in^4*] Moment of area for each wythe*

$P_c = 2 * \frac{\pi^2 E I_e}{(k l_u)^2} = 2 * \frac{\pi^2 2.4*10^5 * 156}{(1*228)^2} = 2.96 * 10^4$ kgf [290 kN] [65 kip] << 802 kN [180 kips]

Therefore, upon failing the shear connectors, the individual panels cannot hold the load and will buckle at the same time.

Similar behavior was observed in the experiment. The failure of the specimen was sudden with no apparent cracks before complete failure of the wall. Before the collapse of the wall loud sounds of the separation of the welding between the horizontal trusses and the two wire mesh faces was heard. The loss of composite action between the two face caused each face to work independently and reduce drastically the capacity of the wall. After the composite action was missing each face experience sufficient buckling to fail. [36].

Diagonal-CSP Under In-Plane Loading

Since a similar cross section of the panel is used as Parallel-CSP that was analyzed in the previous section, the buckling capacity of panel under full-composite action and Non-Composite action is the same.

Here is a summary:

Full-Composite Action

$I_e = I_g / 5$

$I_g = (1/12(b)(t^3) + (b*t) *(h/2-t/2)^2)*2$

$I_g = 28824\ cm^4\ [692.5\ in^4]$

$I_e = I_g/5 = 28824/5 = 5765\ cm4\ [138.5\ in^4]$

$P_c = \frac{\pi^2 EI_e}{(kl_u)^2} = \frac{\pi^2 2.4*10^5 * 5765}{(1*228)^2} = 2.62 * 10^5$ kgf [2576 kN] [578 kip]

Non-Composite Action:

$I_g = (1/12(b)(t^3) = 1/12 * 120 * 25^3 = 156.25\ cm^4\ [3.75\ in^4]$ *Moment of area for each wythe*

$P_c = 2 * \frac{\pi^2 EI_e}{(kl_u)^2} = 2 * \frac{\pi^2 2.4*10^5 * 156}{(1*228)^2} = 2.96 * 10^4$ kgf [290 kN] [65 kip]

To evaluate the Diagonal shear connector capacity due to interface shear, the equation by Nijhawan [37] is used.

$F_h = A_s N \cos(\theta) (f_{st} + f_{sc})/2$ *[Eq. D2]*

Shear Capacity of horizontal shear connectors:

$Ø_{(wire)}$ *= 3mm [0.11 in] Wire Gauge 9 used for Shear connectors*

Wire cross sectional area $A_s = 7.06\ mm^2\ [0.011\ in^2]$

Number of Shear truss connectors in the 1.22m x 2.28m [48in x 90in] (W X H) in Diagonal-CSP design is: 156

The angle of shear connectors $\theta = 63^o$

In order to evaluate the allowable stress in compression wire members, both buckling limit and yielding of the wire should be checked:

Buckling limit of steel wires:

$$P_c = \frac{\pi^2 E I_e}{(k l_w)^2}$$

Assuming Shear connector wires as truss element: K = 1

Moment of Area for Wire $I_w = 4.2\ mm^4\ [1.01 * 10^{-5}\ in4]$

Length of unsupported wire $L_w = 10.1cm\ [4.0in] * csc(63^o) = 11.4cm\ [4.5in]$

$E_s = 200{,}000MPa\ [29{,}000\ ksi]$

$P_c = 647.6\ N\ [145.6\ lbs.]$

$f_{sc} = Pc / A_s = 110\ MPa\ [12.8\ ksi]$

$f_{st} = 0.6*f_y = 0.6*386\ MPa$

$f_{st} = 231.6MPa\ [33600\ psi]$ Using similar wire as used in Parallel-CSP that was tested at UCI for purpose of comparison

Plugging values in [Eq. D2] to evaluate interface shear strength of the panel.

$F_h = A_s\ N \cos(\theta)\ (f_{st} + f_{sc})/2$

$F_h = 165.4kN\ [37.2\ kips]$

$F_h * L_w = M_u$ *(Maximum Moment that shear connectors can handle before failing)*

$165.4 * 101.6 = 16804.6\ kN - mm\ [148.8\ kips - in]$

Axial Force Capacity = Induced Moment to the Panel / Eccentricity

P_c = 16804.6/12.7 = 1323.2 kN [297.6 kips] Diagonal-CSP shear connector Capacity

Crushing strength of the wall

$P_c = 0.85.A_c.f'_c. + (E_s/E_c - 1)(A_{s(Mesh\ Total)}.f'_c)$

P_c = 1387.4 kN [311.9 kips] > 1323.2 kN [297.6 kips]

Shear Connector Failure Dominates before Crushing or Buckling of the Wall

Optimize-CSP Under In-Plane Loading

Since a similar cross section of the panel is used as Parallel-CSP that was analyzed in the previous section, the buckling capacity of panel under full-composite action and Non-Composite action is the same.

Here is a summary:

Full-Composite Action

$I_e = I_g / 5$

$I_g = (1/12(b)(t^3) + (b*t) *(h/2-t/2)^2)*2$

$I_g = 28824\ cm^4\ [692.5\ in^4]$

$I_e = I_g/5 = 28824/5 = 5765\ cm4\ [138.5\ in^4]$

$P_c = \frac{\pi^2 EI_e}{(kl_u)^2} = \frac{\pi^2 2.4*10^5 * 5765}{(1*228)^2} = 2.62 * 10^5$ kgf [2576 kN] [578 kip]

Non-Composite Action:

$I_g = (1/12(b)(t^3) = 1/12 * 120 * 25^3 = 156.25\ cm^4\ [3.75\ in^4]$ *Moment of area for each wythe*

$P_c = 2 * \frac{\pi^2 EI_e}{(kl_u)^2} = 2 * \frac{\pi^2 2.4*10^5 * 156}{(1*228)^2} = 2.96 * 10^4$ kgf [290 kN] [65 kip]

To evaluate the Diagonal shear connector capacity due to interface shear, the equation by Nijhawan [37] is used.

$F_h = A_s N \cos(\theta) (f_{st} + f_{sc})/2$ *[Eq. D2]*

Shear Capacity of horizontal shear connectors:

$Ø_{(wire)}$ *= 3.6mm [0.15 in] Wire Gauge 7 used for Shear connectors*

Wire cross sectional area $A_s = 10.17\ mm^2\ [0.0176\ in^2]$

Number of Shear truss connectors in the 1.22m x 2.28m [48in x 90in] (W X H) in Diagonal-CSP design is: 108

The angle of shear connectors $\theta = 63^o$

In order to evaluate the allowable stress in compression wire members, both buckling limit and yielding of the wire should be checked:

Buckling limit of steel wires:

$$P_c = \frac{\pi^2 E I_e}{(k l_w)^2}$$

Assuming Shear connector wires as truss element: K = 1

Moment of Area for Wire $I_w = 8.24\ mm^4\ [2.48 * 10^{-5}\ in4]$

Length of unsupported wire $L_w = 10.1cm\ [4.0in] * csc(63^o) = 11.4cm\ [4.5in]$

$E_s = 200{,}000MPa\ [29{,}000\ ksi]$

$P_c = 1580.9\ N\ [355.4\ lbs.]$

$f_{sc} = Pc / A_s = 138.7\ MPa\ [20.12\ ksi]$

$f_{st} = 0.6*f_y = 0.6*386\ MPa$

$f_{st} = 231.6MPa\ [33600\ psi]$ Using similar wire as used in Parallel-CSP that was tested at UCI for purpose of comparison

Plugging values in [Eq. D2] to evaluate interface shear strength of the panel.

$F_h = A_s\ N\ cos(\theta)\ (f_{st} + f_{sc})/2$

$F_h = 206.8kN\ [46.5\ kips]$

$F_h * L_w = M_u$ *(Maximum Moment that shear connectors can handle before failing)*

$206.8 * 101.6 = 21010.9\ kN - mm\ [186.1\ kips - in]$

Axial Force Capacity = Induced Moment to the Panel / Eccentricity

P_c = 16804.6/12.7 = 1654.4 kN [372.6 kips] Optimized-CSP shear connector Capacity

- *Crushing strength of the wall*

$P_c = 0.85.A_c.f'_c. + (E_s/E_c - 1)(A_{s(Mesh\ Total)}.f'_c)$

P_c = 1387.4 kN [311.9 kips] < 1654.4 kN [372.6 kips]

Crushing of the concrete failure controls.

APPENDIX E

Effect of Optimization on Economic Thickness of Insulation

A critical factor in making the decision to invest in insulating structural elements is to analyze the cost of the proposed system. The basic rule of insulation is that by increasing the thickness of insulation, the cost of energy due to heat loss decreases. However, increasing the thickness of material comes with increase in cost. Therefore, there is a limit to the amount of insulation that can be justified as cost effective. Beyond the point of optimization, an increase in the thickness of the insulation becomes un-economical, as it cannot be recovered through small heat savings. This limiting value is referred to as the ideal "economic thickness" of the specified insulation.

In order to calculate cost effective thickness of insulation, cost of Material and cost of Energy loss should be calculated for every thickness of insulation for any insulating system. For the base model used in this study, the cost of Material for a unit of CSP is calculated as follows:

Cost of Material = Cost of Steel + Cost of Concrete + Cost of Foam

These three elements are considered in calculation of Cost of Material since, amount of steel and concrete is different in the two designs of CSP (Base Model and Optimized Model). Cost of Foam is directly linked to the Thickness of Insulation.

For Base model the cost is as follows:

Volume of Steel per unit CSP = 7.3 lb (1 Unit of CSP Base model is 1 m^2)

Assume cost of Steel = 1.5 $/lb (Source: http://www.mkmetal.net/)

Volume of Concrete per unit CSP = 487 lb

Assume cost of Concrete = 0.025 $/lb (Source: http://www.cemexusa.com)

Cost of Insulating Foam = 50$ per cubic yard.

Volume of Insulating Foam = Variable per unit thickness.

Approximate Cost of CSP Base Model Unit: $7.3*1.5+487*0.025+50/(12*3/t_f)$ Eq (14)

Where t_f is the thickness of insulating Foam.

For evaluating the Cost of Energy, the following formula is used to evaluate the heat loss through building envelope.

$$E = \frac{T_o - T_{out}}{R_{eff}} \times S \times t \qquad \text{Eq. (17)}$$

Where: **S [m^2]** is the surface area of the building **E [W.hr]** is the heating or cooling energy required to maintain inside temperature of **T_o [K]** when the outside temperature is **T_{out} [K]** during the interval exposure, **t [hr]** and **R_{eff} [m^2 K/ W]** is the effective thermal resistance of the building material.

In order to evaluate the fluctuation of outside temperature base on the temperature inside **($T_0 - T_{out}$)** the building for any location, Degree-days data can be used. Degree days are a specialist type of weather data, calculated from readings of outside air temperature. For example, a Degree-Day data for Dubai, UAE is selected with 3500 Degree-Day in one Year. (Source: www.Degreedays.net).

In the calculation [t is set to 24] to convert Degree-day data to Degree-hr.

Next R_{eff} is calculated for different thickness of insulating material in the base model.

Concrete Thermal Conductivity: k = 0.5 W/mK

Thickness of Concrete = (Top 50mm) + (Bottom 38mm″) = 88mm (3.5″)

$$Rc = {}^{x}/_{(A \times k)} = {}^{0.09}/_{(1 \times 0.5)} = 0.18 \text{ [K/W]}$$ (1.008 h.ft2.oF /BTU R-Value)

Foam Thermal Conductivity: k_f = 0.03 W/mK

Thickness of Foam ranges from (4″ to 8″) (10cm to 20cm) to analyzed in this example.

$$R_{in} = {}^{x}/_{(A \times k)} = {}^{0.1}/_{(1 \times 0.03)} = 3.39 \text{ [K/W]} \quad \text{upto } {}^{0.2}/_{(1 \times 0.03)} = 6.77 \left[\frac{\text{K}}{\text{W}}\right]$$

(37 h.ft^2.^{o}F /BTU R-Value)

Shear Connectors connecting two faces through the insulating foam: 100 Gauge 9:

Diameter = 0.11″ -> As = 100*0.009 = 0.95 in^2 (0.00006 m^2)

Length of Shear connectors connecting the two faces = 5.5″ (0.14m)

Steel wires Thermal Conductivity k_s = 54 W/mK

$$R_s = {}^{0.14}/_{(0.00061 \times 54)} = 4.22 \text{ K/W}$$ (23 h.ft2.^{o}F /BTU R-Value)

$$R_{eff} = R_C + \frac{(R_{in} \times R_s)}{(R_{in}+R_{in})} = 0.18 + \frac{3.39*4.22}{3.39+4.22} = 2.06\ K/W$$ (11.53 h.ft^2.^{o}F /BTU R-Value)

$$R_{eff} = R_C + \frac{(R_{in} \times R_s)}{(R_{in}+R_{in})} = 0.18 + \frac{6.77*4.22}{6.77+4.22} = 2.78\ K/W$$ (15.56 h.ft^2.^{o}F /BTU R-Value)

Next entering R_{eff} into (Eq 13) Heat loss for one year is calculated.

$$E = \frac{T_o - T_{out}}{R_{eff}} \times S \times t = \frac{1500}{2.06} \times 1 \times 24/1000 = 17.84 \text{ kWhr per unit CSP}$$

$$E = \frac{T_o - T_{out}}{R_{eff}} \times S \times t = \frac{1500}{2.78} \times 1 \times 24/1000 = 12.94 \text{ kWhr per unit CSP}$$

Cost of Energy = E * CE where CE is the unit price of Energy. For example, in US unit price of Energy is 0.12 $/kWhr Eq. (14)

These values calculated for Two points, however, to plot the data, Energy loss is required to be calculated for small step sizes insulation thickness.

By comparing and dividing the Cost of Panel for specific thickness of Foam and Cost of Energy due to Heat loss, the number of years for that foam to be cost effective is calculated.

Since the cost of Labor and other machinery is not considered. This payback period is not accurate and with addition of labor cost to the cost of panel, more number of years is required to make using CSP unit cost effective. If the payback period is longer than building life span, then using this insulating material is not feasible.